Measuring platelet contributions to blood clot viscoelasticity using acoustic radiation force

A Dissertation

Presented to the faculty of the

School of Engineering and Applied Sciences

University of Virginia

in partial fulfillment

of the requirements for the degree

Doctor of Philosophy in Biomedical Engineering

by

Caroline Whitaker Wang

May

2015

APPROVAL SHEET

The dissertation
is submitted in partial fulfillment of the requirements
for the degree of
Doctor of Philosophy

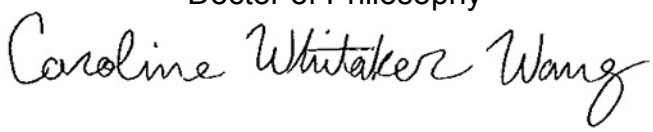

Caroline Whitaker Wang, Author

The dissertation has been read and reviewed by the examining committee:

Michael B. Lawrence, Ph.D., Advisor

Timothy E. Allen, Ph.D., Chair

David L. Green, Ph.D.

William H. Guilford, Ph.D.

Brian P. Helmke, Ph.D.

Jason A. Papin, Ph.D.

Accepted for the School of Engineering and Applied Science:

Dean, School of Engineering and Applied Science
May
2015

Acknowledgements

I'd like to thank my advisor, Dr. Michael Lawrence, for his direction during my time as a graduate student. Your encouragement of me to pursue creative research questions has challenged me and helped me to grow into an independent researcher. I would also like to thank my committee members William Guilford, Brian Helmke, Jason Papin, Timothy Allen, and David Green for all your valuable guidance and insights into my research over the years.

To my labmates past and present, Brian Schmidt, Molly Tinius, Jose Tlaxca, Annika Shuali, Yuhling Wang, Matthew Perez, and Nicole Brackett. Thank you for your friendship, conversation, and all your research assistance. Special thanks to Nicole for carefully reviewing my dissertation. Matt thanks for being my research right hand man and partner in crime. You both were always there to lend a hand or a vein in the lab and I couldn't have done it without you.

I'd like to thank Brittany Earnest for her help on blood clotting protocols and her advice on SEM imaging. To Sunil Unnikrishnan, thanks for offering me frequent opportunities to discuss my research over coffee. Thanks to Francesco Viola and Elisa Ferrante for their help with sonorheometry. I'd also like to thank the Hossack lab for their generous lending of equipment and reagents. I'd especially like to thank Joe Kilroy for his assistance with ultrasound beam characterization, attenuation measurements, and troubleshooting all things ultrasound.

I am so grateful to my family for their love and support. To my parents, thank you for always encouraging and believing in me. To my sister and brother-in-law Elizabeth and Eric, thank you for your perspective and advice on the Phd experience. Thank you to my nephew James for entertaining me and being a welcome distraction during my thesis writing and to my niece, not born yet as of this writing, who fills me with joyful anticipation.

To my husband Harris, thank you for being my cheerleader. You have been there for me as a constant encouraging voice during my time as a graduate student. Thanks for your unconditional love and friendship.

Table of Contents

Abstract

Blood clotting is an enzymatically and cellularly regulated process of stiffening the blood to prevent blood loss. Despite the life-preserving function blood clotting serves in the body, inappropriate blood clot stiffness has been associated with life-threatening diseases such as stroke, hemorrhage, and heart attack. The relationship between clot stiffness and vascular diseases underscores the importance of identifying the mechanisms by which blood clots stiffen. The primary mediators of clot stiffening are fibrin and platelets. Fibrin, when polymerized in a blood clot, provides a protein scaffold to which platelets subsequently bind. Mechanical properties of fibrin have mainly been investigated in the absence of platelets. Research on platelet activation has mainly been examined outside of the context of a fibrin network. It would be desirable to link fibrin clot properties and platelet biology. My dissertation describes the development of an *in vitro* method to measure blood clot stiffness and its application to quantifying the contributions of both fibrin network formation and platelet activation. What is unique about my approach is that I apply ultrasound acoustic radiation force to push on microscopic beads suspended in blood and use microscopy imaging to analyze the resulting bead motion to assess blood clot mechanical properties. To link macro scale clot mechanics to clot microstructure, I have also established an *in vitro* model of blood plasma clotting where platelet-fibrin interactions are visible by several microscopy techniques. With the clot stiffness assessment device and clot microstructure assays I have been investigating the role of platelet enzymatic or adhesive function on clot stiffness and clot structural properties. The experiments differentiate the modulation of clot mechanical properties and structures by platelet thrombin generation from the clot changes due to integrin IIb-IIIa mediated platelet adhesion. Linking platelet thrombin generation and adhesion to modulations of clot mechanical properties and fibrin clot architecture will facilitate identification of targets of anti-platelet drugs that could ultimately prevent thrombosis without interrupting hemostasis.

List of figures and tables

List of abbreviations

°C	degrees Celcius
3D	three dimensional
α	absorption coefficient
α	attenuation coefficient
$\alpha_{IIb}\beta_3$	glycoprotein IIb-IIIa
β_3	integrin beta-3
μ	Kelvin-Voigt viscous parameter
μ	fluid viscosity
μg	microgram
μL	microliter
μm	micrometer
π	mathematical constant pi
Δt	acoustic radiation force pulse interval
c	speed of sound
cm	centimeter
cP	centipoise
dB	decibel
f	frequency
fps	frames per second
g	times gravity
h	hour
k	Kelvin-Voigt elastic parameter
kHz	kilohertz
l	acoustic path length
m	meter
min	minute
mL	milliliter
mm	millimeter
ms	millisecond
pN	piconewton
s	second
t_i	initial time point
t_f	final time point
v	bead velocity
wt%	weight percent
ADP	adenosine diphosphate
AFM	atomic force microscopy
ARF	acoustic radiation force
ATP	adenosine triphosphate
$CaCl_2$	calcium chloride
DIC	differential interference contrast microscopy
D_m	maximum displacement
Dm_{avg}	average maximum displacement
DPBS	Dulbecco's phosphate buffered saline

F	force
F_f	final force
F_i	ideal non-attenuated force
G alpha 13	heterotrimeric G protein alpha 13
GPIB	general purpose interface bus
I	ultrasound intensity
IIb-IIIa	glycoprotein IIb-IIIa
MEMS	microelectromechanical systems
MHz	megahertz
MPa	megapascal
N	newton
Pa	pascal
PDMS	polydimethylsiloxane
PPP	platelet poor plasma
PRF	pulse repetition frequency
PRP	platelet rich plasma
PSGL-1	P-selectin glycoprotein ligand-1
R	bead radius
Re	Reynold's number
RGD	Arg-Gly-Asp peptide sequence
RhoA	Ras homolog gene family member A
RhoGEF	RhoGTPase nucleotide exchange factor
ROCK	Rho kinase
ROTEM™	thromboelastometry
S	stiffness
SEM	scanning electron microscope
Src	tyrosine-protein kinase Src
TAE	tris-acetate-ethylene-diamine-tetra-acetic acid
TEG™	thromboelastography
Txa2	thromboxane A2
VCAM-1	vascular cell adhesion protein-1
V_f	final voltage
V_i	initial voltage
W	power
W	watt

Chapter 1: Introduction

What is blood?

Humans have understood blood to be a bodily fluid vitally important for life since the beginning of human history. Because humanity has this longstanding appreciation of blood's importance, blood holds deep symbolic significance in many cultures. Blood has been equated with life itself in the Bible. Ancient Egyptians, believing blood to carry the human spirit, are said to have bathed in it to cure ailments. Roman gladiators, treating blood as a symbol of strength, are said to have drunk the blood of their slain opponents (Starr 2012). Respect for blood as a life sustaining fluid continues today as blood transfusion has become a workhorse technique of modern medicine.

Blood carries extracellular fluid. It is the body's transport system. It exchanges dissolved constituents with the interstitial fluid in tissues that surround the cells of the body (Hall 2010). Blood shuttles both nutrients and waste through the body from their sources to their destinations. In gas exchange, blood facilitates the transfer of oxygen from the air in the lungs to cells in the body, and carbon dioxide waste product from the cells back to the lungs for removal. Blood also facilitates exchange of nutrients such as carbohydrates, fats, and proteins from the gastrointestinal system to the blood and removal of waste products such as urea by the kidneys. Blood transports cells, liquids, gases, proteins, and chemicals. Major components of blood are red blood cells, leukocytes, platelets, and plasma.

The heart acts as a pump to regulate the flow of blood in the body. Because blood flows through blood vessels, flow is an important feature of the way blood functions. Different flow conditions, such as shear rate and blood vessel structure may elicit different hemostatic blood behaviors. Blood flow conditions contribute to plaque buildup in atherosclerosis, where plaques form most frequently at sites of disrupted flow in blood vessel branch points (Zarins et al. 1983).

Blood as an oxygen transporter

To oxygenate the whole body, blood travels a path starting at the lungs for oxygenation. The blood then travels to the heart, which pumps it out to the arteries and into smaller arterioles and capillaries. The capillaries exchange oxygen and carbon dioxide with the tissues of the body. The blood is then carried through the venuoles, into the veins, and back to the heart and lungs for reoxygenation (Hall 2010).

Blood as an immune defense system

In addition to acting as a transporter of oxygen, blood acts as a system of defense against disease. Bacteria, parasites, fungi, and viruses can infect the body, potentially causing disease or death. The immune system, made up of leukocytes and leukocyte-derived cells, can attack and destroy invaders. These cells work to attack and destroy infectious agents by tagging the agents as targets for destruction using antibodies and by destroying the agents through

phagocytosis (Hall 2010). The leukocyte rolling cascade is a model of how cells undergo a series of interactions with the vessel wall in order to respond to an injury or to a potential breach of the body's physical barrier (e.g. skin and mucous membranes) to infectious agents.

In the leukocyte rolling cascade, membrane proteins (e.g. selectins and integrins) on the leukocyte interact with a series of endothelial cell expressed ligands (e.g. P-selectin glycoprotein ligand-1 (PSGL-1) and vascular cell adhesion protein-1 (VCAM-1)). Through these interactions the leukocyte is captured from the circulating blood and begins rolling on the endothelium. Rolling is slowed by increased endothelium binding and eventually the leukocyte passes through the vessel wall and into the tissue (Ley, Laudanna, and Cybulsky 2007; Wagner and Frenette 2008). The leukocyte, after traversing the vessel wall, is activated or primed to fight an infectious agent.

What are integrins?

Integrins are a class of heterodimeric membrane proteins that signal bi-directionally across the cell membrane and promote cell adhesion (Hynes 2002). The heterodimer of the integrin is made up of an alpha and a beta subunit (Ginsberg, Partridge, and Shattil 2005). With 18 alpha subunits and 8 beta subunits, the heterodimer assembly allows integrins to interact with a variety of ligands that have common peptide binding sequences such as the Arg-Gly-Asp (RGD) sequence (Campbell and Humphries 2011). Integrins are involved in

multiple diverse cell processes, from blood clotting to immune response and leukocyte recruitment. In addition integrins are implicated in auto-immune and genetic diseases as well as cancer (Hynes 2002). In blood clotting, integrin IIb-IIIa ($\alpha_{IIb}\beta_3$) is expressed on platelets. Integrin IIb-IIIa binds to fibrin or fibrinogen, the blood protein that forms the polymer matrix of the blood clot.

What is blood clotting?

Blood clot formation is the change of blood from a viscous fluid to a viscoelastic gel, which prevents blood loss after injury. Blood clotting is another defense system of the body; it maintains blood pressure, aids in the maintenance of the barrier against foreign body entrance, and initiates wound healing.

The formation of a blood clot through the interaction of platelets, fibrin polymers, and the vessel wall is the primary mechanism by which the body prevents blood loss after injury. Platelet activation, fibrinogen polymerization and fibrin fiber crosslinking alter the mechanical properties of blood within minutes, from those of a viscous fluid to that of a viscoelastic gel (J. W. Weisel 2008; Ryan et al. 1999). Effective blood clot formation therefore requires an increase in material stiffness, a characteristic that can be correlated with clinical coagulopathies (Hall 2010; Tran et al. 2013; J. Weisel 2010). Hemostasis is the regulation of blood clotting processes; it maintains blood at the balance between hemorrhage and thrombosis. Platelet plug formation (**Fig. 1-1**) is the process of platelet aggregation at the site of blood vessel injury. Blood vessel injury can occur when the endothelial cell layer is damaged or a blood vessel is severed. Fibrin fiber

formation (**Fig. 1-1**) occurs concurrently with platelet plug formation and involves the formation of a crosslinked polymeric network of fibrin fibers from the precursor blood protein fibrinogen.

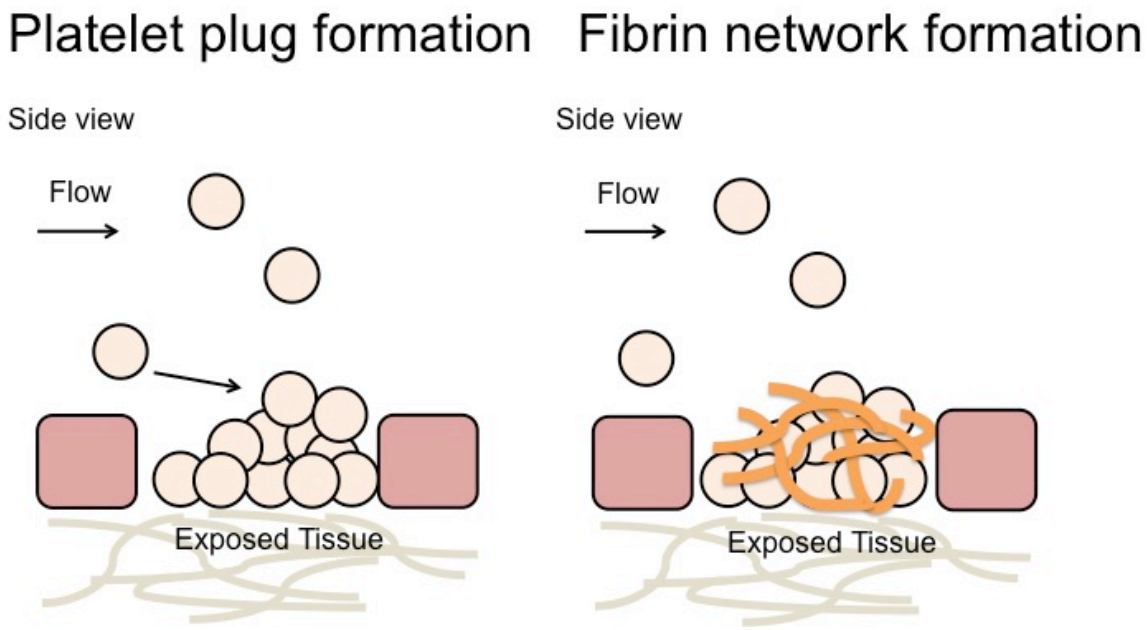

Figure 1-1 | Mechanisms of hemostasis. In platelet plug formation, platelets aggregate at exposed tissue and, in the case of blood vessel severing, block blood flow through the blood vessel with a platelet plug. Fibrin fiber formation, a process concurrent with platelet plug formation, forms a crosslinked fibrin polymer network.

What is a platelet?

Platelets are small anuclear cells approximately 4 μm in diameter (Frojmovic and Milton 1982). They are formed by megakaryocytes in the bone marrow (Hall 2010; Geddis and Kaushansky 2007; Kaushansky 2008; Scurfield and Radley 1981; Junt et al. 2007). Platelets contain actin and myosin, allowing them to perform contractile functions. Additionally platelets store calcium and produce adenosine triphosphate (ATP) and adenosine diphosphate (ADP). On the platelet

surface membrane proteins are expressed that adhere to sites of injury in the blood vessel or exposed collagen tissue (Hall 2010).

Platelet adhesion to the site of vascular injury can result in the formation of a platelet plug. The process of platelet aggregation to form a plug involves release of thromboxane A2 (Txa2), von Willebrand factor, and ADP (Ley, Laudanna, and Cybulsky 2007; Heemskerk and Bevers 2002; Wagner and Frenette 2008). The release of these factors activates nearby platelets, recruiting them to aggregate at the site and amplifying the platelet response. The platelet plug is then filled in by blood coagulation or the formation of fibrin fibers, a polymer network that surrounds and attaches to platelets forming a cohesive blood clot that stops bleeding.

Fibrin is a protein polymer that forms from single monomers of the protein fibrinogen. Fibrinogen is a fibrous protein with two globular regions at its ends connected by coiled coils (Hynes 2002; J. W. Weisel 2005). Fibrinogen has small portions of it, fragment A and fragment B, that are cleaved by the enzyme thrombin to produce the active monomer fibrin that can then begin to polymerize with other active fibrin monomers to form protofibrils (**Fig. 1-2**). These protofibrils then anneal together or laterally aggregate to form larger fibrin fibers (Ginsberg, Partridge, and Shattil 2005; J. Weisel and Nagaswami 1992).

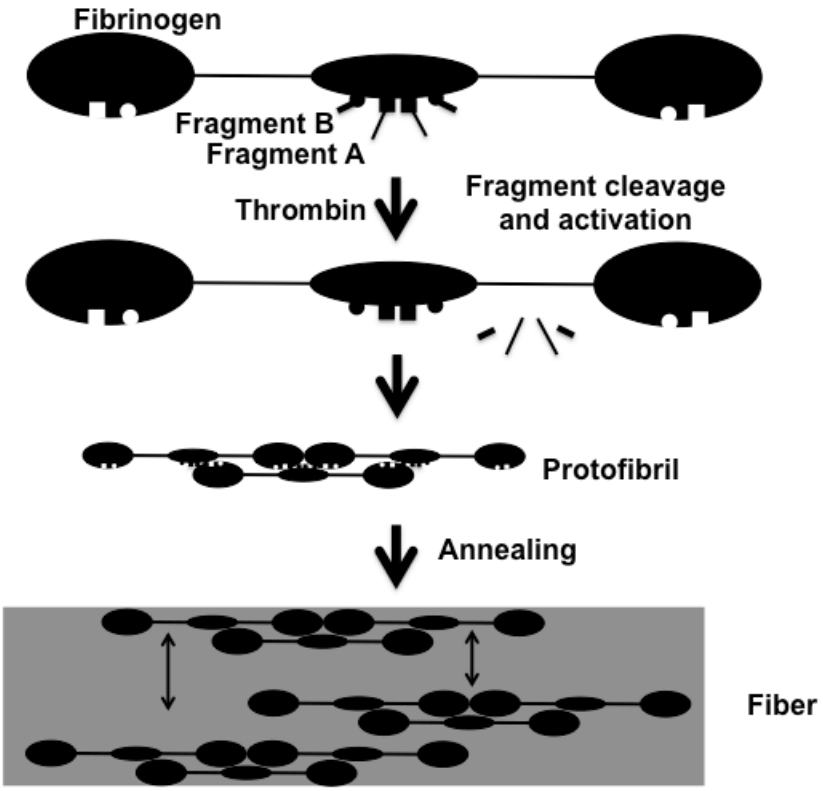

Figure 1-2 | Fibrinogen structure. Fibrinogen is a fibrous protein with two globular regions at its ends connected by coiled coils. Fibrinogen fragments A and B are cleaved by thrombin to form fibrin monomer, which polymerize to form protofibrils and then anneal or laterally aggregate to form fibrin fibers.

A formation of fibrin from its precursor inactive protein in the plasma, fibrinogen results from a series of enzymatic cleavage reactions (**Fig. 1-3**). Activation of the coagulation process can occur either by surface charge or reaction to tissue factor. Since bacteria frequently have charged membranes, surface charge activation of clotting may protect against bacterial infection. These impetuses result in cleavage of a portion of an enzyme, causing activation at each step in the chain, and continuing with cleavage of another enzyme to its active conformation, such that eventually thrombin is activated and fibrinogen is

converted to fibrin resulting in polymerization and coagulation (Campbell and Humphries 2011; J. W. Weisel 2008; Davie 2003; Ryan et al. 1999; Tran et al. 2013; Davie, Fujikawa, and Kisiel 1991; J. Weisel 2010).

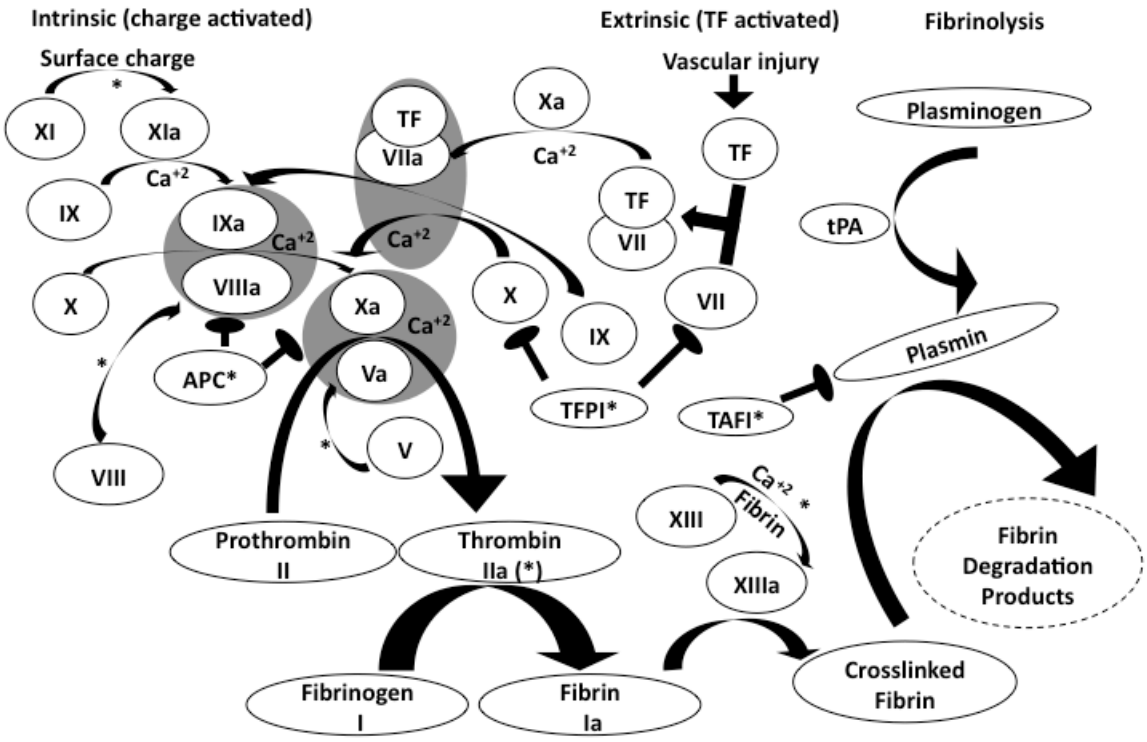

Figure 1-3 | Coagulation cascade. A series of enzymatic reactions, culminating in thrombin generation from prothrombin and conversion of precursor fibrinogen to fibrin monomer, initiates the polymeric reaction that forms fibrin fibers in a blood clot. White ovals (○) denote reagents and products. Pointed arrows (→) denote activations, while flat arrows (⊣) denote inhibitions. Grey ovals (●) denote platelet membrane enzyme complexes. Asterisks (*) denote thrombin catalysis.

Although much useful information has been learned from modeling the process of blood coagulation through this cascade of enzyme reactions, a more recent

model of hemostasis incorporates the cell as a contributing component of coagulation. In this cell-based model of coagulation, the platelet in particular is considered to be a center of the enzymatic reactions of coagulation (Hynes 2002; Hoffman 2001). The cell-based model of coagulation considers many of the reactions of coagulation to be localized on the platelet surface. The kinetic rates of these localized reactions are not diffusion limited, but rather are controlled by platelet surface clusters that facilitate fast thrombin production.

The cell-based model of coagulation has inspired the work presented in this dissertation. The dissertation describes both the development of a device that is particularly sensitive to the contributions of platelets to clot stiffness formation and examines platelet functions that contribute to blood clot mechanical properties.

What are diseases of blood clotting?

Hemostasis is the regulation of blood clotting such that blood neither clots too readily, as in thrombosis, nor too deficiently as in hemorrhage. Diseases of blood clotting include such coagulopathic conditions as hemophilia, which involves a genetically reduced clotting factor enzyme cleavage efficiency (either Factor VIII or Factor IX) that results in a lower rate of thrombin production and a reduced ability to clot (Tanaka, Key, and Levy 2009). Frequent bruising with chronic slow to heal wounds is common in people with hemophilia. In addition heart disease related coagulopathies such as deep vein thrombosis, surgical bleeding, and

stroke are all coagulopathies for which treatments might be improved with the study of the mechanisms of clotting (Knudson and Ikossi 2004; Ganter and Hofer 2008; Elliott et al. 2015).

Current treatments for diseases of blood clotting

For diseases of inadequate blood clotting, blood or blood product donation is a common treatment. For diseases of hypercoagulability, anticoagulants such as heparin can be used for treatment (Hirsh, Raschke, and Warkentin 1995). Platelet drugs are also quite common in the treatment of thrombotic diseases (McNicol and Israels 2003). Factor inhibitors, particularly Factor Xa inhibitors, are another treatment strategy frequently used clinically (Wong et al. 2008). In many cases treatment is guided by blood testing, which can include blood mechanical property testing (van Geffen and van Heerde 2012).

What are clinically relevant blood clot mechanical testing devices?

Ex vivo blood clot mechanical properties have been correlated with a number of disease states. Inadequate clot stiffness, the basis of 'soft' clots, is characteristic of hemorrhagic disorders such as hemophilia, and has been correlated with surgical bleeding in cardiopulmonary bypass (Chitlur et al. 2008; Essell et al. 1993). Hard clots, however, have been linked to the formation of thrombi in stroke, myocardial infarction, and deep vein thrombosis (Elliott et al. 2015; J. W. Weisel 2008; Collet et al. 2006; Lam et al. 2011; Kashuk et al. 2009).

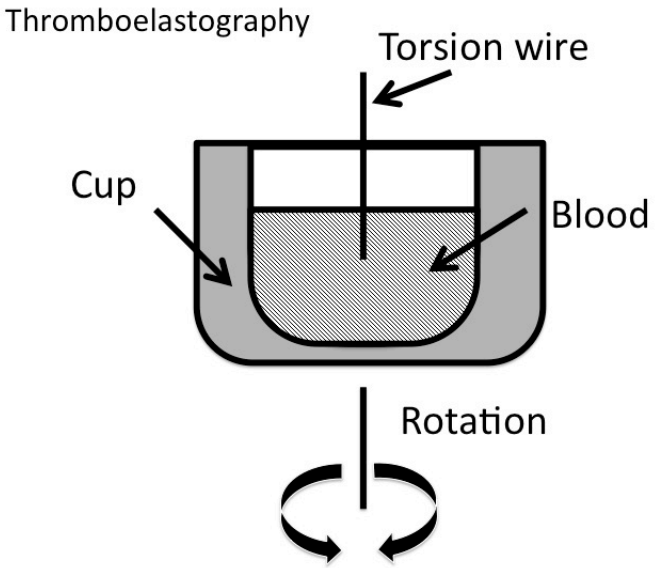

Figure 1-4 | Thromboelastography (TEG™) device. In thromboelastography a clotting blood sample is placed in a rotating cup with a central torsion wire. The cup rotates at an oscillation of 4°45' and the torsion wire tracks the resistance of the blood sample to the rotation of the cup. As the sample viscoelasticity increases with clotting the torsion wire rotation more closely matches the cup rotation.

The relationship between clot mechanics and vascular diseases underscores the importance of identifying the contributory roles of platelets and fibrin to hemostasis. Several mechanical tests of clot stiffness have successfully transitioned into the clinic, most notably the thromboelastogram (TEG™) **(Fig. 1-4)** and rotational thromboelastometry (ROTEM™). TEG™ and ROTEM™ operate by rotation in a pin and cup geometry. Measurement of bulk clot stiffness by either the TEG™ or ROTEM™ can assess the relative contributions of platelets and enzymatic plasma factors to overall clot stiffness (Jen and McIntire 1982; Carr 2003; Evans, Hawkins, and Williams 2006). Recently developed high

resolution measurement of individual platelet contractility and fibrin fiber stiffness have given additional insight into the cellular and enzymatic basis of clot mechanics, though single cell and molecule assessments have yet to be linked to global or bulk rheological properties of clots (Lam et al. 2011; Collet et al. 2005).

There are other rotational mechanical testing devices that can measure shear modulus by strain controlled or shear controlled methods. In addition, indentation, compressive, or tensile loading devices are also used when measuring mechanical properties of biological gels such as blood. Although mechanical testing by the array of methods described may be largely similar for a given material, the specific probing design of each test system likely identifies features of the material that are uniquely measured by that device. Therefore, when choosing a mechanical testing device to study a material, it is important to know what information you hope to ascertain and to ultimately choose the appropriate device for obtaining that information.

Platelet function tests

There are several assays that provide additional readouts about the process of hemostasis. A clot retraction assay **(Fig. 1-5)** looks at later stages of clotting, on the order of hours to days, in which the volume of the thrombus is reduced resulting in serum around the more compact clot (Weiner 1963; Nicholson et al. 1998; Tucker, Sage, and Gibbins 2012). Platelet contraction is thought to contribute to the clot retraction process. A thrombus stability test **(Fig. 1-6)** uses

flow, such as in a flow chamber assay, to examine the size of a platelet clot and the adhesive strength of the clot on a fibrinogen or collagen coated surface (Baumgartner and Sakariassen 2006). A platelet-spreading assay **(Fig. 1-7)** on fibrinogen or collagen also looks at the ability of the platelet to interact with fibrin. In the platelet-spreading assay, the surface area and the shape of the platelet on the substrate is assessed, where greater surface area and formation of filopodia or lamellipodia is an indication of platelet activation (K. Park, Mao, and Park 1990; Goodman 1999).

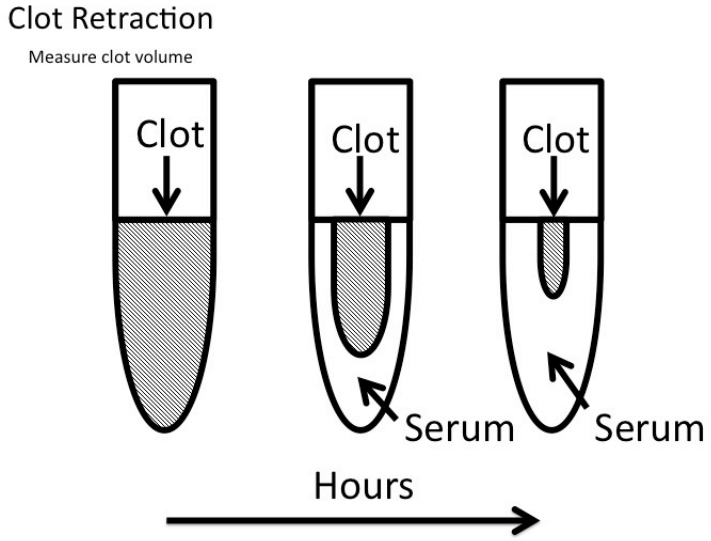

Figure 1-5 | Clot retraction assay. In the clot retraction assay, a clotting blood sample is placed in a tube. With clotting over the course of hours, the clot volume is reduced. The reduced clot volume is either assessed by visual inspection or pipetting to measure amount of serum extracted from the clot.

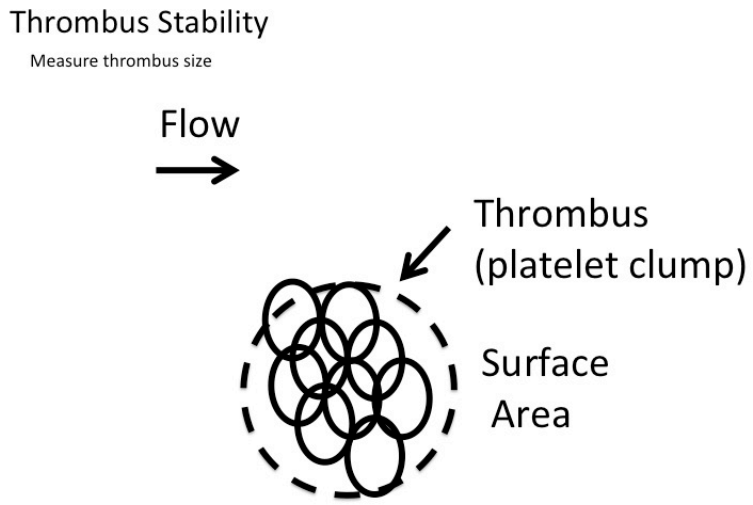

Figure 1-6 | Thrombus stability assay. In a thrombus stability assay, clotting blood is drawn through a flow chamber, and platelet clumping is assessed by measurement of thrombus size.

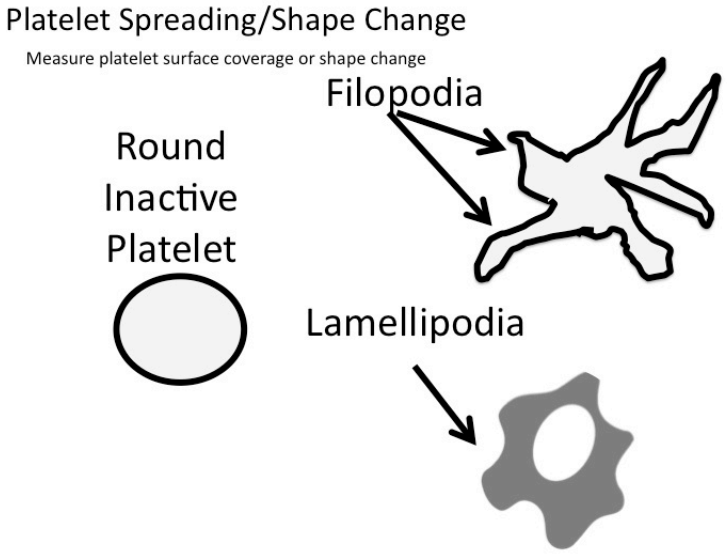

Figure 1-7 | Platelet shape change assessment. In platelet shape change assessment, platelets contact a surface and their morphological characteristics, in response to various clotting stimuli from the surface, are visually assessed. Platelet shape changes include a round inactive shape, platelet spreading, formation of sheet-like protrusions called lamellipodia, or formation of long thin protrusions called filopodia.

The role of platelets in blood clotting

Platelets perform many functions in the clot when activated (**Fig. 1-8**), including enzymatic modulation of fibrin polymerization, granule secretion to release coagulation factors that act in the clot in diverse functions, and expression of IIb-IIIa integrin which binds to fibrinogen and fibrin. Development of tenase and prothrombinase complexes on the platelet membrane catalyze the production of thrombin and fibrin polymerization (Heemskerk and Bevers 2002). Granule secretion of factors such as ADP, fibrinogen, von Willebrand factor, Factor V, P-selectin, IIb-IIIa, and plasminogen activator inhibitor-1 is required for the initial hemostatic response and also promotes the inflammatory and wound healing responses in the clot tissue (Harrison and Martin Cramer 1993; Whiteheart 2011). Integrin IIb-IIIa, as the platelet receptor for fibrin, (Sidelmann et al. 2000) acts as the link between the platelet and the fibrin mesh of the clot, which may primarily adhere the platelet to the site of the clot under flow conditions, and additionally may affect clot stiffness.

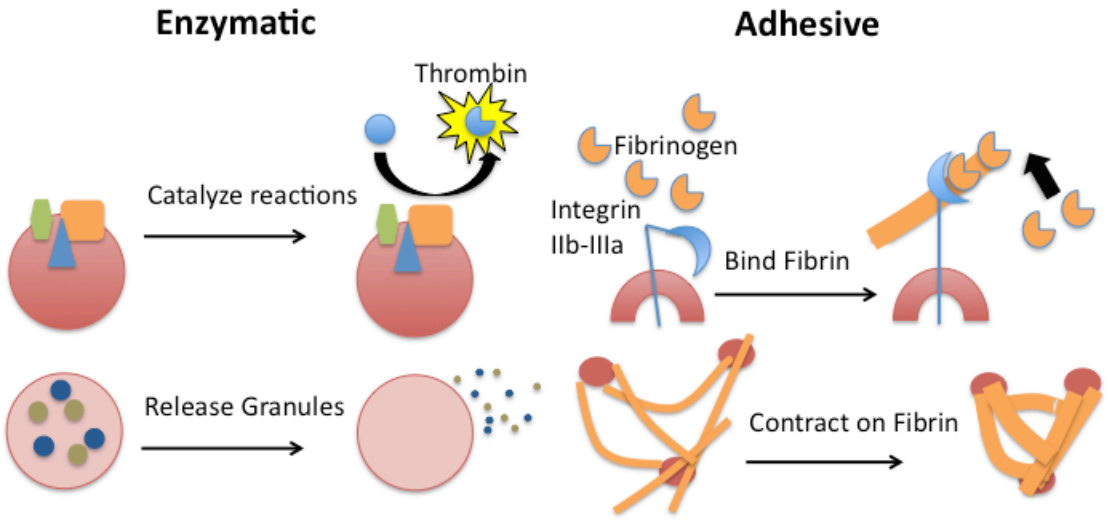

Figure 1-8 | Platelet functions in blood clotting. In blood clotting, platelets contribute both enzymatically, catalyzing thrombin generation, and adhesively, binding to fibrin through integrin IIb-IIIa. Platelet enzymatic catalysis includes (i) activation of membrane localized clotting factors (e.g. the tenase and prothrombinase complexes) leading to thrombin generation and (ii) granule secretion, which results in release of a cocktail of procoagulant and anticoagulant factors. Adhesive functions of the platelet include (i) binding of integrin IIb-IIIa to fibrin fibers and (ii) platelet contraction.

The integrin can be activated and inactivated by signaling processes in hemostasis that involve both “inside-out” and “outside-in” signal transduction (Goggs and Poole 2012). Inside-out signaling involves mediation of signals from ADP, thrombin, and Txa2 receptors to the IIb-IIIa integrin, which promote a transient conformational shift in the integrin from its bent “off” conformation to its extended “on” conformation,(Cosemans et al. 2008) which has faster kinetics for binding to fibrin (Ma, Qin, and Plow 2007). Binding of fibrin to IIb-IIIa initiates outside-in signaling which mediates the performance of platelet functions that

include platelet aggregation, granule release, shape change, and platelet contractility (Shattil, Kashiwagi, and Pampori 1998).

It is thought that IIb-IIIa mediates clot retraction through the platelet contractile apparatus and the activity of myosin IIa (Suzuki-Inoue et al. 2007; Kovacs 2004). The role of platelet contractile mechanism and IIb-IIIa on clot retraction and later stages of clot formation is well understood, however any influence of the platelet contractile apparatus on primary hemostasis or early stages of clotting is limited (Ono et al. 2008).

Because most platelet biology research has been done out of the context of the fibrin network, and most fibrin mechanics and structure research has been done in the absence of platelets, the impact of all platelet functions, both enzymatic and adhesive, on clot stiffness and clot structure is ill defined.

Ultrasound and momentum transfer by acoustic radiation force

A wave of any form (e.g. light, electromagnetic, sound) can generate a force upon contacting the surface of an object. The phenomenon of force application by ultrasound waves on an object is called acoustic radiation force (ARF) (Torr 1984). The force is applied to the object either by absorption or scattering of the wave (**Fig. 1-9**), both of which involve a transfer of energy from the wave to the object. The energy transfer results in transfer of momentum to the object. The

force applied to a medium, where absorption is the dominant form of energy transfer, as is the case in soft biological gels, is defined by the equation

$$F = \frac{W}{c} = \frac{2\alpha I}{c} \quad (1)$$

where F is the acoustic radiation force applied to a volume of the medium (N/cm^3), W is the power from the wave absorbed at the point of interest in the medium (W/cm^3), c is the speed of sound in the medium (m/s), α is the absorption coefficient of the medium (cm^{-1}), and I is the average intensity of the ultrasound wave at the point of interest in the medium (W/cm^2) (Nightingale et al. 2002).

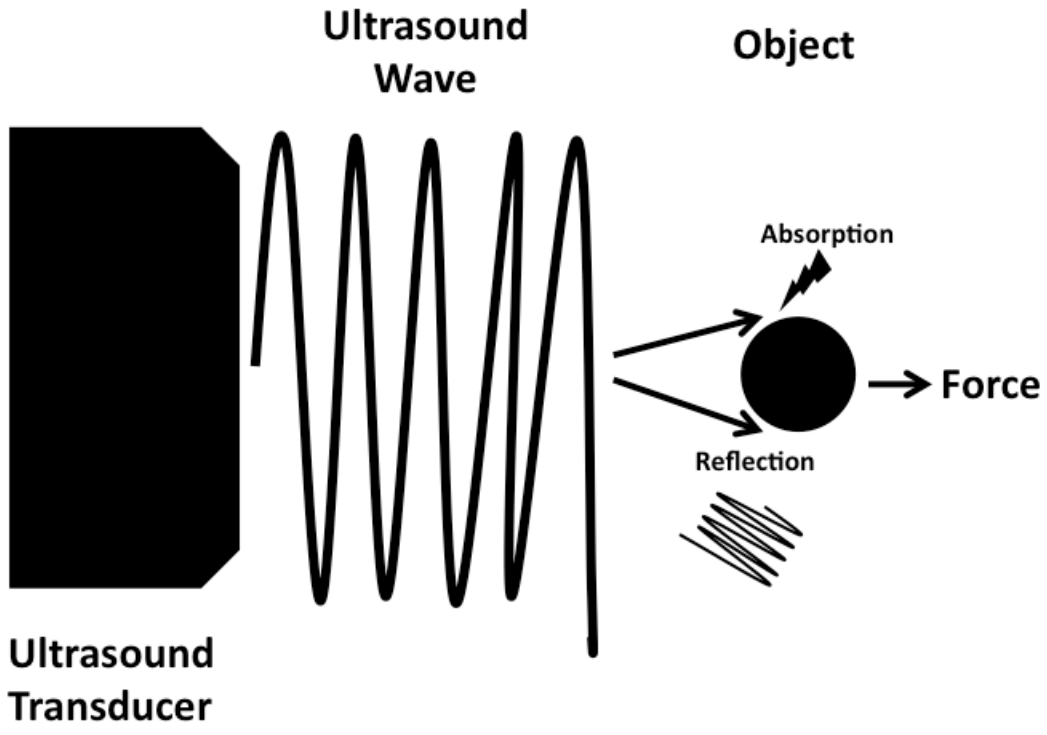

Figure 1-9 | Acoustic radiation force (ARF). The phenomenon of ARF causes a transfer of momentum from an ultrasound wave to an object, due to transfer of energy by absorption or reflection of the wave.

Ultrasound based techniques for mechanical testing of biomaterials

ARF has been previously used to characterize the viscoelastic properties of various biological tissues including the liver, tumor tissue, and the vitreous body of the eye (Nightingale, McAleavey, and Trahey 2003; Palmeri et al. 2008; Negron et al. 2002; Fatemi, Manduca, and Greenleaf 2003). In a more recent development to assess viscoelastic properties of blood, ultrasound ARF is coupled with echo time delay estimation of red blood cell displacement in a technique called sonorheometry (Viola et al. 2004; Mauldin et al. 2010; Viola et al. 2010). Other technologies that employ ultrasound in their approach to detect material properties of blood include supersonic shear imaging (Bercoff, Tanter, and Fink 2004). Ultrasound imaging has been used for detection of material strains in tissue following external application of force (Parker et al. 1990; Greenleaf, Fatemi, and Insana 2003).

Study Objectives

The purpose of this dissertation was two pronged: 1) to develop a system to measure blood clot stiffness that provides unique insight about blood clot mechanical properties, and 2) to determine whether platelet thrombin production or platelet adhesion are primarily responsible for changes in blood clot mechanical properties and blood clot structure (**Fig. 1-10**). Designing a new device for blood clot stiffness measurement was motivated by a desire to better understand material property contributions to diseases of clotting. The study of

mechanisms of platelet contribution to clot stiffness was motivated by the goal of identifying potential targets for therapies that might exploit key modulators of clot stiffness in order to better maintain hemostasis.

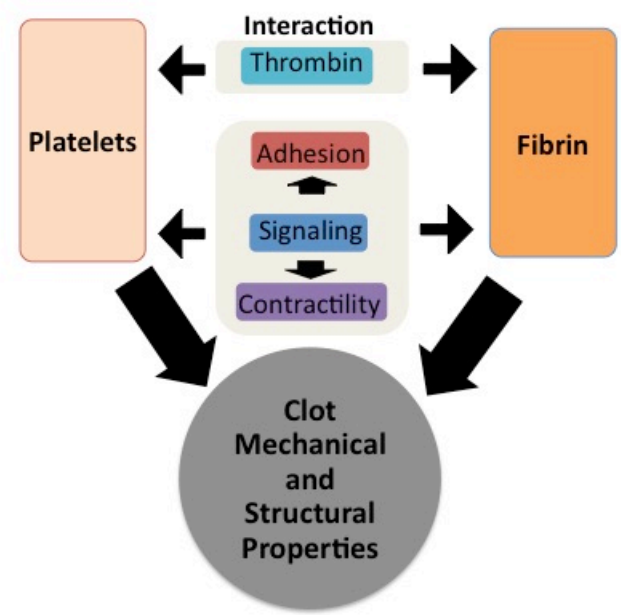

Figure 1-10 | Platelets and clot mechanics and structure. Platelets may interact with fibrin through enzymatic catalysis of thrombin generation and adhesion through integrin IIb-IIIa, which involves platelet signaling and contractility, to modulate clot mechanical and structural properties.

The method developed and utilized in this dissertation measures blood clot viscoelasticity on the scale of platelet aggregate and fibrin network complexes, applying pN magnitude forces in a region of clot on the order of a hundredth of a microliter, making it useful for studying platelet modulation of clot stiffness. The technique is quantitative and can measure both early and late stage clot stiffness. The ultrasound based technique allows for measurement of the mechanical response of the clot, both during and after removal of force application, which allows for assessment both of viscoelasticity and clot plasticity.

The platelet mechanistic study involved examination of both structural and material properties of blood, because structure is fundamentally linked to mechanical properties. We tested the hypothesis that both platelet thrombin generation and adhesions contribute to modification of the fibrin network, and change the clot stiffness.

What is not currently understood or appreciated in the field is that blood clotting depends on adhesion, particularly because larger fibrin fibers generate greater stiffness than smaller fibers. The process of generating thrombin, which is critical for quickly generating a clot, also tends to make weaker clots with smaller fibrin fibers. The adhesive action of the platelet through IIb-IIIa enables quick formation of a stronger fibrin clot. Platelet adhesion allows strong clot formation with high thrombin concentrations, through a possible mechanism of integrin clustering on the platelet surface, collecting fibrin protofibril chains into large fibrin bundles. Additionally platelet contractility, which involves the actin cytoskeleton, may pull on the fibrin fibers, collecting the integrins and fibrin fibers together into larger fibers. This study is suggestive that integrins cluster fibrin fibers, and that contractility contributes to the clustering and the stiffness generation, although the mechanism has not been proven.

This study identifies adhesion as important for platelet mechanical contributions to the clot, and also supports the role of platelet thrombin generation as important

for quick clot formation, which has been thought of as the primary way that platelets contribute to clot stiffness in the past.

Outline of the Study

Chapter 2 focuses on developing a device for assessment of clot stiffness that is sensitive to platelet contributions. Chapter 3 assesses whether thrombin generation alone could account for platelet contributions to clot stiffness and clot architecture. In Chapter 4, the influence of platelet adhesive function on clot stiffness and clot architecture is determined. To allow each chapter to stand alone, each has its own methods section, relevant to the techniques used to generate data. Methods information, for techniques used in more than one chapter, may appear more than once.

REFERENCES

Baumgartner, H R, and K S Sakariassen. 2006. “Factors Controlling Thrombus Formation on Arterial Lesions.” *Annals of the New York Academy of Sciences* 454 (1): 162–77. doi:10.1111/j.1749-6632.1985.tb11855.x.

Bercoff, Jérémy, Mickael Tanter, and Mathias Fink. 2004. “Supersonic Shear Imaging: a New Technique for Soft Tissue Elasticity Mapping.” *IEEE Transactions on Ultrasonics, Ferroelectrics, and Frequency Control* 51 (4): 396–409. doi:10.1109/TUFFC.2004.1295425.

Campbell, I D, and M J Humphries. 2011. “Integrin Structure, Activation, and Interactions.” *Cold Spring Harbor Perspectives in Biology* 3 (3): a004994. doi:10.1101/cshperspect.a004994.

Carr, Marcus E, Jr. 2003. “Development of Platelet Contractile Force as a Research and Clinical Measure of Platelet Function.” *Cell Biochemistry and Biophysics* 38 (1): 55–78. doi:10.1385/CBB:38:1:55.

Chitlur, Meera, Indira Warrier, Madhvi Rajpurkar, Wendy Hollon, Lolita Llanto, Carol Wiseman, and Jeanne M Lusher. 2008. “Thromboelastography in Children with Coagulation Factor Deficiencies.” *British Journal of Haematology* 142 (2): 250–56. doi:10.1111/j.1365-2141.2008.07063.x.

Collet, J P, Y Allali, C Lesty, M L Tanguy, J Silvain, A Ankri, B Blanchet, et al. 2006. “Altered Fibrin Architecture Is Associated with Hypofibrinolysis and Premature Coronary Atherothrombosis.” *Arteriosclerosis, Thrombosis, and Vascular Biology* 26: 2567–73. doi:10.1161/01.ATV.0000241589.52950.4c.

Collet, Jean-Philippe, Henry Shuman, Robert E Ledger, Seungtaek Lee, and John W Weisel. 2005. “The Elasticity of an Individual Fibrin Fiber in a Clot.” *Proceedings of the National Academy of Sciences* 102 (26): 9133–37. doi:10.1073/pnas.0504120102.

Cosemans, J M E M, B F Iserbyt, H Deckmyn, and J W M Heemskerk. 2008. “Multiple Ways to Switch Platelet Integrins on and Off.” *Journal of Thrombosis and Haemostasis* 6 (8): 1253–61. doi:10.1111/j.1538-7836.2008.03041.x.

Davie, E W. 2003. “A Brief Historical Review of the Waterfall/Cascade of Blood Coagulation.” *Journal of Biological Chemistry* 278 (51): 50819–32. doi:10.1074/jbc.X300009200.

Davie, Earl W, Kazuo Fujikawa, and Walter Kisiel. 1991. “The Coagulation Cascade: Initiation, Maintenance, and Regulation.” *Biochemistry* 30 (43): 10363–70. doi:10.1021/bi00107a001.

Elliott, Andrea, Jeremy Wetzel, Tiffany Roper, Evan Pivalizza, James McCarthy, Cristina Wallace, Mary Jane Hess, et al. 2015. “Thromboelastography in Patients with Acute Ischemic Stroke.” *International Journal of Stroke : Official Journal of the International Stroke Society* 10 (2): 194–201. doi:10.1111/j.1747-4949.2012.00919.x.

Essell, J.H., T.J. Martin, J. Salinas, J.M. Thompson, and V.C. Smith. 1993. “Comparison of Thromboelastography to Bleeding Time and Standard Coagulation Tests in Patients After Cardiopulmonary Bypass.” *Journal of Cardiothoracic and Vascular Anesthesia* 7 (4): 410–15. doi:10.1016/1053-

0770(93)90161-D.
Evans, PA, K. Hawkins, and PR Williams. 2006. “Rheometry for Blood Coagulation Studies.” *Rheology Reviews*. The British Society of Rheology, 255–91.
Fatemi, M, A Manduca, and J.F Greenleaf. 2003. “Imaging Elastic Properties of Biological Tissues by Low-Frequency Harmonic Vibration.” *Proc. IEEE* 91 (10): 1503–19. doi:10.1109/JPROC.2003.817865.
Frojmovic, M M, and J G Milton. 1982. “Human Platelet Size, Shape, and Related Functions in Health and Disease.” *Physiological Reviews* 62 (1): 185–261.
Ganter, Michael T, and Christoph K Hofer. 2008. “Coagulation Monitoring: Current Techniques and Clinical Use of Viscoelastic Point-of-Care Coagulation Devices.” *Anesthesia and Analgesia* 106 (5): 1366–75. doi:10.1213/ane.0b013e318168b367.
Geddis, A E, and K Kaushansky. 2007. “The Root of Platelet Production.” *Science* 317: 1689. doi:10.1126/science.1148946.
Ginsberg, M H, A Partridge, and S J Shattil. 2005. “Integrin Regulation.” *Current Opinion in Cell Biology* 17: 509–16.
Goggs, Robert, and Alastair W Poole. 2012. “Platelet Signaling-a Primer.” *Journal of Veterinary Emergency and Critical Care* 22 (1): 5–29. doi:10.1111/j.1476-4431.2011.00704.x.
Goodman, S L. 1999. “Sheep, Pig, and Human Platelet-Material Interactions with Model Cardiovascular Biomaterials.” *Journal of Biomedical Materials Research* 45 (3): 240–50. doi:10.1002/(SICI)1097-4636(19990605)45:3<240::AID-JBM12>3.0.CO;2-C.
Greenleaf, James F, Mostafa Fatemi, and Michael Insana. 2003. “Selected Methods for Imaging Elastic Properties of Biological Tissues..” *Annual Review of Biomedical Engineering* 5: 57–78. doi:10.1146/annurev.bioeng.5.040202.121623.
Hall, J E. 2010. *Guyton and Hall Textbook of Medical Physiology*. Elsevier Health Sciences.
Harrison, P., and E Martin Cramer. 1993. “Platelet A-Granules.” *Blood Reviews* 7 (1): 52–62. doi:10.1016/0268-960X(93)90024-X.
Heemskerk, JWM, and E M Bevers. 2002. “Platelet Activation and Blood Coagulation.” *Thrombosis and Haemostasis* 88: 186–93.
Hirsh, J, R Raschke, and T E Warkentin. 1995. “Heparin: Mechanism of Action, Pharmacokinetics, Dosing Considerations, Monitoring, Efficacy, and Safety.” *Chest* 108 (4_Supplement): 258S–275S. doi:10.1378/chest.108.4_Supplement.258S.
Hoffman, M. 2001. “A Cell-Based Model of Hemostasis.” *Thrombosis and Haemostasis* 85: 958–65.
Hynes, Richard O. 2002. “IntegrinsBidirectional, Allosteric Signaling Machines.” *Cell* 110 (6): 673–87. doi:10.1016/S0092-8674(02)00971-6.
Jen, Chauying J, and Larry V McIntire. 1982. “The Structural Properties and Contractile Force of a Clot.” *Cell Motility* 2 (5): 445–55. doi:10.1002/cm.970020504.
Junt, T, H Schulze, Z Chen, S Massberg, T Goerge, A Krueger, D D Wagner, et

al. 2007. “Dynamic Visualization of Thrombopoiesis Within Bone Marrow.” *Science* 317 (5845): 1767–70. doi:10.1126/science.1146304.

Kashuk, Jeffry L, Ernest E Moore, Allison Sabel, Carlton Barnett, James Haenel, Tuan Le, Michael Pezold, et al. 2009. “Rapid Thrombelastography (R-TEG) Identifies Hypercoagulability and Predicts Thromboembolic Events in Surgical Patients.” *Surgery* 146 (4): 764–74. doi:10.1016/j.surg.2009.06.054.

Kaushansky, Kenneth. 2008. “Historical Review: Megakaryopoiesis and Thrombopoiesis.” *Blood* 111 (3): 981–86. doi:10.1182/blood-2007-05-088500.

Knudson, M Margaret, and Danagra G Ikossi. 2004. “Venous Thromboembolism After Trauma.” *Current Opinion in Critical Care* 10 (6): 539–48. doi:10.1097/01.ccx.0000144941.09650.9f.

Kovacs, M. 2004. “Mechanism of Blebbistatin Inhibition of Myosin II.” *Journal of Biological Chemistry* 279 (34): 35557–63. doi:10.1074/jbc.M405319200.

Lam, Wilbur A, Ovijit Chaudhuri, Ailey Crow, Kevin D Webster, Tai-De Li, Ashley Kita, James Huang, and Daniel A Fletcher. 2011. “Mechanics and Contraction Dynamics of Single Platelets and Implications for Clot Stiffening.” *Nature Materials* 10 (1): 61–66. doi:10.1038/nmat2903.

Ley, K, C Laudanna, and M Cybulsky. 2007. “Getting to the Site of Inflammation: the Leukocyte Adhesion Cascade Updated.” *Nature Reviews Immunology* 7 (9): 678–89. doi:10.1016/j.cca.2010.01.018.

Ma, Y Q, Hao Qin, and E F Plow. 2007. “Platelet Integrin αIIb B3: Activation Mechanisms.” *Journal of Thrombosis and Haemostasis* 5 (7): 1345–52. doi:10.1111/j.1538-7836.2007.02537.x.

Mauldin, F William, Francesco Viola, Theresa C Hamer, Eman M Ahmed, Shawna B Crawford, Doris M Haverstick, Michael B Lawrence, and William F Walker. 2010. “Adaptive Force Sonorheometry for Assessment of Whole Blood Coagulation.” *Clinica Chimica Acta* 411 (9-10): 638–44. doi:10.1016/j.cca.2010.01.018.

McNicol, A, and SJ Israels. 2003. “Platelets and Anti-Platelet Therapy.” *Journal of Pharmacological Sciences* 93 (4): 381–96. doi:10.1254/jphs.93.381.

Negron, L.A, F Viola, E.P Black, C.A Toth, and W.F Walker. 2002. “Development and Characterization of a Vitreous Mimicking Material for Radiation Force Imaging.” *IEEE Transactions on Ultrasonics, Ferroelectrics, and Frequency Control* 49 (11): 1543–51. doi:10.1109/TUFFC.2002.1049736.

Nicholson, Nancy S, Susan G Panzer-Knodle, Neal F Haas, Beatrice B Taite, James A Szalony, Jimmy D Page, Larry P Feigen, David M Lansky, and Anita K Salyers. 1998. “Assessment of Platelet Function Assays.” *American Heart Journal* 135 (5): S170–78. doi:10.1016/S0002-8703(98)70245-5.

Nightingale, K, M S Soo, R Nightingale, R Bentley, D Stutz, M Palmeri, J Dahl, and G Trahey. 2002. “Acoustic Radiation Force Impulse Imaging: Remote Palpation of the Mechanical Properties of Tissue.” *IEEE Ultrasonics Symposium*, 1821–30. doi:10.1109/ULTSYM.2002.1192652.

Nightingale, K, S McAleavey, and G Trahey. 2003. “Shear-Wave Generation Using Acoustic Radiation Force: in Vivo and Ex Vivo Results.” *Ultrasound in Medicine and Biology* 29 (12): 1715–23. doi:10.1016/j.ultrasmedbio.2003.08.008.

Ono, A, E Westein, S Hsiao, W S Nesbitt, J R Hamilton, S M Schoenwaelder, and S P Jackson. 2008. “Identification of a Fibrin-Independent Platelet Contractile Mechanism Regulating Primary Hemostasis and Thrombus Growth.” *Blood* 112 (1): 90–99. doi:10.1182/blood-2007-12-127001.

Palmeri, M.L., M H Wang, J J Dahl, K.D. Frinkley, and K.R. Nightingale. 2008. “Quantifying Hepatic Shear Modulus in Vivo Using Acoustic Radiation Force.” *Ultrasound in Medicine and Biology* 34 (4): 546–58. doi:10.1016/j.ultrasmedbio.2007.10.009.

Park, K, F W Mao, and H Park. 1990. “Morphological Characterization of Surface-Induced Platelet Activation.” *Biomaterials* 11 (1): 24–31. doi:10.1016/0142-9612(90)90047-T.

Parker, K J, S R Huang, R A Musulin, and R M Lerner. 1990. “Tissue Response to Mechanical Vibrations for ‘Sonoelasticity Imaging’.” *Ultrasound in Medicine and Biology* 16: 241–46. doi:10.1016/0301-5629(90)90003-U.

Ryan, Esther A, Lyle F Mockros, John W Weisel, and Laszlo Lorand. 1999. “Structural Origins of Fibrin Clot Rheology.” *Biophysical Journal* 77 (5): 2813–26. doi:10.1016/S0006-3495(99)77113-4.

Scurfield, G, and J M Radley. 1981. “Aspects of Platelet Formation and Release.” *American Journal of Hematology* 10 (3): 285–96. doi:10.1002/ajh.2830100308.

Shattil, Sanford J, Hirokazu Kashiwagi, and Nisar Pampori. 1998. “Integrin Signaling: the Platelet Paradigm.” *Blood* 91: 2645–57.

Sidelmann, JJ, J Gram, J Jespersen, and C Kluft. 2000. “Fibrin Clot Formation and Lysis: Basic Mechanisms.” *Seminars in Thrombosis and Hemostasis* 26 (6): 605–18.

Starr, D. 2012. *Blood: an Epic History of Medicine and Commerce*. Knopf Doubleday Publishing Group.

Suzuki-Inoue, K, C E Hughes, O Inoue, and M Kaneko. 2007. “Involvement of Src Kinases and PLCγ2 in Clot Retraction.” *Thrombosis Research* 120: 251–58. doi:10.1016/j.thromres.2006.09.003.

Tanaka, Kenichi A, Nigel S Key, and Jerrold H Levy. 2009. “Blood Coagulation: Hemostasis and Thrombin Regulation.” *Anesthesia and Analgesia* 108 (5): 1433–46. doi:10.1213/ane.0b013e31819bcc9c.

Torr, G R. 1984. “The Acoustic Radiation Force.” *American Journal of Physics* 52 (5): 402–8. doi:10.1119/1.13625.

Tran, Reginald, David R Myers, Jordan Ciciliano, Elaissa L Trybus Hardy, Yumiko Sakurai, Byungwook Ahn, Yongzhi Qiu, Robert G Mannino, Meredith E Fay, and Wilbur A Lam. 2013. “Biomechanics of Haemostasis and Thrombosis in Health and Disease: From the Macro- to Molecular Scale.” *Journal of Cellular and Molecular Medicine* 20 (10): 1–18. doi:10.1111/jcmm.12041.

Tucker, Katherine L, Tanya Sage, and Jonathan M Gibbins. 2012. “Clot Retraction.” *Methods in Molecular Biology* 788: 101–7. doi:10.1007/978-1-61779-307-3_8.

van Geffen, Mark, and Waander L van Heerde. 2012. “Global Haemostasis Assays, From Bench to Bedside.” *Thrombosis Research* 129 (6): 681–87.

doi:10.1016/j.thromres.2011.12.006.
Viola, F, MD Kramer, MB Lawrence, JP Oberhauser, and WF Walker. 2004. "Sonorheometry: a Noncontact Method for the Dynamic Assessment of Thrombosis." *Annals of Biomedical Engineering* 32 (5): 696–705. doi:10.1023/B:ABME.0000030235.72255.df.
Viola, Francesco, F William Mauldin, Xiefan Lin-Schmidt, Doris M Haverstick, Michael B Lawrence, and William F Walker. 2010. "A Novel Ultrasound-Based Method to Evaluate Hemostatic Function of Whole Blood." *Clinica Chimica Acta* 411: 106–13. doi:10.1016/j.cca.2009.10.017.
Wagner, Denisa D, and Paul S Frenette. 2008. "The Vessel Wall and Its Interactions." *Blood* 111 (11): 5271–81. doi:10.1182/blood-2008-01-078204.
Weiner, Murray. 1963. "Clot Retraction and Fibrinolysis." *Clinical Chemistry* 9 (2): 182–87.
Weisel, J, and C Nagaswami. 1992. "Computer Modeling of Fibrin Polymerization Kinetics Correlated with Electron Microscope and Turbidity Observations: Clot Structure and Assembly Are Kinetically Controlled." *Biophysical Journal* 63 (1): 111–28. doi:10.1016/S0006-3495(92)81594-1.
Weisel, John W. 2005. *Fibrinogen and Fibrin*. Vol. 70. Advances in Protein Chemistry. doi:10.1016/S0065-3233(05)70008-5.
Weisel, John W. 2008. "Enigmas of Blood Clot Elasticity." *Science* 320: 456–57. doi:10.1126/science.1154210.
Weisel, JW. 2010. "Biomechanics in Hemostasis and Thrombosis." *Journal of Thrombosis and Haemostasis* 8: 1027–29. doi:10.1111/j.1538-7836.2010.03808.x.
Whiteheart, Sidney W. 2011. "Platelet Granules: Surprise Packages.." *Blood* 118 (5): 1190–91. doi:10.1182/blood-2011-06-359836.
Wong, P C, E J Crain, B Xin, R R Wexler, P Y S Lam, D J Pinto, J M Luettgen, and R M Knabb. 2008. "Apixaban, an Oral, Direct and Highly Selective Factor Xa Inhibitor: in Vitro, Antithrombotic and Antihemostatic Studies." *Journal of Thrombosis and Haemostasis* 6 (5): 820–29. doi:10.1111/j.1538-7836.2008.02939.x.
Zarins, C K, D P Giddens, B K Bharadvaj, V S Sottiurai, R F Mabon, and S Glagov. 1983. "Carotid Bifurcation Atherosclerosis. Quantitative Correlation of Plaque Localization with Flow Velocity Profiles and Wall Shear Stress." *Circulation* 53: 502–14. doi:10.1161/01.RES.53.4.502.

Chapter 2: Integration of acoustic radiation force and optical imaging for blood plasma clot stiffness measurement

INTRODUCTION

The formation of a blood clot through the interaction of platelets, fibrin polymers, and the vessel wall is the primary mechanism by which the body arrests blood loss after injury. Platelet activation, fibrinogen polymerization and fibrin fiber crosslinking alter the mechanical properties of blood within minutes from those of a viscous fluid to that of a viscoelastic gel (J. W. Weisel 2008; Ryan et al. 1999). Effective blood clot formation therefore requires an increase in material stiffness, a characteristic that can be correlated with clinical coagulopathies (Tran et al. 2013; J. Weisel 2010).

Ex vivo blood clot mechanical properties have been correlated with a number of disease states. Inadequate clot stiffness, manifested as a 'soft' clot, is characteristic of hemorrhagic disorders such as hemophilia and has been correlated with surgical bleeding in cardiopulmonary bypass (Chitlur et al. 2008; Essell et al. 1993). 'Hard' clots, by contrast, have been linked to the formation of thrombi in stroke, myocardial infarction, and deep vein thrombosis (Elliott et al. 2015; J. W. Weisel 2008; Collet et al. 2006; Lam et al. 2011; Kashuk et al. 2009).

The relationship between clot mechanics and vascular diseases underscores the importance of identifying the contributory roles of platelets and fibrin to

hemostasis. Several *ex vivo* mechanical tests of clot stiffness have successfully transitioned into the clinic, most notably the thromboelastogram (TEG™) and rotational thromboelastometry (ROTEM™). Measurement of bulk clot stiffness by either the TEG™ or ROTEM™ can be structured as a differential test to assess the relative contributions of platelets and plasma factors to overall clot stiffness (Jen and McIntire 1982; Carr 2003; Evans, Hawkins, and Williams 2006).

Recent innovations in blood clot mechanical testing

There are a number of new technologies that are being developed based on diverse approaches to look at the dynamics of blood clotting both *in vivo* and *ex vivo.* Dynamic light scattering analysis has been used to measure *in vivo* the clotting of blood by comparing motion of red blood cells in flow or in stasis (Fine et al. 2011). Dynamic light scattering can be used to assess motion of particles in suspensions. Information about the particle properties such as size and solution viscosity can also be determined by analysis of the light scatter from the sample solution. In the application of dynamic light scattering described by Fine et al. 2011, the blood flow to the base of the finger was obstructed by application of a pressure cuff in order to create a condition of blood stasis and the motion of red blood cells was examined using a laser and a photo detector. With the measurement of dynamic light scattering in the finger model described they were able to show a reduction in red blood cell diffusion with increasing time over the course of seconds.

Similarly, laser speckle rheology has been used to correlate changes in light scattering speckle intensity with viscoelastic property changes *ex vivo* (Tripathi et al. 2014). The laser speckle phenomenon is characterized by fluctuations in laser light scattering from tissue. In Tripathi et al. 2014 an *ex vivo* blood clot viscoelasticity testing system was implemented that detected laser light scattering by high speed CMOS camera. The system detected clotting time differences in samples with increasing concentrations of several procoagulant factors (thromboplastin, prothrombin, and fibrinogen).

A novel approach that combines laser detection of material motion and mechanical oscillation of the blood sample is RheoSpectris™ (Schmitt et al. 2013). In RheoSpectris™ a cylindrical tube is made to oscillate perpendicular to its longitudinal axis and shear waves are generated. A laser and light sensor are used to detect shear wave motion by measurement of laser light scattering.

Ultrasound imaging is the principle of using acoustic wave transmission into a material and measurement of the subsequent reflection of the acoustic waves off of objects in the wave path (Leighton 2007). The reflection of the acoustic waves can be interpreted to construct images of the material through which the wave was transmitted. Ultrasound imaging has been used for detection of material strains in tissue following external application of force (Parker et al. 1990; Greenleaf, Fatemi, and Insana 2003).

In addition there are multiple microelectromechanical systems (MEMS) technologies that incorporate microcantilever or piezoelectric approaches to measure the changes in material properties of blood *ex vivo* (Xu, Appel, and Chae 2012; Cakmak et al. 2013).

Recently developed high resolution measurements of individual platelet contractility and fibrin fiber stiffness have given additional insight into the cellular and molecular basis of clot mechanics, though single cell and molecule assessments have yet to be linked to global or bulk rheological properties of clots (Lam et al. 2011; Collet et al. 2005). The majority of viscometric assessments of clot rheology require removal of a blood sample from the subject for analysis and therefore may not capture fully the pathophysiology of an arterial or venous clot *in situ*. Within this admittedly severe limitation, *ex vivo* approaches to studying blood clotting can give significant insight into detailed molecular and cellular mechanisms that regulate coagulation. The *ex vivo* approaches of TEG^{TM} and ROTEM^{TM} have been shown to generate useful information for clinical transfusion management and fibrinogen supplementation (Shore-Lesserson et al. 1999; Meybohm, Zacharowski, and Weber 2013)1.

In contrast to approaches to assess *ex vivo* blood clot stiffness based on either light scattering or mechanical testing, ultrasound can assess tissue stiffness by generation of acoustic radiation force (ARF), which transfers momentum from the ultrasound waves to the propagating medium and any embedded reflective or

absorptive objects (Torr 1984; K. Nightingale, Soo, Nightingale, and Trahey 2002). ARF has been previously used to characterize the viscoelastic properties of various biological tissues including the liver, tumor tissue, and the vitreous body of the eye (K. Nightingale, McAleavey, and Trahey 2003; Palmeri et al. 2008; Negron et al. 2002; Fatemi, Manduca, and Greenleaf 2003). In a more recent development to assess viscoelastic properties of blood, ultrasound ARF is coupled with echo time delay estimation of red blood cell displacement in a technique called sonorheometry (Viola et al. 2004; Mauldin et al. 2010; Viola et al. 2010). Other technologies that employ ultrasound in their approach to detect material properties of blood include supersonic shear imaging (Bercoff, Tanter, and Fink 2004).

Here I describe the development of an optical ARF-based method of strain application to blood plasma clots that exploits high resolution particle tracking to assess stiffness. Sonorheometry, by contrast, depends on time analysis of ultrasound pulse echos from a displaced volume to determine stiffness. Due to the unknown parameter of speed of sound in blood samples whose hematocrit varies, the sonorheometry approach can only generate a relative stiffness estimate. Using optical particle tracking, I can calibrate the force acting on acoustically reflective objects and therefore generate estimates of mechanical parameters in absolute terms.

To implement this concept, I developed an approach in which acoustically reflective microbeads were embedded in the clot to act as force transducers and strain gauges (**Fig. 2-1a**). Ultrasound ARF was then used to induce bead displacement within a plasma sample that was then tracked by video microscopy to evaluate clot stiffness (**Fig. 2-1b**). The focal point of the ultrasound transducer corresponded to a microliter-sized region of a blood clot that was positioned away from container walls so that it acted on a relatively small numbers of platelet clusters within the 3D clot matrix. ARF was controlled to generate rapid and highly transient (subsecond) mechanical strains of a few 10s of microns to quantify local plasma clot stiffness. Because the method perturbed a small clot region and applied small strains, it measured blood clot stiffness at an intermediate length scale between the milliliter volumes of conventional rheometric approaches and single molecule and cell approaches such as optical tweezers or atomic force microscopy (AFM). ARF-based assessment of clot stiffness may therefore be useful for investigating the cooperative role of platelet signaling and fibrin dynamics in the elastic transformation of a blood clot.

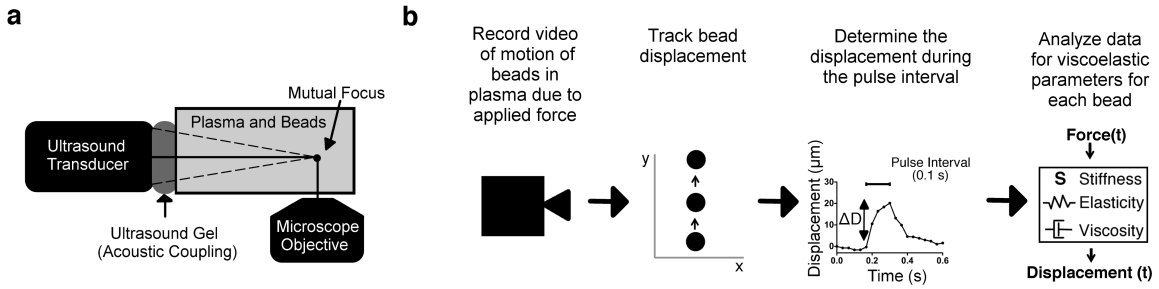

Figure 2-1 | Acoustic radiation force (ARF) based clot stiffness measurement. (**a**) The ARF based measurement setup used a 10 MHz ultrasound transducer to apply ARF to blood plasma in which beads were suspended. A microscope with 10 X objective and video camera had a mutual focus with the ultrasound transducer so application of ARF to the sample was imaged. (**b**) To assess blood plasma stiffness: 1) Video microscopy of the blood plasma sample was collected during application of ARF, 2) The bead motion due to applied ARF was tracked by an ImageJ program, 3) Displacements during the ARF pulse interval were determined, and 4) The displacement data was analyzed for the sample's viscoelastic parameters.

METHODS

The Ethics statement and Blood clotting experiments sections are included in Chapters 2-4. Optical ARF Clot Stiffness Assessment: Experimental Setup and Bead tracking and processing of displacement data sections are included in Chapters 2 and 4. This repetition allows for each chapter to stand alone.

Ethics statement

All participants provided written signed informed consent after explanation of study procedures. Experiments and study protocol as described in IRB-HSR # 12600 were approved by the Institutional Review Board for Health Sciences Research of the University of Virginia.

Experimental setup

The experimental setup (**Fig. 2-1a**) consisted of a platform, which positioned the ultrasound transducer relative to the microscope objective at the transducer focal distance. The sample was held in place over the objective and acoustically coupled to the transducer with ultrasound gel (Aquasonic, Parker Laboratories, Fairfield, NJ, USA). The sample container was slightly larger than the transducer diameter in order to minimize beam interference with the container walls. A 2.54 cm square polystyrene box (8.2 mL) (Ted Pella, Redding CA, USA) was used to hold the fluid or plasma sample. An acoustically absorbent V-shaped polydimethylsiloxane (PDMS) form (**Fig. 2-2**) was inserted into the box to minimize acoustic reflections and reduce the required sample volume to 2 mL. A 10 MHz single-element focused transducer (model IBMF103, NDT Systems, Huntington Beach, CA, USA) was coupled to the sample holder with ultrasound gel. The 10 MHz transducer had a diameter of 9.5 mm and a focal length of 19 mm. The transducer and sample holder were held in place by a custom stage mounted on an air table. The sample holder was mounted above a microscope (Diaphot 300, Nikon, Melville, NY, USA) with a 10 X microscope air objective, which permitted focusing into the sample at varying depths. For optimal foci alignment of the ultrasound beam with the objective plane of focus, the optical focal plane was fixed at 1300 μm above the sample holder surface for all stiffness measurements. The effect of different optical focal depths on bead displacement was investigated (**Fig. 2-3**). The motion of beads dispersed within the sample was acquired at 30 fps by a video camera (Canon Vixia HF S21,

Canon, Melville, NY, USA) mounted to the microscope camera port. As beads experiencing ARF move more slowly than material shear waves due to their size relative to fundamental material components (e. g. molecules, fibers), standard frame rate (30 fps) video microscopy can be used to assess bead trajectories with a high degree of precision.

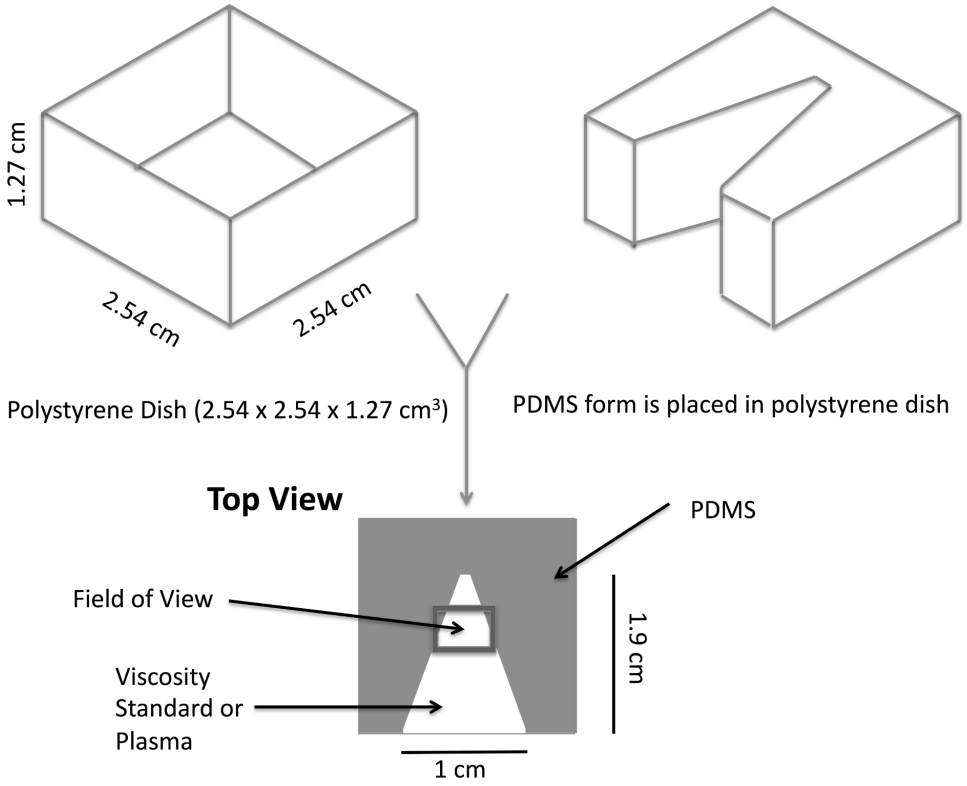

Figure 2-2 | The sample holder. The field of view for the 10 x objective is 2000 μm x 1200 μm. The shape of the polydimethylsiloxane (PDMS) mold works to reduce volume requirements for the blood sample, while the PDMS material properties allow it to act as an ultrasonic absorber reducing container reflections.

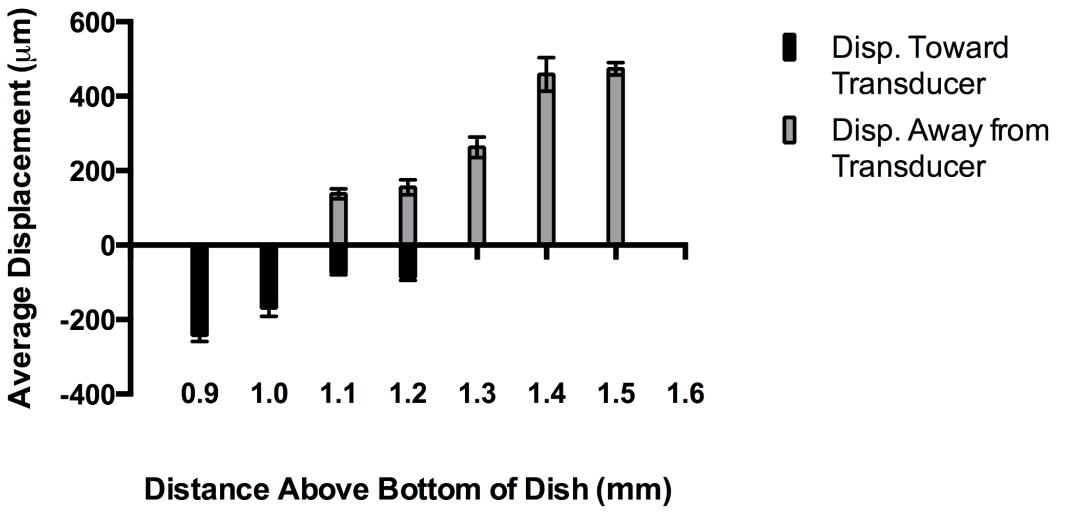

Figure 2-3 | Bead displacement in optical focal planes. To find the focal plane at the center of the ultrasound beam the bead displacement during ultrasound pulsing was measured at multiple focal planes within the sample. The plane at which measurements were made in the sample was chosen at 1.3 mm above the bottom of the sample holder. At 1.3 mm backflow, bead displacement opposite to the direction of ultrasound beam application, likely due to convection, was not present.

An acoustic beamforming model

The ultrasound beam intensity and pressure profiles were modeled using Field II (http://field-ii.dk/), a well characterized ultrasound simulation tool (Jensen and Svendsen 1992). The example code provided by the designer for producing intensity and pressure profiles, calc_int.m, was modified for the specific transducer specifications and settings used in this study: transducer center frequency (10 MHz), transducer radius (9.525 mm), focal length (19.05 mm), cycles per pulse (8), pulse repetition frequency (7.5 kHz), number of elements (1). The transducer aperture was modeled using the function xdc_concave. The intensity was set to 202 W/m^2 in order to match the peak pressure 2.5MPa to that

which was measured with the hydrophone. The program then generated simulated beam intensity and pressure profiles.

Bead tracking and processing of displacement data

Two methods of single particle tracking implemented in the image processing software ImageJ (NIH, Bethesda, MD, USA) were used to quantify bead displacement due to incident ARF: a manual particle tracking protocol and an automated tracking algorithm (Schneider, Rasband, and Eliceiri 2012). Manual tracking was used when bead velocities were greater than 400 μm/s and the automated algorithm was used in all other cases. At high velocities manual tracking was more effective due to edge detection limitations in the automated tracking algorithm. The automated tracking algorithm utilized a cross-correlation technique to measure sub-pixel and sub-micron displacements (Cheezum, Walker, and Guilford 2001).

Manual tracking was performed using the point tool in ImageJ with the "auto-measure" and "auto-next slice" features turned on. Determination of the elastic and viscous parameters of the Kelvin-Voigt viscoelastic model from position data was performed using curve fitting with the built-in function lsqcurvefit in the computational software Matlab® (Natick, MA, USA) where the lower and upper bounds for viscosity (μ) and elasticity (k) were set to 0.1 and 10 $pN \cdot s \cdot \mu m^{-1}$ and 0.1 and 10,000 $pN \cdot \mu m^{-1}$, respectively.

Because beads like those used in optical ARF move much more slowly than material shear waves due to bead size relative to fundamental material components (e. g. molecules, fibers), standard frame rate (30 fps) video microscopy can be used to assess ARF induced bead motion.

Force calibration experiments

For determining stiffness and for modeling viscoelasticity, the magnitude of force applied must be known. The ARF was estimated by tracking beads and analyzing their trajectories and terminal velocities in known viscosity fluids. Stokes' law was applied to determine the force on an object moving through a fluid of known viscosity. Three fluids with known viscosities were used, two NIST traceable viscosity standards (S3 and S6) (Cole Parmer, Court Vernon Hills, IL, USA) and blood plasma to calibrate ARF on the bead.

To estimate force, 15 μm diameter latex polystyrene beads were suspended in the fluid samples Polybead, Polysciences, Warrington, PA, USA). The S3 and S6 fluids have precisely known viscosities of 4.063 cP and 8.743 cP, respectively, at 25° C. At room temperature blood plasma has a viscosity of 1.6 ± 0.1 cP (Shinton 2010).

The sample holder was filled with a viscosity standard in which beads were suspended. The 10 MHz transducer used to generate ARF was triggered in all experiments (except where noted) by a custom amplifier circuit connected to a Macbook 2,1 laptop computer (Apple, Cupertino, CA) running a Matlab®/C++ program that controlled the ultrasound transducer firing pattern. A 0.8 μs pulse length (8 wave cycles) was applied (**Fig. 2-4**). I define the rate of pulse generation used to create an impulse sequence by a pulse repetition frequency (PRF). Pulses were generated at a PRF of 7.5 kHz over a pulse train interval of 0.5 s. Pulse train intervals were separated by 6 s of rest. In place of the custom amplifier circuit, a waveform generator and power amplifier were substituted to increase dynamic range in selected experiments.

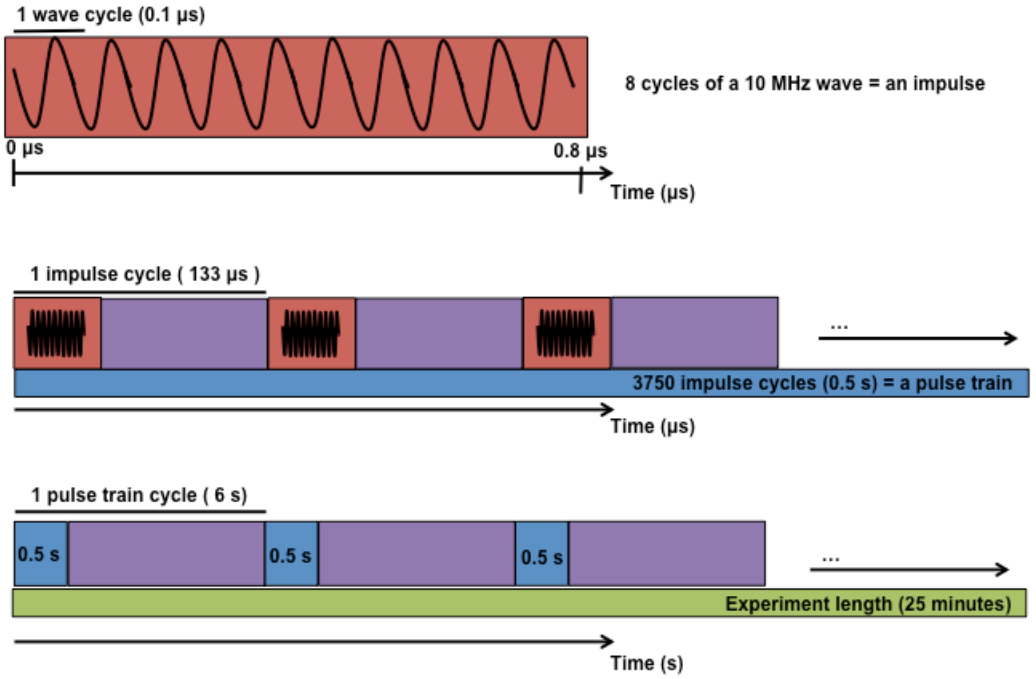

Figure 2-4 | Ultrasound pulsing sequence. 8 wave cycles, an impulse ( ) , were applied. The impulses were applied once every 133 µs in pulse trains ( ) of 3750 impulses lasting 0.5 s. Pulse trains were applied once every 5 seconds for the duration of the experiment ( ).

To investigate the effect of changing the PRF on bead displacement the PRF was varied in the viscosity standards. PRFs of 15, 7.5, 3.75, and 1.875 kHz were used at a time interval of 0.5 s. The result was a total of 7500, 3750, 1875, and 937 pulses fired per burst for each respective condition.

Measurement and analysis of ultrasound attenuation in viscosity standards and in agarose gels

A 10 MHz ultrasound transducer for transmitting ultrasound signals and a signal receiver, either a bullet hydrophone (Onda Corporation, Sunnyvale, CA) or 10

MHz ultrasound transducer, were immersed in a degassed water bath. A two-axis micron precision stepper motor controlled the relative positions of the transmit transducer and the signal receiver (hydrophone or receive transducer). For measurement of ultrasound attenuation in the viscosity standards and in agarose, sample holders with varying acoustic path lengths were built (**Fig. 2-5**). An arbitrary waveform generator AFG 3022B (Tektronix, Beaverton, OR, USA) and 55dB amplifier ENI A-150 (E & I, Rochester, NY, USA) was used to drive the transducer. A Lecroy 334A oscilloscope (Lecroy, Chestnut Ridge, NY, USA) collected waveforms from each transducer or hydrophone that were transferred by general purpose interface bus (GPIB) to computer for analysis. The attenuation was determined by comparing ultrasound signal amplitudes at different path lengths of viscosity standard (**Fig. 2-6**) and using analysis techniques described in a later section.

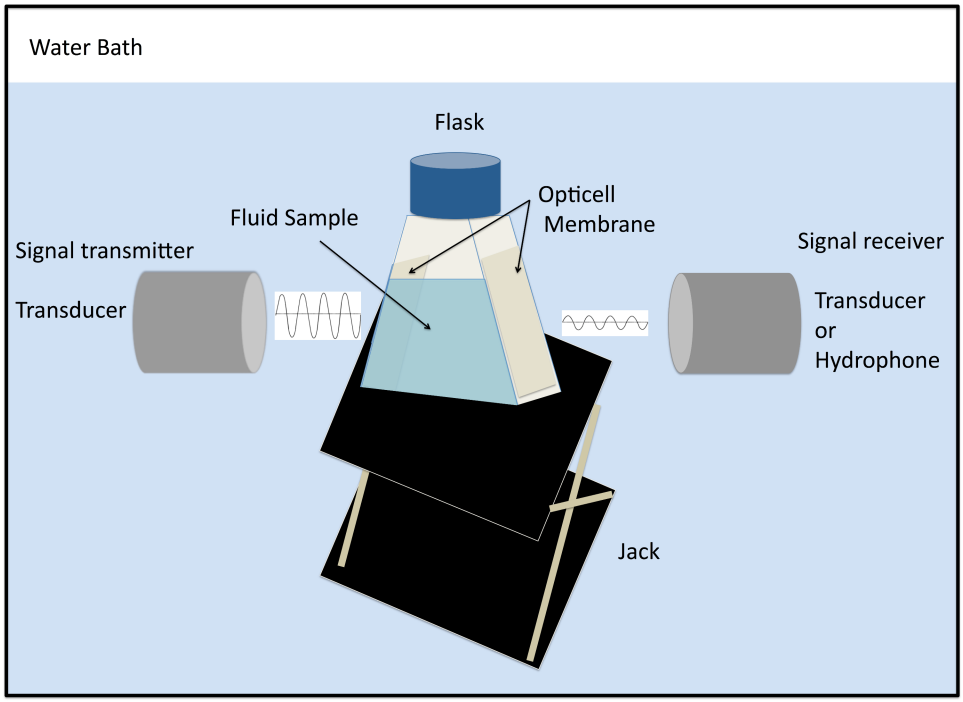

Figure 2-5 | Schematic of setup for attenuation measurement in fluids. In a water bath, a signal transmitting transducer was fired into the fluid sample at 3 path lengths of fluid. The signal receiver recorded the resulting waveform. For agarose gel samples, slabs of gel were placed between the transmitter and receiver in the place of the flask, with 3 thicknesses. The change in amplitude of the waveform between the path lengths of fluid or gel were used to calculate the attenuation of each material.

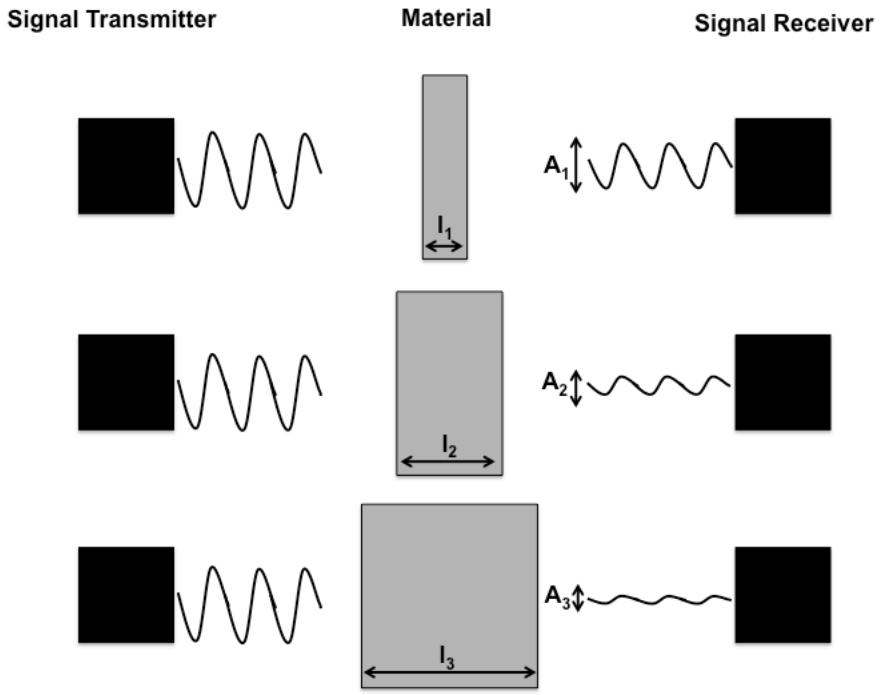

Figure 2-6 | Attenuation conceptual schematic. The attenuation of a material can be ascertained by measurement of signal amplitude after the signal has been transmitted through several path lengths of the material. With increasing path length ($l_1 < l_2 < l_3$) the amplitude of the received signal decreases ($A_1 > A_2 > A_3$).

The total path length between the transmit and receive transducer or hydrophone was determined by the measurement of the time delay between the pulse transmission and the pulse receipt with the speed of sound in water (1497 m/s) (Del Grosso and Mader 1972). Change in signal voltage due to signal path length within the material was determined by the average absolute value of the waveform. A trend of reduced signal voltage with material thickness was measured. The voltage attenuation data was used to form a system of equations specific for each thickness of material and solved for the attenuation coefficient of

the material using the Matlab® function lsqnonlin. The attenuation of water was 0.0022 $dB \cdot cm^{-1} \cdot MHz^{-1}$ (Culjat et al. 2010).

Agarose gel formation

Agarose gel was made with UltraPure™ Agarose (Life Technologies, Grand Island, NY, USA). The agarose was added to tris-acetate-ethylene-diamine-tetra-acetic acid (TAE) buffer in proportions to generate a 0.5 wt % gel in an Erlenmeyer flask. The solution was heated for 30 s in the microwave and then poured into either a 2.54 cm or 10 cm square polystyrene box to a volume appropriate for the thickness of gel desired (8.2 mL or 500 mL, respectively). Agarose was allowed to cool for 1 h before removal from the mold and measurement of attenuation.

Agarose gel and blood plasma bead displacement measurement

The agarose gel was made as described above with the exception that 10 µL of 5 µm carboxylated YG fluorescent beads ($2x10^6$)(Fluoresbrite, Polysciences, Warrington, PA, USA) were added. Similarly PRP was doped with 10 µL of 5 µm carboxylated YG fluorescent beads before initiating clotting. Both agarose and plasma gelled in molds for 1 h to maximize stability and permit transfer to a gel holder mounted in a water bath on the stage of the microscope. In this way acoustic attenuation was minimized to increase force transmittal and permit analysis of the much stiffer agarose gel. A ziplock bag was used to enclose each

sample in its appropriate buffer (TAE in the case of agarose or Dulbecco's phosphate buffered saline (DPBS) in the case of plasma). The sample was then aligned at the mutual focus of the 10 MHz transducer and a 40 X water immersion microscope objective. The fluorescent beads allowed imaging in a turbid gel. For generation of ARF the transducer was driven by an arbitrary waveform generator AFG 3022B (Tektronix, Beaverton, OR, USA) and 55dB amplifier ENI A-150 (E & I, Rochester, NY, USA).

Bead sedimentation velocity measurement

Bead sedimentation velocity was determined experimentally in citrated platelet rich plasma (PRP) by measuring bead time of flight over the thickness of a gasket in a flow chamber. The gasket thickness allowed for precise measurement of distance travelled due to gravity from one surface to the other.

Blood clotting experiments

Blood was collected from two healthy volunteers using the protocol described in IRB-HSR # 12600 in 2.7 mL citrated 3.2% Vacutainer® tubes (BD, Franklin Lakes, NJ, USA). Venipuncture drawn by syringe resulted in more variable levels of platelet activation, hence the use of Vacutainers® for sample acquisition. The blood was centrifuged at 100 x g for 20 min to separate phases of PRP, buffy coat, and red blood cells. To obtain PRP, the supernatant of the centrifuged samples was collected by pipette. An additional centrifugation step of 2000 x g

for 40 min was used to obtain platelet poor plasma (PPP). Samples consisted of 2 mL of fluid volume mixed with 0.5 x 10^6 / mL of 15 μm diameter latex polystyrene beads (Polybead, Polysciences, Warrington, PA, USA). Plasma samples were pipetted into the experimental sample chamber. To initiate clotting, samples were recalcified with $CaCl_2$ (Sigma, St. Louis, MO, USA) to bring the PRP to a concentration of 9.525 mM $CaCl_2$. Kaolin (JT Baker, VWR, Radnor, PA, USA) was added to a final concentration of 5 μg/mL, except where otherwise noted. Clotting and the ARF pulsing sequence were initiated within 15 s of kaolin addition. Particle motion within the sample was recorded for 30 s intervals every 3 min throughout the initial 30 min of clotting for each sample.

RESULTS

Spatial distribution of acoustic radiation force

A focused ultrasound beam was aimed into a 2 mL sample volume container coupled acoustically via ultrasound gel (**Fig. 2-1a**). In order to determine the focal point and shape of the beam, the pressure field was simulated in FIELD II (**Fig. 2-7a**) (Jensen and Svendsen 1992). Pressure was directly measured by hydrophone in a region spanning the analytically determined ultrasound focus (**Fig. 2-7b**). A 2-D heat map defined the region of maximum pressure and the -6 dB beam boundaries (delineated by the dotted line). The -6 dB lateral beam width was 400 μm, which could be entirely observed within the 10 X microscope field of view (**Fig. 2-7b**). The -6 dB axial beam length was 5 mm, resulting in a

shallow pressure gradient relative to the optical field of view (2 mm in the axial direction), which allowed us to assume that the beads were in a relatively constant pressure field in the direction of wave propagation. Assumption of constant pressure field is supported by velocity data with viscosity standards, where terminal velocities (constant velocities for multiple tenths of a second during the pulse) are reached (**Fig. 2-8a**).

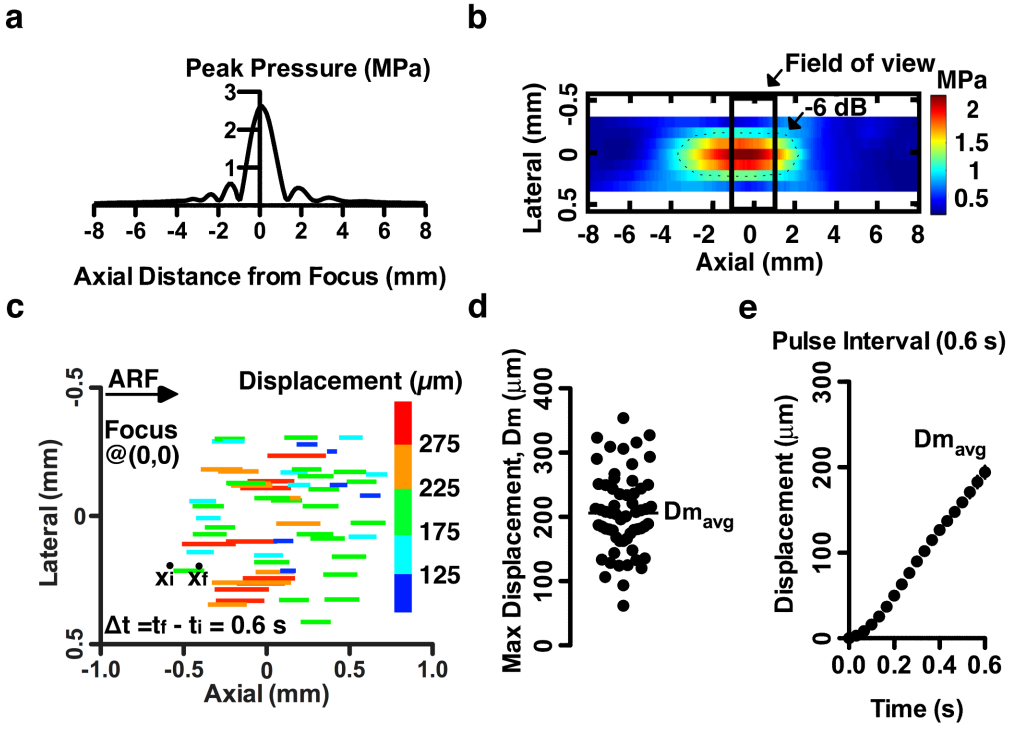

Figure 2-7 | Ultrasound transducer pressure field and bead displacement in a viscous fluid. (**a**) The pressure field of the 10 MHz focused ultrasound transducer at the focal length (19 mm) was simulated in Field II software. (**b**) Hydrophone measurements of the acoustic pressure produced by the ultrasound transducer were used to determine the -6 dB lateral beam width (400 μm) and the -6 dB axial beam length (5 mm) at the focus. The microscope field of view is shown. In **b** & **c**, the y-axis is expanded in the interest of clarity. (**c - e**) The microscope field of view was positioned on the beam focus by centering over the largest bead displacements. The ARF induced displacement of 15 μm beads was analyzed in the S6 viscosity standard (8.743 cP). Bead displacement was measured during the 0.6 s ARF pulse interval, $\Delta t = t_f - t_i$ where maximum displacement D_m was determined at t_f.

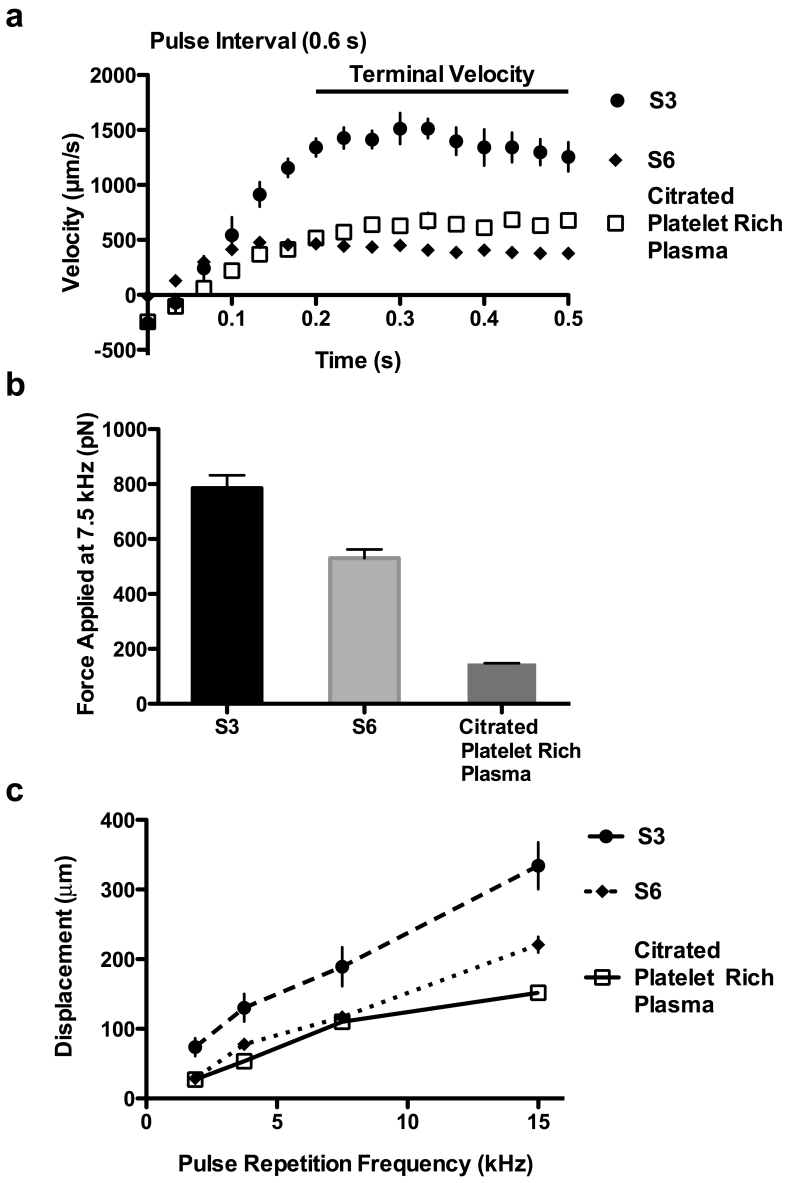

Figure 2-8 | The effects of attenuation and pulse repetition frequency (PRF) on bead velocities and force magnitude. (**a**) Bead terminal velocities under applied ARF at 7.5 kHz PRF in the viscosity standards S6 (8.743 cP) and S3 (4.063 cP), and in citrated platelet rich plasma were measured. Standard error is shown with n=10 beads. (**b**) Applied ARF magnitude at 7.5 kHz was determined using Stokes' law and terminal bead velocities. Distinct acoustic attenuations between the fluids account for much of the difference in the applied force in the fluids. At 7.5 kHz the force applied in citrated blood plasma was estimated to be 147 pN. Standard error is shown with n=10 beads. (**c**) Bead displacement after 0.3 s of pulsing due to applied ARF increased linearly with increasing PRF in the three fluids. Standard error is shown with n=9 beads.

Region of bead displacement

The bead displacements during application of a 7.5 kHz ARF impulse were tracked by video microscopy (**Fig. 2-1b**). Bead displacements were measured by recording trajectories in a S6 viscosity standard (8.743 cP at room temperature). Maximum bead displacement (D_m) induced by an ARF impulse relative to position in the pressure field is shown in **Fig. 2-7c**. Since the ultrasound beam has an approximately Gaussian power distribution with respect to its axis, we anticipated that there would be a gradient in the bead displacements across the microscope's 10 X objective field of view. As expected bead displacements were largest at the center of the transducer focus and smallest near the edges (**Fig. 2-7c**). The average of the maximum bead displacement due to application of an ARF impulse (Dm_{avg}) was 206.2 +/- 62.6 μm (n = 60). The distribution of D_m across the field of view (1 x 2 mm) was approximately Gaussian (**Fig. 2-7d**). Average bead displacement during the pulse approached a terminal velocity within 0.1 s of pulse initiation (**Fig. 2-7e)**.

Bead sedimentation

To control for bead sedimentation effects in clotting plasma prior to reaching the gel-point, I measured bead sedimentation velocity in citrated plasma. Bead sedimentation velocity was determined experimentally in anti-coagulated platelet rich plasma (PRP) by measuring settling time. The 15 μm polystyrene beads

settled at an average velocity of 3.84 +/- 0.15 μm/s (n = 250). The distance a bead fell during a 0.5 s pulse train was approximately 1.92 μm. The bead sedimentation distance constituted a 0.5% change in bead position within the -6 dB lateral beam depth (400 μm). Because bead sedimentation was small relative to the beam diameter, and sedimentation would be abolished once the clot was past the gel-point, it was assumed to negligibly influence observed bead trajectories.

Magnitude of force application

The magnitude of ARF applied to beads in clotting blood plasma was estimated by measuring displacements in citrated PRP and correlating motion to force using Stokes' law (**Eq. 1**). Bead motion in citrate anticoagulated PRP was compared to that in viscous standards. Terminal bead velocities during ARF application were measured (**Fig. 2-8a)** and Stokes' law for drag force was used to calculate the force applied to the beads (**Fig. 2-8b**) (Dayton, Allen, and Ferrara 2002). Stokes' law is:

$$F = 6\,\pi\,\mu\,Rv \quad , \qquad (1)$$

where F is the force applied to the beads, μ is the fluid viscosity, R is the bead radius, and v is the bead terminal velocity (Deen 1998). The bead terminal

velocities in the viscosity standards S6 (8.743 cP at room temperature) and S3 (4.063 cP at room temperature) and citrated PRP (1.6 cP at room temperature) (Shinton 2010) were 429.4 +/- 57.2 μm/s, 1367.4 +/- 256.4 μm/s, and 646.5 +/- 120.4 μm/s respectively. From Stokes' law (**Eq. 1**) it was determined that the force magnitude applied at 7.5 kHz pulse repetition frequency on the beads in S6, S3, and citrated PRP was 530.7 +/- 70.7 pN, 785.4 +/- 147.3 pN, and 147.0 +/- 27.2 pN respectively (**Fig. 2-8b**). The differences in the applied force on the beads may reflect differences in the degree of ultrasound attenuation between the three fluids, so attenuation of the viscosity standards was measured.

The relationship between attenuation and force magnitude

All materials attenuate acoustic waves (Torr 1984). The attenuation in S6 and S3 viscosity standards and in the agarose elastic standard was measured to determine the influence of attenuation on force experienced by the beads. Acoustic signal amplitudes in the viscous and elastic standards were measured to determine attenuation and force applied to the beads for each material.

The attenuation coefficient of a material is described by the equation

$$\frac{V_f}{V_i} = 10^{-\alpha l f/10}, \qquad (2)$$

where V_i is the voltage of the signal before entering the material, V_f is the voltage of the signal after traveling a distance (*l*) through the material, *f* is the frequency of the signal, and α is the attenuation coefficient. The transducer frequency (*f*) was 10 MHz and the acoustic path length (*l*) in the sample was 1.9 cm.

Change in signal voltage due to signal path length and material attenuation was determined by the average absolute value of the waveform. In all samples signal voltage decreased linearly with thickness. With the voltage attenuation data, a version of **Eq. 2** specific for each thickness of material was established. The system of equations was solved for the attenuation coefficient of the material using the Matlab® function lsqnonlin. The attenuation of water was set to a previously reported value (0.0022 $dB \cdot cm^{-1} \cdot MHz^{-1}$) (Culjat et al. 2010). The attenuation coefficient of 0.5% agarose was found to be 0.0109 $dB \cdot cm^{-1} \cdot MHz^{-1}$. The attenuation coefficients of the S3 and S6 viscosity standards were determined to be 0.0764 $dB \cdot cm^{-1} \cdot MHz^{-1}$ and 0.1056 $dB \cdot cm^{-1} \cdot MHz^{-1}$, respectively.

Eq. 2, which describes attenuation of ultrasound signal voltage, can be extended to reflect a proportional change in applied force with the change in voltage across a signal path length within the material, such that

$$\frac{F_f}{F_i} = \frac{V_f}{V_i} = 10^{-\alpha l f/10}, \quad (3)$$

where α is the material attenuation, F_i is the ideal (non-attenuated) force delivered by the transducer, F_f is the force calculated on beads in the material from Stokes' law (**Eq. 1**) (Leighton 2007), V_i is the voltage of the signal before entering the material, V_f is the voltage of the signal after traveling a distance (*l*) through the material, and *f* is the transducer frequency. The lower ultrasound attenuation of S3 compared to S6 was consistent with the greater force experienced by beads in the S3 fluid than in the S6 fluid.

To determine the expected force differential between two materials a ratio of **Eqn. 3** can be made. When the settings of applied ultrasound are the same for each material such that the F_i in each material are equal

$$\frac{\frac{F_{material\,1}}{F_i}}{\frac{F_{material\,2}}{F_i}} = \frac{F_{material\,1}}{F_{material\,2}} = 10^{-\alpha_1 l f/10}/10^{-\alpha_2 l f/10}, \quad (4)$$

where $F_{material\ 1}$ is the force on beads in a material, $F_{material\ 2}$ is the force on beads in a second material, α_1 and α_2 are the attenuation coefficients for the respective materials, *f is* the transducer frequency and *l* is the acoustic path length.

The expected force differential between S6 and S3 viscosity standards was determined from the attenuation coefficients measured previously using **Eqn. 4** such that

$$\frac{F_{S6}}{F_{S3}} = \frac{10^{-\frac{\alpha_{S6} lf}{10}}}{10^{-\frac{\alpha_{S3} lf}{10}}} = \frac{0.630}{0.715} = 0.881 \quad . \quad (5)$$

The statistically bounded range of the F_{S6} to F_{S3} ratio using bead displacement analysis by Stokes' law was

$$\frac{F_{S6}}{F_{S3}} = \frac{530.7 \pm 70.7\ pN}{785.4 \pm 147.3\ pN} = 0.493 – 0.942 \quad . \quad (6)$$

Since the ratio predicted by the fluid attenuations was within the Stokes analysis range (**Eqn. 6**), the agreement of the force and attenuation measurements suggested that fluid attenuation accounted for the difference in force (F_f) experienced by the beads in their respective fluids.

The lower force experienced by beads in citrated PRP relative to S3 or S6 standards predicts that blood plasma has a greater attenuation than S3 and S6 viscous standards, or even a 0.5% agarose gel. Previously reported attenuation

coefficients (α) for unclotted and clotted blood plasma are 0.104 $dB \cdot cm^{-1} \cdot MHz^{-1}$ and 0.126 $dB \cdot cm^{-1} \cdot MHz^{-1}$ respectively (Calor-Filho and Machado 2006). The expected force differential between clotted and unclotted plasma was determined from the attenuation coefficients measured previously using **Eqn. 4** such that

$$\frac{F_{clotted}}{F_{unclotted}} = \frac{10^{-\frac{\alpha_{clotted} lf}{10}}}{10^{-\frac{\alpha_{unclotted} lf}{10}}} = \frac{0.575}{0.634} = 0.907 \quad . \qquad (7)$$

As the relative difference between the estimated force acting on a bead in clotted and unclotted plasma differs by less than 10% based on the relationship between force and attenuation described in **Eqn. 4**, I chose to use the average of the two coefficients for all plasma conditions. Therefore, given the assumption of constant attenuation coefficient 0.115 $dB \cdot cm^{-1} \cdot MHz^{-1}$, a constant force of 147 pN at 7.5 kHz PRF was assumed for all blood plasma material property measurements with the optical ARF technique.

The relationship between pulse repetition frequency (PRF) and force magnitude

Based on previous ARF theory (Mauldin et al. 2010), I hypothesized that varying the PRF (the number of ultrasound impulses applied within one second) would adjust the force applied to the beads and lead to a corresponding modulation of

bead displacements. To test our hypothesis the PRF was varied in the S3 and S6 viscosity standards and in citrated PRP (**Fig. 2-8c**). Material stiffness was correlated with PRF and bead displacement by the equation

$$D_m \propto \frac{\mathrm{PRF}}{S}, \qquad (8)$$

where D_m was the maximum displacement of the bead after the ARF impulse, S was material stiffness, and PRF was the pulse repetition frequency of the material (Viola et al. 2004). Reducing the PRF resulted in a linear reduction in the bead displacements, consistent with theory (**Eq. 8**).

Viscoelastic measurement of platelet poor plasma (PPP) clotting

Fibrin contributions to stiffness were assessed by removing platelets from plasma through centrifugation to generate PPP. Bead displacement due to ARF pulsing decreased over the course of 17 min (**Fig. 2-9a,b,c**). Signs of increasing elasticity developed early after clot initiation; within 1 min of kaolin activation beads recoiled after removal of an ARF impulse (**Fig. 2-9a**). Based on bead velocities, the PPP sample at 1 min had a Re ~ 0.07 (Deen 1998), suggesting that the sample was experiencing significant viscous damping of the developing elastic response, characteristics of a viscoelastic fluid. At later time points, the Reynolds number reduced further (Re < 0.002) as the viscosity increased and

the velocity of the beads was reduced (**Fig. 2-9b,c**). At 15 (**Fig. 2-9b**) and 18 (**Fig. 2-9c**) min the beads reached a plateau of maximum displacement during the ARF impulse, recoiling 100% after force application stopped, indicative of a high degree of material elasticity.

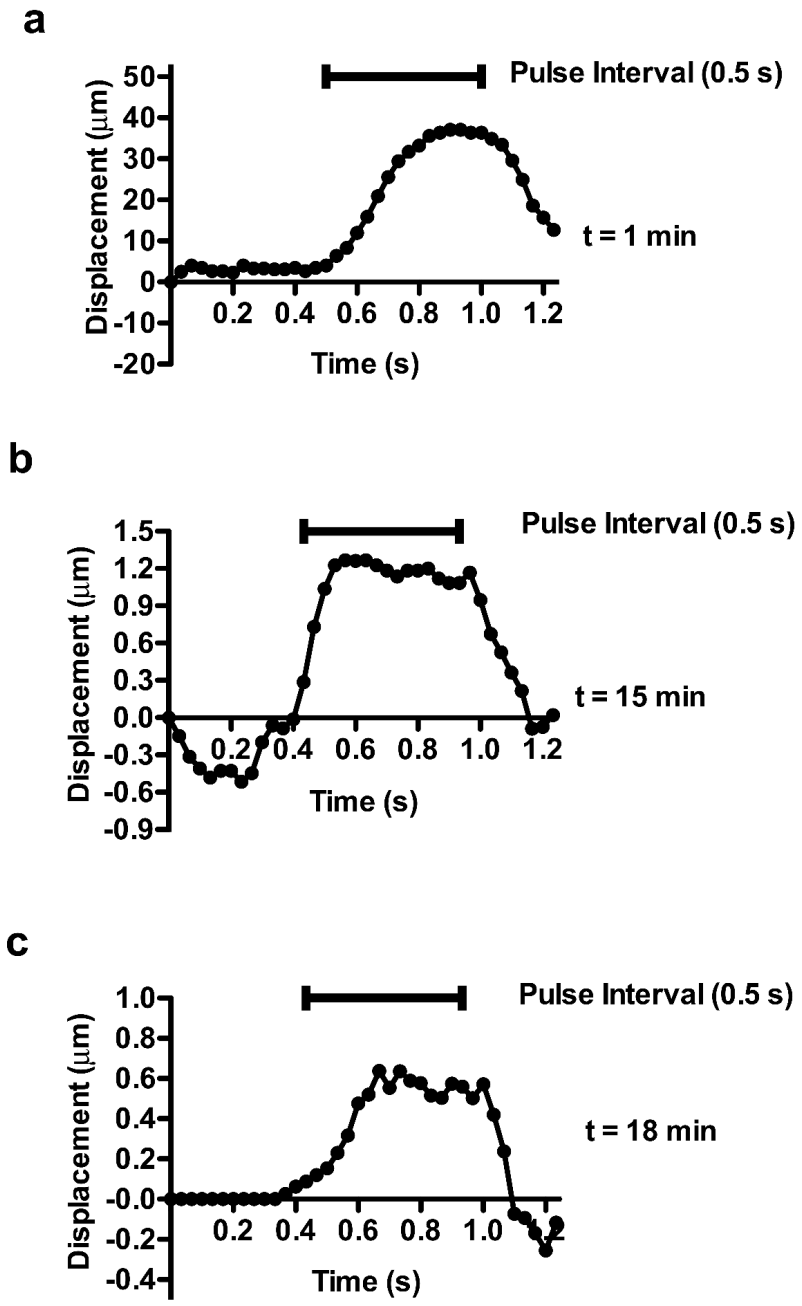

Figure 2-9 | Characteristic bead displacement due to applied ARF at 7.5 kHz in clotting platelet poor plasma. (**a**) At t = 1 min the bead displaced 40 μm during a 0.5 s pulse interval and recoiled after the pulse stopped. (**b**) At t = 15 min the bead displaced 0.9 μm during the pulse interval and recoiled after the pulse stopped. (**c**) At t = 18 min the bead displaced 0.5 μm during the pulse interval and recoiled after the pulse stopped. Optical noise was reduced by smoothing with a 3 data point moving average filter.

Viscoelastic model fitting of platelet poor plasma

Clot stiffness in PPP was determined by the equation:

$$S = \frac{F_{plasma}}{D_m}, \quad (9)$$

where S is the clot stiffness, F_{plasma} is the ARF applied to beads in plasma, and D_m is the average of bead maximum displacements after application of 0.5 s of an ARF pulse (**Fig. 2-10a**). As a form of Hooke's law, the inverse relationship between applied force and resultant displacement defines stiffness (S) (**Eq. 9**) (Hooke 1678). Acoustic radiation force has been used in defining material stiffness in previous work (Mauldin et al. 2010). The clot appeared to have near constant stiffness from 0 - 9 min and then stiffness increased 78-fold between 9 and 18 min. In order to quantify the changes in viscous and elastic components of the plasma during clotting the displacement data was fitted with the Kelvin-Voigt model.

The Kelvin-Voigt model consists of a spring and a dashpot in parallel (**Fig. 2-10b**). The spring constant, viscous dashpot constant, and the equation that defines the system together describe the displacement of the point of interest due to a given force. To evaluate the viscoelastic properties the characteristic

equation for the Kelvin-Voigt model was fit to the displacement data during the application of a pulse train (see the Methods bead tracking section). The Kelvin-Voigt model captures the coupled effects of viscosity and material elasticity on force-induced material displacements and has been widely used in biological materials modeling (Park and Lakes 2007).

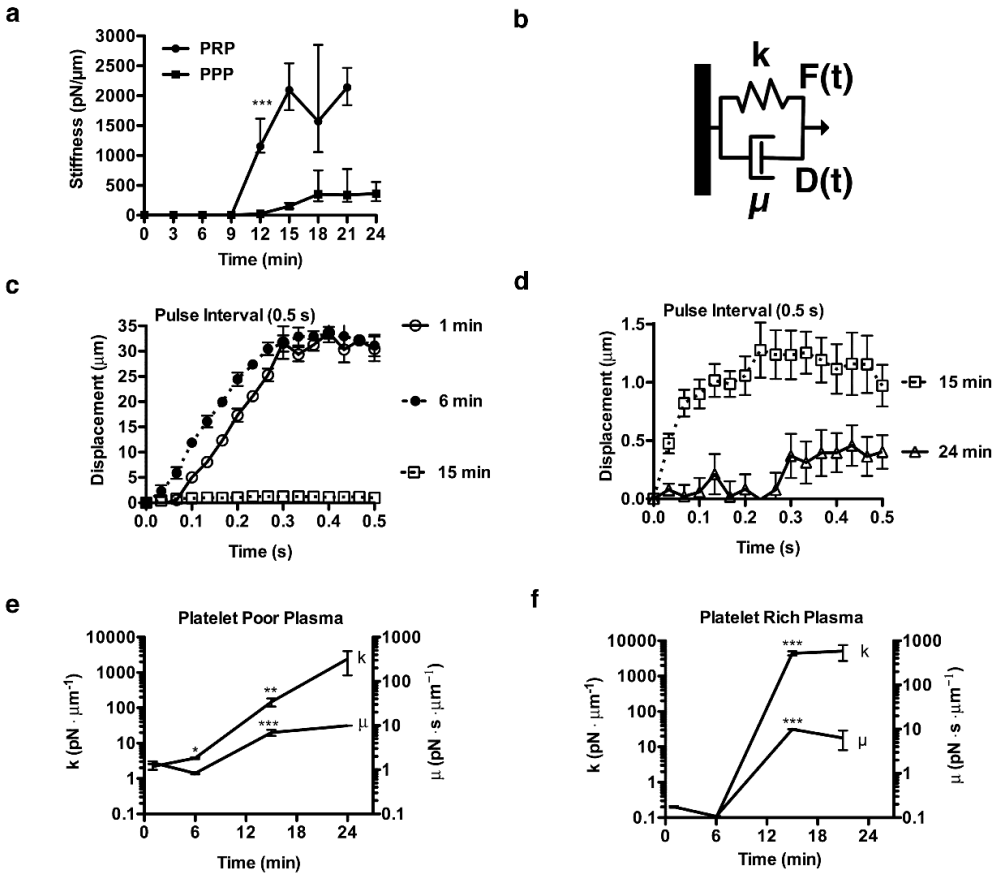

Figure 2-10 | Characteristic mechanical properties of clotting platelet rich (PRP) and platelet poor plasma (PPP) as assessed by application of ARF at 7.5 kHz. (**a**) Clot stiffness (S), $S(t) = F_{plasma}/Dm_{avg}$, of clotting PRP and PPP was determined. Bead displacements (n = 5) were averaged to compute stiffness, which is displayed with 60% quartiles (***, $p<0.0005$ between PPP and PRP from $t > 12$ min). (**b**) In the Kelvin-Voigt model, which predicts the displacement D(t) response of viscoelastic materials to applied force F(t), a viscous element (dashpot) is in parallel with an elastic element (spring). The parameters k and μ describe the elastic and viscous properties respectively. (**c-e**) The Kelvin-Voigt model was fit to bead displacement data in clotting PPP (**c**) where displacement decreased abruptly between 6 - 15 min. (**d**) From 15 - 24 min the model was fit to bead displacement data and displacement continued to decrease. At all time points, in contrast to measurements in the viscous fluids, the displacement approached a maximum. Standard error is shown with n=5 beads per time point. (**e-f)** Kelvin-Voigt viscous (μ) and elastic (k) parameters of PPP and PRP were determined. Standard error is shown with n=5 beads per time point (* ,$p<0.05$)(**, $p<0.006$)(***,$p<0.0005$). (**e**) During clotting in the PPP sample the Kelvin-Voigt viscous (μ) and elastic (k) parameters increased 1107 fold and 6.9 fold respectively. (**f**) During clotting in the PRP sample the average fold difference of viscous (μ) and elastic (k) parameters of the clot as compared to PPP between 15 and 21 min were 1.3 fold and 11 fold larger, respectively.

Assumptions of the Kelvin-Voigt model include application of constant force, which is appropriate if the analysis is limited to the displacements measured during the pulse train interval. The force applied on the blood plasma sample can be considered constant during a pulse train interval because the ratio of the time constant of blood plasma viscoelastic response (~0.01 s) (K. Nightingale, Soo, Nightingale, Bentley, et al. 2002; Long et al. 2005; Viola and Walker 2003) to the pulse repetition period (~10^{-4} s/cycle) is so large. Tissue (or blood clot) movement is negligible between each impulse, and therefore during the microsecond pulse train application the force is effectively constant on the tissue. Momentum of the bead, because of low Reynolds number, is assumed negligible and therefore not accounted for in the model.

The Kelvin-Voigt model was fit to bead displacement during force application to assess the viscoelastic behavior of blood (Viola et al. 2004; Schmitt, Hadj Henni, and Cloutier 2011; Gennisson, Lerouge, and Cloutier 2006). Within a minute of PPP clot initiation spring-like behavior (displacement plateau during impulse) was evident and increased at all times measured (**Fig. 2-10c,d**). In contrast, viscous fluid-like behavior (constant velocity during impulse) was observed with bead motion in the S6 viscosity standard at all time points measured**.** The elastic parameter k of S6 fluid, as expected, was near zero (**Fig. 2-11**). Viscous (μ) and elastic (k) parameters of PPP determined by the model at 24 min were 9.999 +/-

0.001 $pN \cdot s \cdot \mu m^{-1}$ and 2430 +/- 1600 $pN \cdot \mu m^{-1}$ respectively (**Fig. 2-10e**). This is an increase in viscous and elastic parameters of 6.9 fold and 1107 fold respectively from unclotted PPP. The clot properties changed most significantly between 6 and 15 min, when elasticity (k) rapidly increased.

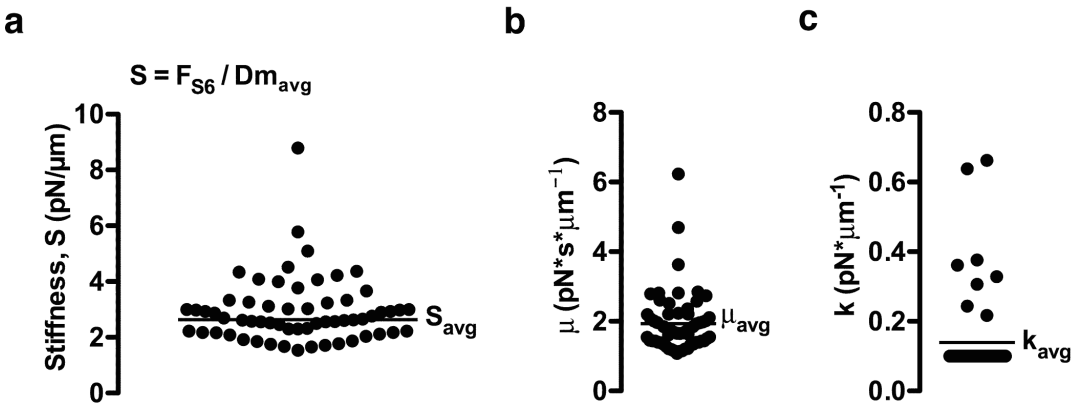

Figure 2-11 | Viscoelastic measurement of viscous fluid S6. (**a**) The stiffness (S) of the material was determined with the force applied on beads in S6 (F_{S6}) and the bead displacement during a 0.6 s pulse interval (Dm_{avg}) by the equation $S = F_{S6}/Dm_{avg}$. (**b-c**) The Kelvin-Voigt model was fit to the displacement during the pulse interval from which (**b**) viscous parameter μ and (**c**) elastic parameter k were calculated, which showed, as expected, a viscous-dominated mechanical response.

Platelet depletion and clot stiffness

Stiffness of PPP samples was compared to that of PRP to assess platelet contributions to clot stiffness (**Fig. 2-10a**). PRP increased clot stiffness 6.9 fold relative to PPP. Where significant elasticity developed, beads in both PPP and PRP recoiled after ARF induced displacement (**Fig. 2-9**), a hallmark of reversible elastic deformation. Viscous (μ) and elastic (k) parameters determined by the model at 21 min in PRP are 6.364 +/- 2.988 $pN \cdot s \cdot \mu m^{-1}$ and 5127 +/- 2440 $pN \cdot \mu m^{-1}$ respectively (**Fig. 2-10f**). To assess the clot properties of PRP after

initial hemostasis, the average fold difference of viscous (μ) and elastic (k) parameters of the clot as compared to PPP between 15 and 21 min were 1.3 fold and 11 fold larger, respectively. In PRP, elasticity and viscosity both developed most significantly between 9 and 15 min, paralleling the kinetics of viscosity and elasticity changes in clotting PPP. Video of PRP clotting is available in the supplemental section (see Supplemental Video 1).

Measuring stiffness ratio of agarose elastic standard to blood plasma

For interpretation of the measurements made by the optical ARF method relative to standard material property testing techniques, the stiffness of PRP was related to that of a 0.5 wt % agarose elastic standard. Both PRP and agarose have been measured by standard material property testing techniques such as the parallel plate rheometer. Stiffness comparison required the previously determined attenuation coefficients for plasma and agarose. The range of reported shear modulus of 0.5 wt% agarose is 1400 - 4530 Pa (Barrangou, Daubert, and Allen Foegeding 2006; Adams, Frith, and Stokes 2004; Fernández et al. 2007; Hamhaber et al. 2002). Previously reported shear moduli of PRP range from 406 - 600 Pa (Jen and McIntire 1982; Riha et al. 1999; Huang et al. 2011). The ratio of the shear moduli of 0.5 wt% agarose to PRP as previously reported ranges from 2.3 - 11.2.

The ratio of stiffness of 0.5 wt% agarose and PRP measured by our optical ARF technique was compared directly to the ratio of previously reported shear moduli in order to validate the material property measurement capabilities of the optical ARF technique (**Fig. 2-12**).

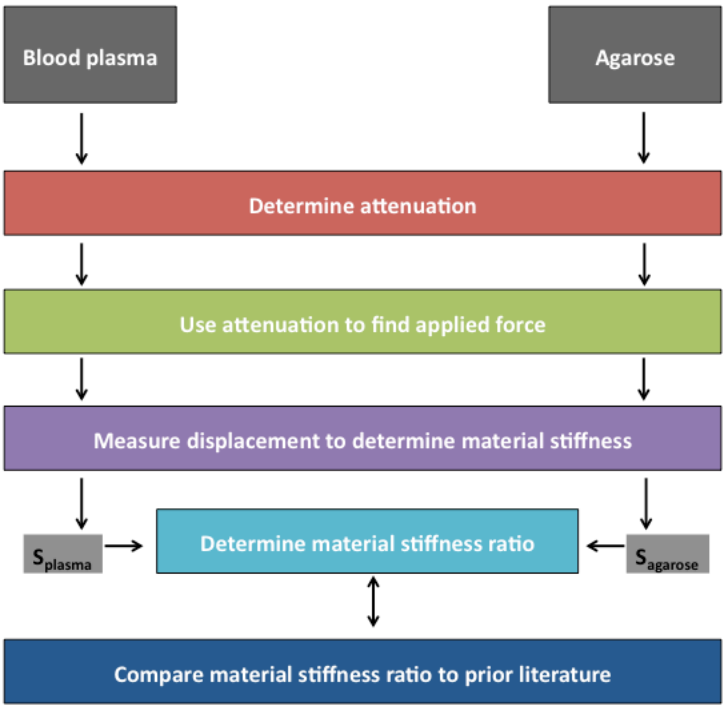

Figure 2-12 | Comparison of optical ARF based clot stiffness assessment to existing mechanical testing devices. In order to validate the material properties measurement capabilities of the optical ARF technique (1) attenuation of platelet rich plasma and 0.5 wt% agarose were determined. (2) Material attenuation was used to find the force applied for each material. (3) Displacement of each material was measured to determine stiffness. (4) The stiffness ratio of the two materials was determined. (5) The material stiffness ratio was compared to prior literature.

The expected force differential between PRP and agarose was determined from the attenuation coefficients measured previously using **Eqn. 4** such that

$$\frac{F_{plasma}}{F_{agarose}} = \frac{10^{-\frac{\alpha_{plasma}lf}{10}}}{10^{-\frac{\alpha_{agarose}lf}{10}}} = \frac{0.588}{0.953} = 0.617 \quad . \quad (10)$$

With the difference in force application between PRP and agarose determined, the displacements of beads in each material were measured. The beads in PRP were displaced 8.25 +/- 0.91 μm and those in agarose were displaced 1.369 +/- 0.13 μm. In order to compare the stiffness of the plasma to that of agarose the following equation was used

$$\frac{S_{agarose}}{S_{plasm}} = \frac{F_{agarose}}{F_{plasma}} \times \frac{d_{plasma}}{d_{agarose}} \quad , \quad (11)$$

where $S_{agarose}$ is the stiffness of agarose, S_{plasma} is the stiffness of plasma, $d_{agarose}$ is the bead displacement in agarose, and d_{plasma} is the bead displacement in plasma. Using **Eqn. 11** the 0.5 wt % agarose gel was approximately 9.8 fold more stiff than a clotted PRP sample. This was within the ratio range (2.3 - 11.2) of the shear moduli reported previously for 0.5 wt% agarose and clotted PRP in independent determinations.

Measurement technique sensitivity to strength of clotting stimulus

Clotting of PRP was stimulated over a range of kaolin concentrations to assess the sensitivity of the optical ARF based clot stiffness assessment technique to

strength of clotting stimulus (**Fig. 2-13**). The measurements showed the capability of the ARF based bead-tracking technique to detect differences in kinetics of stiffness development that occur with variation in coagulation stimulus.

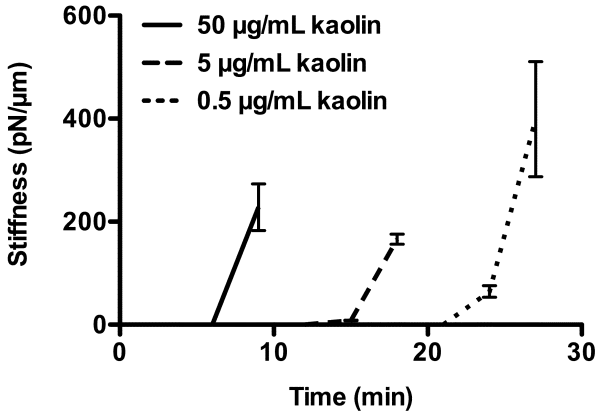

Figure 2-13 | Sensitivity of optical ARF clot stiffness assessment to strength of kaolin clotting stimulus. Clot stiffness of PRP stimulated with 0.5, 5, and 50 µg/mL kaolin was measured by optical ARF. Optical ARF detected kaolin concentration dependent kinetics of clot stiffness. Standard error is shown with at least n=5 beads per time point.

DISCUSSION

In this study we describe an application of acoustic radiation force (ARF) to measure blood plasma clot stiffness. In this approach microbeads were embedded in the plasma to serve as coupled force transducers and strain gauges. ARF induced micron-scale displacements of acoustically reflective beads that were tracked by video microscopy. Bead forces were calibrated in viscosity standards to quantify viscoelasticity changes in blood plasma due to fibrin network formation. The motion of beads under ARF was initially dominated by blood plasma viscosity and later, as clotting progressed, was marked by

increased elasticity. Comparison of the stiffness ratio of plasma and agarose gels measured by optical tracking of ARF-induced bead displacement to their previously reported shear moduli provided a point of reference to other rheometric techniques. Optical measurement of ARF-induced bead displacement (optical ARF) to assess blood plasma viscoelasticity was sensitive to biologically relevant characteristics of blood clotting such as strength of activation stimulus and platelet stiffness contributions.

ARF generation requires ultrasound scatterers in the material to reflect and absorb energy. While the material itself experiences force, additional scatterers, such as embedded beads, significantly increase force application. ARF results from the millisecond integration of thousands of individual acoustic pressure waves into what is effectively a sustained impulse. Pressure wave integration occurs because the pulse repetition period (~10^{-4} s/cycle) is much smaller than the time required for tissues to relax between acoustic pulses (~1 ms) (K. Nightingale, Soo, Nightingale, Bentley, et al. 2002; Long et al. 2005; Viola and Walker 2003). Key to the utility of beads as force transducers are their greater attenuation of acoustic energy compared to the suspending medium, a difference of approximately 6-fold for polystyrene beads relative to plasma (Kopecheck et al.). The bead radius is another significant determinant of optical ARF, as surface area is directly proportional to the resultant force (Bouchard et al. 2009). A related application of ARF to blood clot stiffness estimation, sonorheometry,

relies on the red blood cells at the beam focal point to reflect ultrasound and act as force transducers (Viola et al. 2004; Mauldin et al. 2010; Viola et al. 2010).

While material attenuation and bead radius influence the transmittal of ARF, ultrasound wave characteristics also affect the resultant force. Variation of pulse repetition frequency (PRF) was shown to proportionally modulate the force on the bead. By varying the PRF, the force per bead could be varied from 10 - 294 pN. These forces are on the order of those required for rupture of a fibrin fiber bond (200 pN) or to stretch a monomer in a fibrin fiber to 100% strain (140 pN) (L. E. Averett et al. 2009; Liu et al. 2010). Since rupture of fibrin fibers in a network requires greater force than that needed to rupture a single fibrin bond, I assume the forces applied by ARF in this study to be largely non-destructive to the fibrin network, allowing evaluation of its viscoelasticity.

The assessment of plasma clot viscoelasticity by optical ARF was further validated by comparison with an elastic standard, agarose. Stiffness measurements of PRP, PPP and agarose were compared shear moduli determined in conventional rotational rheometers. In our case, agarose was determined by optical ARF to be 9.8-fold stiffer than PRP. This stiffness ratio was used to estimate a shear modulus ratio of agarose to PRP. Assuming the relationship was approximately proportional, the known shear modulus of 0.5% agarose ranging from 1400 - 4530 Pa would predict a shear modulus range of

143 - 462 Pa for PRP (Barrangou, Daubert, and Allen Foegeding 2006; Adams, Frith, and Stokes 2004; Fernández et al. 2007; Hamhaber et al. 2002; Ilinskii et al. 2005). The estimate of the shear modulus for PRP was on the order of the 406 - 600 Pa range estimated in previous reports at equivalent times (Jen and McIntire 1982; Riha et al. 1999; Huang et al. 2011). The 6.9 fold stiffness ratio of PRP to PPP measured by optical ARF was also of similar proportion to the reported stiffness ratio of 8.6 measured with the parallel plate rheometer (Jen and McIntire 1982). Optical ARF estimates of stiffness therefore scales closely to a classic rheologic test and therefore can be extrapolated, within appropriate limitations, to a wider range of biologic testing of plasma blood clotting mechanics.

With the use of optical ARF there are several considerations that may confound the interpretation of the results. For instance, Brownian motion of the embedded bead could conceivably influence the estimation of the ARF-induced viscoelastic response. However, the diffusion coefficient of a 15 μm diameter bead in blood plasma was estimated to be $2.6\times10^{-14}m^2/s$, therefore the average bead would move only $0.33\ \mu m$/s (Cicuta and Donald 2007; Deen 1998; Weihs, Mason, and Teitell 2006). Brownian motion was therefore considered to contribute negligibly in unclotted blood plasma relative to ARF induced bead displacement (>100 μm). Once a fibrin network has formed the bead diffusivity would drop even further. A related factor that could influence the interpretation of bead motion is the relative size of the beads compared to the fibrin network pore size and potential molecular interactions between bead and fibrin. However, polystyrene beads

have been shown to non-specifically adhere to fibrin fibers (Collet et al. 2005) and the bead size (15 μm) is more than an order of magnitude larger than estimates of the fibrin mesh pore size (0.6 μm) (Scott et al. 2011), suggesting that the beads are likely trapped in the gel by adhesion and physical entanglement. Another potential concern is that bead motion under the influence of shear waves would be too fast to be captured at standard video rates. However, the maximum velocity at which beads moved when unconstrained in plasma was 600 μm/s, thus their frame to frame displacement was ~ 20 μm — a distance easily resolvable by microscopy. A final point of consideration is the potential effect of the beads on the coagulation process. Embedding beads in a blood sample reduced time to clot and increased clot stiffness in a sonorheometry measurement (**Fig. 2-14**), However, in our study, the presence of the beads was a constant and thus all samples experienced the same level of contact-pathway stimulation.

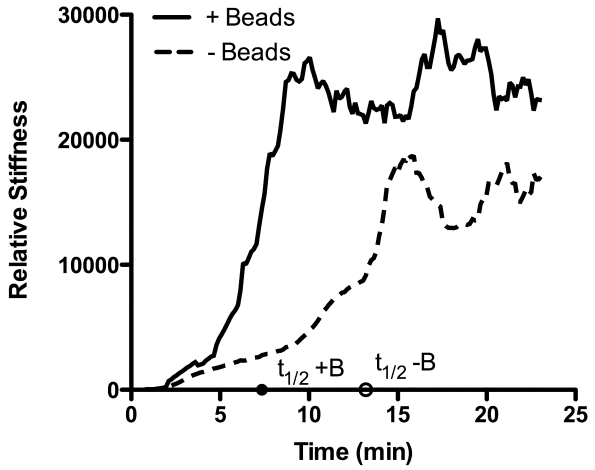

Figure 2-14 | Influence of polystyrene beads on clot stiffness. The addition of beads to whole blood samples as measured by sonorheometry resulted in increased kinetics of clot stiffness and maximum clot stiffness as compared to whole blood samples without beads.

The detection of viscoelastic material properties by ARF-induced bead motion has several experimental limitations. For one, a microscope-based bead tracking approach has an inherent stiffness detection limit defined by video resolution and the optical signal to noise ratio; i.e, once the gel becomes very stiff relative to the force on the bead, motion stops. Further increases in gel stiffness are undetectable. However, improved signal detection can be achieved by increasing transducer power to increase bead displacement or by raising microscope magnification to increase spatial resolution. Increases in plasma clot turbidity, which becomes a significant optical limitation after 45 minutes, can also reduce bead displacement measurement accuracy. In this study, fluorescent beads (**Fig. 2-15**) were used to allow optical ARF analysis at advanced stages of PRP clot development (~1 h).

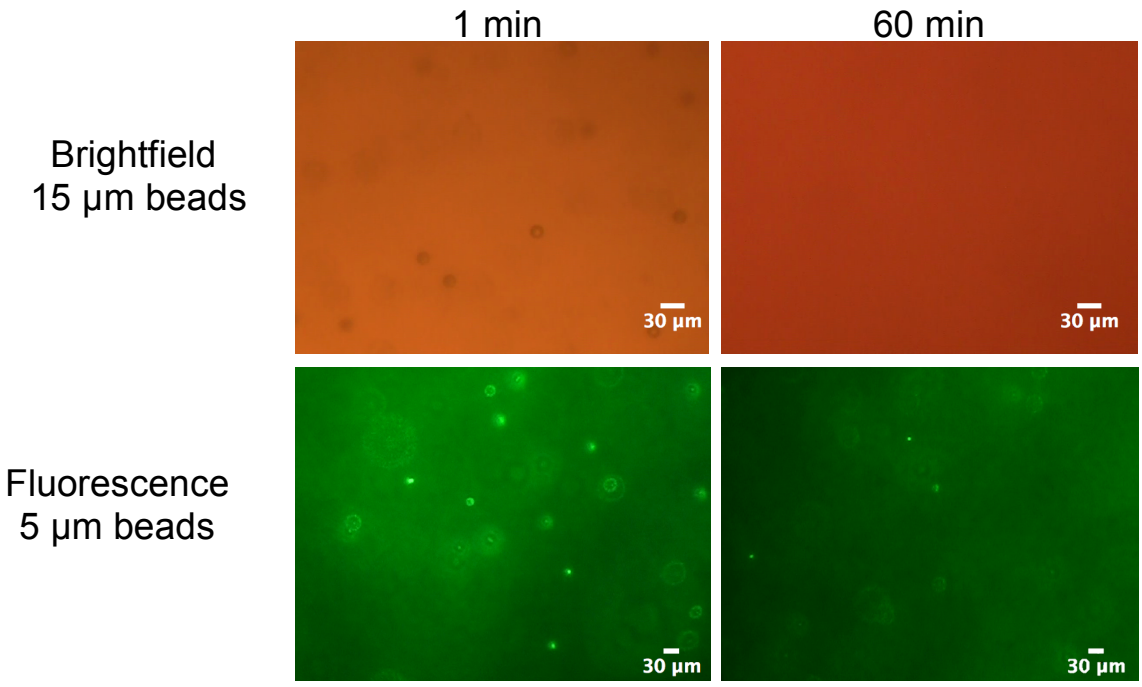

Figure 2-15 | Fluorescent beads extend measurement capabilities in an advanced stage platelet rich plasma clot. Imaging was performed at 10 x magnification in clotting platelet rich plasma. Polystyrene beads were observed in bright field (15 µm) and fluorescence (5 µm fluorescent) imaging at 0 minutes after initiation of clotting. In turbid platelet rich plasma clots after 1 hour, beads were detected by fluorescence imaging (5 µm fluorescent) while beads were obscured in brightfield imaging (15 µm).

The mechanics of blood clots is complex. One of the more intriguing features of fibrin networks is their strain-hardening characteristic, or increased material stiffness with application of large strains (>10-100%) (Shah and Janmey 1997; R. D. Averett et al. 2012; Guthold et al. 2007; Liu et al. 2010). A component of the strain hardening is thought to be a consequence of network deformation such that the slack is essentially taken out of the fibrin fibers. In platelet-rich plasma clots strain hardening does not occur (Shah and Janmey 1997), possibly by platelets pre-tensioning the network. Consequently, at low strains a PRP clot will have a larger elastic modulus than a PPP clot. But at progressively higher strains

the difference between the two decreases as the PPP clot strain hardens, eventually becoming almost equivalent to PRP at strains of 20% and greater. Rotational rheometers such as thromboelastography (TEG™) and rotational thromboelastometry (ROTEM™), which introduce strain at levels of 8-16%, could therefore potentially strain-harden of blood clots as they assess viscoelasticity. Under conditions where strain-hardening occurs, platelet contributions to clot stiffness may be less evident (Burghardt et al. 1995; Riha et al. 1999; Evans et al. 2008).

When PRP and PPP clots have been compared in the TEG™ assay, it has been observed that the stiffness ratio varies from 1.2 – 4 fold using TEG™ maximum amplitude (MA) assessment, depending on laboratory (Katori et al. 2005; Lang et al. 2004; Nielsen, Geary, and Baird 2000; Khurana et al. 1997). In contrast, the optical ARF method described here indicated the presence of platelets increased the clot stiffness by 6.9 fold, which was consistent with a previous study using ARF in whole blood (Viola et al. 2010). The relative softness of the ARF probe described here, where induced strains were 2% or less, may therefore be useful in the analysis of platelet contributions to fibrin network stiffness, as sub-optimal platelet function would conceivably be more evident in the absence of fibrin network strain hardening.

Ex vivo measurements of clotting, such as the optical ARF method described in this study, almost all suffer a potential limitation in accuracy with regard to inferences of coagulopathies *in vivo* due to the fact that the blood sample is clotted under quiescent conditions. Since blood clot formation under stasis may increase fibrin and decrease platelet concentration as compared to *in vivo* arterial clots (Jerjes-Sanchez 2005; Hathcock 2006), it is important to qualify interpretations of clot mechanics depending on whether the test is based on quiescent or shear conditions, and additionally how the specific magnitude of shear might influence clotting; i.e., is the shear arterial or venous? With that consideration in mind, static condition measurement techniques, such as optical ARF, may be more appropriate when assessing coagulopathies characterized by venous flows, trauma, or surgical bleeding.

Optical ARF viscoelasticity measurements as described in this study appeared to be sensitive to both the contribution of platelets to clot stiffness and the level of clotting stimulus. Consequently, the approach could potentially be employed for studies on early stages of clot formation, which likely involves activation of the platelet contractile apparatus in addition to contributions of fibrin polymerization (Huveneers and Danen 2009). In addition, ARF measured platelet contributions to stiffness in a 3D clot matrix rather than on a surface, differentiating it from direct measures of platelet contractility such as micropost and AFM assays that typically require testing of isolated platelets on a substrate (Liang et al. 2010; Chaudhuri et al. 2009). During clot formation, platelet contractile activity is

translated to larger length scales through fibrin filaments and concurrent platelet aggregation. The ARF method I've described here may be useful in characterizing how single platelet force generation ultimately leads to the generation of tensioned fibrin networks and clot stiffness.

REFERENCES

Adams, S, W J Frith, and J R Stokes. 2004. “Influence of Particle Modulus on the Rheological Properties of Agar Microgel Suspensions.” *Journal of Rheology* 48 (6): 1195. doi:10.1122/1.1795193.

Averett, Laurel E, Mark H Schoenfisch, Boris B Akhremitchev, and Oleg V Gorkun. 2009. “Kinetics of the Multistep Rupture of Fibrin ‘a-a’ Polymerization Interactions Measured Using Atomic Force Microscopy.” *Biophysical Journal* 97 (10): 2820–28. doi:10.1016/j.bpj.2009.08.042.

Averett, Rodney D, Bryant Menn, Eric H Lee, Christine C. Helms, Thomas Barker, and Martin Guthold. 2012. “A Modular Fibrinogen Model That Captures the Stress-Strain Behavior of Fibrin Fibers.” *Biophysical Journal* 103 (7): 1537–44. doi:10.1016/j.bpj.2012.08.038.

Barrangou, Lisa M, Christopher R Daubert, and E Allen Foegeding. 2006. “Textural Properties of Agarose Gels. I. Rheological and Fracture Properties.” *Food Hydrocolloids* 20 (2-3): 184–95. doi:10.1016/j.foodhyd.2005.02.019.

Bercoff, Jérémy, Mickael Tanter, and Mathias Fink. 2004. “Supersonic Shear Imaging: a New Technique for Soft Tissue Elasticity Mapping.” *IEEE Transactions on Ultrasonics, Ferroelectrics, and Frequency Control* 51 (4): 396–409. doi:10.1109/TUFFC.2004.1295425.

Bouchard, Richard R., Mark L Palmeri, Gianmarco F. Pinton, Gregg E Trahey, Jason E. Streeter, and Paul A Dayton. 2009. “Optical Tracking of Acoustic Radiation Force Impulse-Induced Dynamics in a Tissue-Mimicking Phantom.” *The Journal of the Acoustical Society of America* 126 (5): 2733–45. doi:10.1121/1.3238235.

Burghardt, W R, T K Goldstick, J Leneschmidt, and K Kempka. 1995. “Nonlinear Viscoelasticity and the Thrombelastograph: 1. Studies on Bovine Plasma Clots.” *Biorheology* 32 (6): 621–30. doi:10.1016/0006-355X(95)00041-7.

Cakmak, O, C Elbuken, E Ermek, A Mostafazadeh, I Baris, E Alaca, I H Kavakli, and H Urey. 2013. “Microcantilever Based Disposable Viscosity Sensor for Serum and Blood Plasma Measurements.” *Methods* 63: 225–32. doi:10.1016/j.ymeth.2013.07.009.

Calor-Filho, Marcos Muniz, and João Carlos Machado. 2006. “Measurement of the Ultrasonic Attenuation Coefficient of Human Blood Plasma During Clotting in the Frequency Range of 8 to 22 MHz.” *Ultrasound in Medicine and Biology* 32 (7): 1055–64. doi:10.1016/j.ultrasmedbio.2006.04.002.

Carr, Marcus E, Jr. 2003. “Development of Platelet Contractile Force as a Research and Clinical Measure of Platelet Function.” *Cell Biochemistry and Biophysics* 38 (1): 55–78. doi:10.1385/CBB:38:1:55.

Chaudhuri, Ovijit, Sapun H Parekh, Wilbur A Lam, and Daniel A Fletcher. 2009. “Combined Atomic Force Microscopy and Side-View Optical Imaging for Mechanical Studies of Cells.” *Nature Methods* 6 (5): 383–87. doi:10.1038/nmeth.1320.

Cheezum, M K, WF Walker, and W H Guilford. 2001. “Quantitative Comparison of Algorithms for Tracking Single Fluorescent Particles.” *Biophysical Journal*

81: 2378–88. doi:10.1016/S0006-3495(01)75884-5.
Chitlur, Meera, Indira Warrier, Madhvi Rajpurkar, Wendy Hollon, Lolita Llanto, Carol Wiseman, and Jeanne M Lusher. 2008. “Thromboelastography in Children with Coagulation Factor Deficiencies.” *British Journal of Haematology* 142 (2): 250–56. doi:10.1111/j.1365-2141.2008.07063.x.
Cicuta, Pietro, and Athene M Donald. 2007. “Microrheology: a Review of the Method and Applications.” *Soft Matter* 3 (10): 1449–55. doi:10.1039/b706004c.
Collet, J P, Y Allali, C Lesty, M L Tanguy, J Silvain, A Ankri, B Blanchet, et al. 2006. “Altered Fibrin Architecture Is Associated with Hypofibrinolysis and Premature Coronary Atherothrombosis.” *Arteriosclerosis, Thrombosis, and Vascular Biology* 26: 2567–73. doi:10.1161/01.ATV.0000241589.52950.4c.
Collet, Jean-Philippe, Henry Shuman, Robert E Ledger, Seungtaek Lee, and John W Weisel. 2005. “The Elasticity of an Individual Fibrin Fiber in a Clot.” *Proceedings of the National Academy of Sciences* 102 (26): 9133–37. doi:10.1073/pnas.0504120102.
Culjat, Martin O, David Goldenberg, Priyamvada Tewari, and Rahul S Singh. 2010. “A Review of Tissue Substitutes for Ultrasound Imaging.” *Ultrasound in Medicine and Biology* 36 (6): 861–73. doi:10.1016/j.ultrasmedbio.2010.02.012.
Dayton, Paul A, John S Allen, and Katherine W Ferrara. 2002. “The Magnitude of Radiation Force on Ultrasound Contrast Agents..” *The Journal of the Acoustical Society of America* 112 (5): 2183–92. doi:10.1121/1.1509428.
Deen, William Murray. 1998. *Analysis of Transport Phenomena*. New York: Oxford University Press.
Del Grosso, V A, and C W Mader. 1972. “Speed of Sound in Pure Water.” *The Journal of the Acoustical Society of America* 52 (5): 1442–46. doi:10.1121/1.1913258.
Elliott, Andrea, Jeremy Wetzel, Tiffany Roper, Evan Pivalizza, James McCarthy, Cristina Wallace, Mary Jane Hess, et al. 2015. “Thromboelastography in Patients with Acute Ischemic Stroke.” *International Journal of Stroke : Official Journal of the International Stroke Society* 10 (2): 194–201. doi:10.1111/j.1747-4949.2012.00919.x.
Essell, J.H., T.J. Martin, J. Salinas, J.M. Thompson, and V.C. Smith. 1993. “Comparison of Thromboelastography to Bleeding Time and Standard Coagulation Tests in Patients After Cardiopulmonary Bypass.” *Journal of Cardiothoracic and Vascular Anesthesia* 7 (4): 410–15. doi:10.1016/1053-0770(93)90161-D.
Evans, P A, K. Hawkins, M Lawrence, R L Williams, M S Barrow, N Thirumalai, and P R Williams. 2008. “Rheometry and Associated Techniques for Blood Coagulation Studies.” *Medical Engineering & Physics* 30 (6): 671–79. doi:10.1016/j.medengphy.2007.08.005.
Evans, PA, K. Hawkins, and PR Williams. 2006. “Rheometry for Blood Coagulation Studies.” *Rheology Reviews*. The British Society of Rheology, 255–91.
Fatemi, M, A Manduca, and J.F Greenleaf. 2003. “Imaging Elastic Properties of

Biological Tissues by Low-Frequency Harmonic Vibration." *Proc. IEEE* 91 (10): 1503–19. doi:10.1109/JPROC.2003.817865.

Fernández, Emiliano, Daniel López, Carmen Mijangos, Miroslava Duskova-Smrckova, Michal Ilavsky, and Karel Dusek. 2007. "Rheological and Thermal Properties of Agarose Aqueous Solutions and Hydrogels." *Journal of Polymer Science Part B: Polymer Physics* 46 (3): 322–28. doi:10.1002/polb.21370.

Fine, I, A Kaminsky, B Kuznik, and L Shenkman. 2011. "A Non-Invasive Method for the Assessment of Hemostasis in Vivo by Using Dynamic Light Scattering." *Laser Physics* 22 (2): 469–75. doi:10.1134/S1054660X12020090.

Gennisson, Jean-Luc, Sophie Lerouge, and Guy Cloutier. 2006. "Assessment by Transient Elastography of the Viscoelastic Properties of Blood During Clotting." *Ultrasound in Medicine and Biology* 32 (10): 1529–37. doi:10.1016/j.ultrasmedbio.2006.06.008.

Greenleaf, James F, Mostafa Fatemi, and Michael Insana. 2003. "Selected Methods for Imaging Elastic Properties of Biological Tissues.." *Annual Review of Biomedical Engineering* 5: 57–78. doi:10.1146/annurev.bioeng.5.040202.121623.

Guthold, M, W Liu, EA Sparks, LM Jawerth, L Peng, M Falvo, R Superfine, R R Hantgan, and S T Lord. 2007. "A Comparison of the Mechanical and Structural Properties of Fibrin Fibers with Other Protein Fibers." *Cell Biochemistry and Biophysics* 49: 165–81. doi:10.1007/s12013-007-9001-4.

Hamhaber, U, F A Grieshaber, J H Nagel, and U Klose. 2002. "Comparison of Quantitative Shear Wave MR-Elastography with Mechanical Compression Tests." *Magnetic Resonance in Medicine* 49 (1): 71–77. doi:10.1002/mrm.10343.

Hathcock, J J. 2006. "Flow Effects on Coagulation and Thrombosis." *Arteriosclerosis, Thrombosis, and Vascular Biology* 26 (8): 1729–37. doi:10.1161/01.ATV.0000229658.76797.30.

Hooke, Robert. 1678. *Lectures De Potentia Restitutiva, or, of Spring: Explaining the Power of Springing Bodies: to Which Are Added Some Collections*. Printed for J. Martyn.

Huang, Chih-Chung, Cho-Chiang Shih, Ting-Yu Liu, and Po-Yang Lee. 2011. "Assessing the Viscoelastic Properties of Thrombus Using a Solid-Sphere-Based Instantaneous Force Approach." *Ultrasound in Medicine and Biology* 37 (10): 1722–33. doi:10.1016/j.ultrasmedbio.2011.06.026.

Huveneers, Stephan, and Erik H J Danen. 2009. "Adhesion Signaling – Crosstalk Between Integrins, Src and Rho." *Journal of Cell Science* 122 (8): 1059–69. doi:10.1242/jcs.039446.

Ilinskii, Yurii A, G Douglas Meegan, Evgenia A Zabolotskaya, and Stanislav Y Emelianov. 2005. "Gas Bubble and Solid Sphere Motion in Elastic Media in Response to Acoustic Radiation Force." *The Journal of the Acoustical Society of America* 117 (4): 2338. doi:10.1121/1.1863672.

Jen, Chauying J, and Larry V McIntire. 1982. "The Structural Properties and Contractile Force of a Clot." *Cell Motility* 2 (5): 445–55. doi:10.1002/cm.970020504.

Jensen, J A, and N B Svendsen. 1992. "Calculation of Pressure Fields From

Arbitrarily Shaped, Apodized, and Excited Ultrasound Transducers." *IEEE Transactions on Ultrasonics, Ferroelectrics, and Frequency Control* 39 (2): 262–67. doi:10.1109/58.139123.

Jerjes-Sanchez, C. 2005. "Venous and Arterial Thrombosis: a Continuous Spectrum of the Same Disease?." *European Heart Journal* 26 (11): 3–4. doi:10.1093/eurheartj/ehi041.

Kashuk, Jeffry L, Ernest E Moore, Allison Sabel, Carlton Barnett, James Haenel, Tuan Le, Michael Pezold, et al. 2009. "Rapid Thrombelastography (R-TEG) Identifies Hypercoagulability and Predicts Thromboembolic Events in Surgical Patients." *Surgery* 146 (4): 764–74. doi:10.1016/j.surg.2009.06.054.

Katori, Nobuyuki, Kenichi A Tanaka, Fania Szlam, and Jerrold H Levy. 2005. "The Effects of Platelet Count on Clot Retraction and Tissue Plasminogen Activator-Induced Fibrinolysis on Thrombelastography." *Anesthesia and Analgesia* 100: 1781–85. doi:10.1213/01.ANE.0000149902.73689.64.

Khurana, S, J C Mattson, S Westley, W W O'Neill, Gerald C Timmis, and Robert D Safian. 1997. "Monitoring Platelet Glycoprotein IIb/IIIa—Fibrin Interaction with Tissue Factor—Activated Thromboelastography." *Journal of Laboratory and Clinical Medicine* 130 (4): 401–11. doi:10.1016/S0022-2143(97)90040-8.

Kopecheck, Jonathan A., Kevin J Haworth, Jason L Raymond, T Douglas Mast, Stephen R Perrin, Melvin E Klegerman, Shaoling Huang, Tyrone M Porter, David D McPherson, and Christy K Holland. "Acoustic Characterization of Echogenic Liposomes: Frequency-Dependent Attenuation and Backscatter.." *The Journal of the Acoustical Society of America* 130 (5 Pt. 2): 3472–81. doi:10.1121/1.3626124.

Lam, Wilbur A, Ovijit Chaudhuri, Ailey Crow, Kevin D Webster, Tai-De Li, Ashley Kita, James Huang, and Daniel A Fletcher. 2011. "Mechanics and Contraction Dynamics of Single Platelets and Implications for Clot Stiffening." *Nature Materials* 10 (1): 61–66. doi:10.1038/nmat2903.

Lang, T, W Toller, M Gutl, E Mahla, H Metzler, P Rehak, W Marz, and G Halwachs-Baumann. 2004. "Different Effects of Abciximab and Cytochalasin D on Clot Strength in Thrombelastography." *Journal of Thrombosis and Haemostasis* 2 (1): 147–53. doi:10.1111/j.1538-7836.2004.00555.x.

Leighton, T. 2007. "What Is Ultrasound?." *Progress in Biophysics and Molecular Biology* 93 (1-3): 3–83. doi:10.1016/j.pbiomolbio.2006.07.026.

Liang, Xin M, Sangyoon J Han, Jo-Anna Reems, Dayong Gao, and Nathan J Sniadecki. 2010. "Platelet Retraction Force Measurements Using Flexible Post Force Sensors." *Lab Chip* 10 (8): 991–98. doi:10.1039/b918719g.

Liu, W, C R Carlisle, E A Sparks, and M Guthold. 2010. "The Mechanical Properties of Single Fibrin Fibers." *Journal of Thrombosis and Haemostasis* 8: 1030–36. doi:10.1111/j.1538-7836.2010.03745.x.

Long, Jennifer A, Akif Ündar, Keefe B Manning, and Steven Deutsch. 2005. "Viscoelasticity of Pediatric Blood and Its Implications for the Testing of a Pulsatile Pediatric Blood Pump." *ASAIO Journal* 51 (5): 563. doi:10.1097/01.mat.0000180353.12963.f2.

Mauldin, F William, Francesco Viola, Theresa C Hamer, Eman M Ahmed, Shawna B Crawford, Doris M Haverstick, Michael B Lawrence, and William F

Walker. 2010. “Adaptive Force Sonorheometry for Assessment of Whole Blood Coagulation.” *Clinica Chimica Acta* 411 (9-10): 638–44. doi:10.1016/j.cca.2010.01.018.

Meybohm, Patrick, Kai Zacharowski, and Christian F Weber. 2013. “Point-of-Care Coagulation Management in Intensive Care Medicine..” *Critical Care* 17 (2): 218. doi:10.1186/cc12527.

Negron, L.A, F Viola, E.P Black, C.A Toth, and W.F Walker. 2002. “Development and Characterization of a Vitreous Mimicking Material for Radiation Force Imaging.” *IEEE Transactions on Ultrasonics, Ferroelectrics, and Frequency Control* 49 (11): 1543–51. doi:10.1109/TUFFC.2002.1049736.

Nielsen, Vance G, Brian T Geary, and Manuel S Baird. 2000. “Evaluation of the Contribution of Platelets to Clot Strength by Thromboelastography in Rabbits: the Role of Tissue Factor and Cytochalasin D.” *Anesthesia and Analgesia* 91 (1): 35–39. doi:10.1213/00000539-200007000-00007.

Nightingale, K, M S Soo, R Nightingale, R Bentley, D Stutz, M Palmeri, J Dahl, and G Trahey. 2002. “Acoustic Radiation Force Impulse Imaging: Remote Palpation of the Mechanical Properties of Tissue.” *IEEE Ultrasonics Symposium*, 1821–30. doi:10.1109/ULTSYM.2002.1192652.

Nightingale, K, S McAleavey, and G Trahey. 2003. “Shear-Wave Generation Using Acoustic Radiation Force: in Vivo and Ex Vivo Results.” *Ultrasound in Medicine and Biology* 29 (12): 1715–23. doi:10.1016/j.ultrasmedbio.2003.08.008.

Nightingale, Kathryn, Mary Scott Soo, Roger Nightingale, and Gregg Trahey. 2002. “Acoustic Radiation Force Impulse Imaging: in Vivo Demonstration of Clinical Feasibility.” *Ultrasound in Medicine and Biology* 28 (2): 227–35. doi:10.1016/S0301-5629(01)00499-9.

Palmeri, M.L., M H Wang, J J Dahl, K.D. Frinkley, and K.R. Nightingale. 2008. “Quantifying Hepatic Shear Modulus in Vivo Using Acoustic Radiation Force.” *Ultrasound in Medicine and Biology* 34 (4): 546–58. doi:10.1016/j.ultrasmedbio.2007.10.009.

Park, Joon, and R S Lakes. 2007. *Biomaterials*. 3rd ed. New York: Springer.

Parker, K J, S R Huang, R A Musulin, and R M Lerner. 1990. “Tissue Response to Mechanical Vibrations for ‘Sonoelasticity Imaging’.” *Ultrasound in Medicine and Biology* 16: 241–46. doi:10.1016/0301-5629(90)90003-U.

Riha, P, X Wang, R Liao, and J F Stoltz. 1999. “Elasticity and Fracture Strain of Whole Blood Clots.” *Clinical Hemorheology and Microcirculation* 21 (1): 45–49.

Ryan, Esther A, Lyle F Mockros, John W Weisel, and Laszlo Lorand. 1999. “Structural Origins of Fibrin Clot Rheology.” *Biophysical Journal* 77 (5): 2813–26. doi:10.1016/S0006-3495(99)77113-4.

Schmitt, C, E Montagnon, A Hadj Henni, S Qi, and G Cloutier. 2013. “Shear Wave Induced Resonance Elastography of Venous Thrombi: a Proof-of-Concept.” *IEEE Transactions on Medical Imaging* 32 (3): 565–77. doi:10.1109/TMI.2012.2231093.

Schmitt, Cédric, Anis Hadj Henni, and Guy Cloutier. 2011. “Characterization of Blood Clot Viscoelasticity by Dynamic Ultrasound Elastography and Modeling

of the Rheological Behavior..” *Journal of Biomechanics* 44 (4): 622–29. doi:10.1016/j.jbiomech.2010.11.015.

Schneider, C A, W S Rasband, and K W Eliceiri. 2012. “NIH Image to ImageJ: 25 Years of Image Analysis.” *Nature Methods* 9 (7): 671–75. doi:10.1038/nmeth.2089.

Scott, D Julian A, Priya Prasad, Helen Philippou, Sheikh Tawqeer Rashid, Soroush Sohrabi, Daniel Whalley, Andy Kordowicz, et al. 2011. “Clot Architecture Is Altered in Abdominal Aortic Aneurysms and Correlates with Aneurysm Size.” *Arteriosclerosis, Thrombosis, and Vascular Biology* 31: 3004–10. doi:10.1161/ATVBAHA.111.236786.

Shah, Jagesh V, and Paul A Janmey. 1997. “Strain Hardening of Fibrin Gels and Plasma Clots.” *Rheologica Acta* 36 (3): 262–68. doi:10.1007/BF00366667.

Shinton, N K. 2010. *Desk Reference for Hematology*. 2nd ed. Boca Raton: CRC Press.

Shore-Lesserson, Linda, Heather E Manspeizer, Marietta DePerio, Sanjeev Francis, Frances Vela-Cantos, and M Arisan Ergin. 1999. “Thromboelastography-Guided Transfusion Algorithm Reduces Transfusions in Complex Cardiac Surgery.” *Anesthesia and Analgesia* 88: 312–19. doi:10.1097/00000539-199902000-00016.

Torr, G R. 1984. “The Acoustic Radiation Force.” *American Journal of Physics* 52 (5): 402–8. doi:10.1119/1.13625.

Tran, Reginald, David R Myers, Jordan Ciciliano, Elaissa L Trybus Hardy, Yumiko Sakurai, Byungwook Ahn, Yongzhi Qiu, Robert G Mannino, Meredith E Fay, and Wilbur A Lam. 2013. “Biomechanics of Haemostasis and Thrombosis in Health and Disease: From the Macro- to Molecular Scale.” *Journal of Cellular and Molecular Medicine* 20 (10): 1–18. doi:10.1111/jcmm.12041.

Tripathi, Markandey M, Zeinab Hajjarian, Elizabeth M Van Cott, and Seemantini K Nadkarni. 2014. “Assessing Blood Coagulation Status with Laser Speckle Rheology.” *Biomedical Optics Express* 5 (3): 817–31. doi:10.1364/BOE.5.000817.

Viola, F, and W.F Walker. 2003. “Radiation Force Imaging of Viscoelastic Properties with Reduced Artifacts.” *IEEE Transactions on Ultrasonics, Ferroelectrics, and Frequency Control* 50 (6): 736–42. doi:10.1109/TUFFC.2003.1209564.

Viola, F, MD Kramer, MB Lawrence, JP Oberhauser, and WF Walker. 2004. “Sonorheometry: a Noncontact Method for the Dynamic Assessment of Thrombosis.” *Annals of Biomedical Engineering* 32 (5): 696–705. doi:10.1023/B:ABME.0000030235.72255.df.

Viola, Francesco, F William Mauldin, Xiefan Lin-Schmidt, Doris M Haverstick, Michael B Lawrence, and William F Walker. 2010. “A Novel Ultrasound-Based Method to Evaluate Hemostatic Function of Whole Blood.” *Clinica Chimica Acta* 411: 106–13. doi:10.1016/j.cca.2009.10.017.

Weihs, Daphne, Thomas G Mason, and Michael A Teitell. 2006. “Bio-Microrheology: a Frontier in Microrheology..” *Biophysical Journal* 91 (11): 4296–4305. doi:10.1529/biophysj.106.081109.

Weisel, John W. 2008. “Enigmas of Blood Clot Elasticity.” *Science* 320: 456–57. doi:10.1126/science.1154210.

Weisel, JW. 2010. “Biomechanics in Hemostasis and Thrombosis.” *Journal of Thrombosis and Haemostasis* 8: 1027–29. doi:10.1111/j.1538-7836.2010.03808.x.

Xu, Wencheng, J Appel, and Junseok Chae. 2012. “Real-Time Monitoring of Whole Blood Coagulation Using a Microfabricated Contour-Mode Film Bulk Acoustic Resonator.” *J Microelectromech Syst* 21 (2): 302–7. doi:10.1109/JMEMS.2011.2179011.

Chapter 3: Influence of platelet thrombin generation on clot stiffness

INTRODUCTION

In blood clotting platelets release clotting factors, provide a catalytic surface for enzymatic reactions, and interact with fibrin fibers through integrin IIb-IIIa. One of the main enzymatic reactions on the platelet plasma membrane is thrombin generation from prothrombin. Thrombin transforms fibrinogen into the reactive fibrin monomer, initiating the polymeric reaction that results in formation of fibrin fibers. Fibrin fiber formation is the main process that transforms blood clot material properties from those of a viscous fluid to a viscoelastic gel (Weisel 2010; Ryan et al. 1999).

The tenase and prothrombinase complexes (**Fig. 3-1**) are responsible for catalysis of thrombin generation by the platelet. The tenase complex is composed of coagulation Factors IXa and VIIa and activates Factor Xa while the prothrombinase complex is composed of coagulation Factors Xa and Va and activates thrombin (Factor IIa) (Rivera et al. 2009).The role of the platelet as a reactive site for the enzymatic reactions of the coagulation cascade has only recently been appreciated. The functions of the platelet that contribute to the mechanical properties of the blood clot are a largely unexplored area of research.

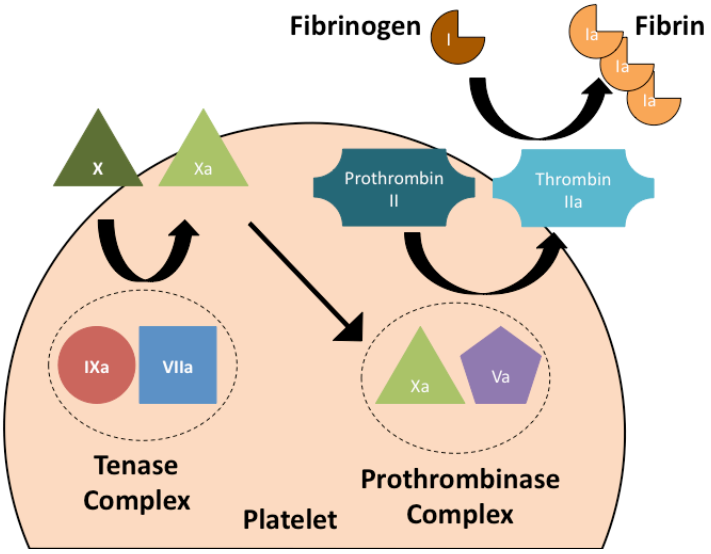

Figure 3-1 | Platelet catalysis of thrombin generation. Thrombin generation occurs on the platelet surface by tenase and prothrombinase complex activity.

Experimental design

Since thrombin is the central enzyme of the coagulation cascade this study is directed toward assessing the importance of the tenase complex and platelet thrombin generation to the mechanical properties and structural characteristics of the blood clot. Sonorheometry, an acoustic radiation force based clot stiffness assessment technique was used in order to assess changes in clot stiffness due to thrombin concentration. Sonorheometry differs from the optical acoustic radiation force based clot stiffness assessment technique described in Chapter 2 in that it estimates displacements in the sample from time delay estimation of the ultrasound signal whereas the optical technique employs microscopy to assess displacement. Sonorheometry can use either beads in plasma or the red blood cells in whole blood as scatterers of ultrasound in order to apply force on the sample and obtain time delay estimation of sample displacement.

Previous studies on fibrin gels have shown that increasing levels of thrombin increase the fibrin polymerization rate, decrease fibrin fiber diameter, and increase the branch points of fibrin networks (Weisel 2004; Wolberg 2007). With increasing thrombin levels, fibrin monomer may be produced at high concentrations and polymerize into multiple smaller fibrin fibers, whereas low thrombin levels may generate a lower concentration of fibrin monomer and force the formation of fewer larger fibrin fibers. An optimal thrombin concentration (**Fig. 3-2**) for maximum fibrin gel stiffness may exist at approximately 1U/mL (Ryan et al. 1999). With experiments controlling for Factor XIII levels, it has also been shown that Factor XIII increases fibrin gel stiffness while not altering fibrin fiber diameter of fibrin network branch point number (Mockros, Roberts, and Lorand 1974; Bale and Ferry 1988; Ryan et al. 1999). Since these studies were all performed in fibrin gels, the role of platelets in thrombin concentration dependent changes to clot stiffness and clot structure has not been investigated.

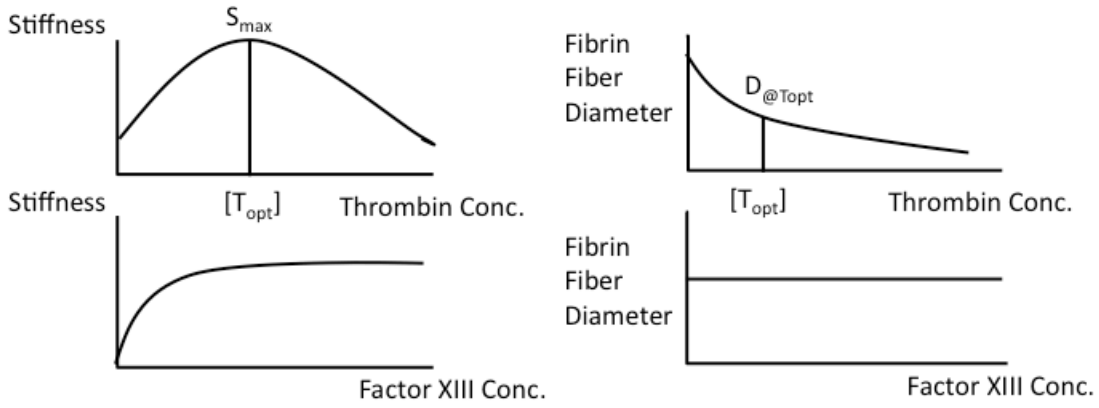

Figure 3-2 | Clot stiffness and fibrin fiber diameter dependence on thrombin and Factor XIII concentration. An optimal clot stiffness with thrombin concentration may exist such that at lower thrombin concentrations increasing thrombin levels increases clot stiffness, while after the thrombin inflection point increasing thrombin concentrations reduces clot stiffness. Increasing thrombin concentration may reduce fibrin fiber diameter. Factor XIII initially increases clot stiffness while at high concentrations it does not continue to influence clot stiffness. Factor XIII does not influence fibrin fiber diameter.

Platelet functions independent of thrombin generation, such as platelet adhesion, may increase fibrin network density relative to clots formed without platelets at equivalent thrombin concentrations (**Fig. 3-3**). Additional clot modulations that may be influenced by thrombin generation independent platelet functions include clot stiffness and fibrin fiber diameter (**Fig. 3-4**). In order to assess platelet functions excluding platelet thrombin generation, Factor Xa, the enzyme activated by the tenase complex on the platelet and the enzyme that directly activates thrombin, was inhibited.

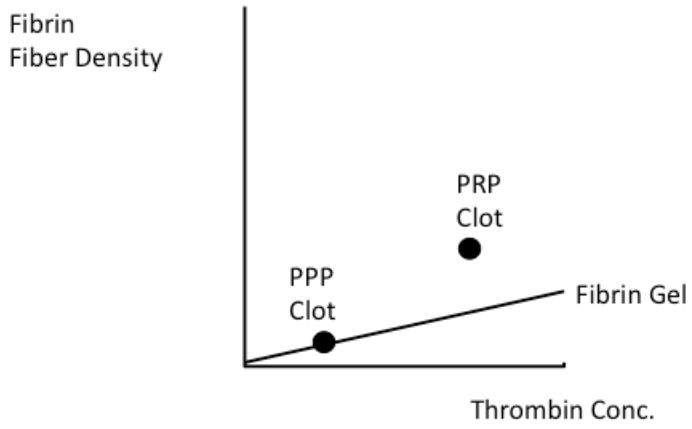

Figure 3-3 | Fibrin fiber density dependence on platelet functions independent of thrombin concentration. Platelet functions independent of thrombin generation may increase fibrin fiber density in plasma clots.

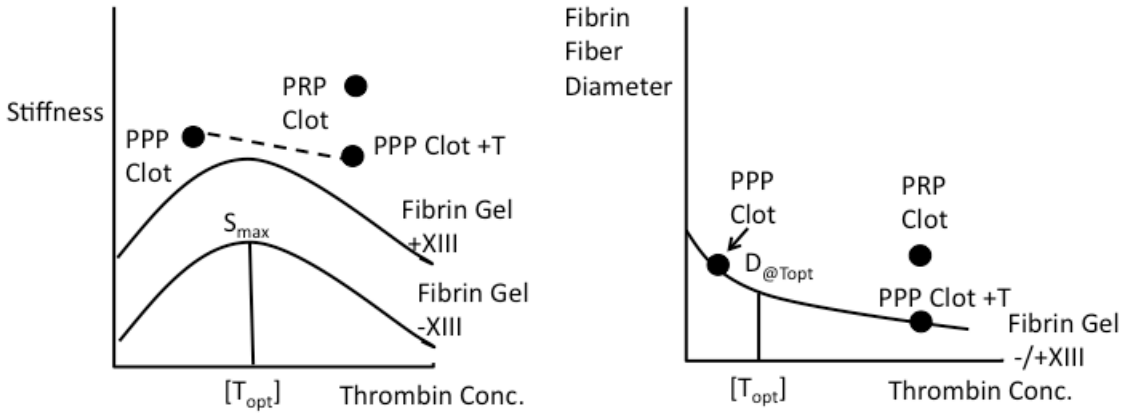

Figure 3-4 | Clot stiffness and fibrin fiber diameter dependence on platelet functions independent of thrombin concentration. Platelet functions independent of thrombin generation may increase clot stiffness and fibrin fiber diameter in plasma clots.

METHODS

The Ethics statement and Blood clotting experiments sections are included in Chapters 2-4. Reagents, Sonorheometry, Sonorheometry blood clot sample preparation, and Instrumentation and acoustic pulse sequence sections are

included in Chapters 3 and 4. This repetition allows for each chapter to stand alone.

Ethics statement

All participants provided written signed informed consent after explanation of study procedures. Experiments and study protocol as described in IRB-HSR # 12600 were approved by the Institutional Review Board for Health Sciences Research of the University of Virginia.

Blood clotting experiments

Blood was collected from three healthy volunteers using the protocol described in IRB-HSR # 12600 in 1.8 mL or 2.7 mL citrated 3.2% Vacutainer® tubes (BD, Franklin Lakes, NJ, USA). Venipuncture drawn by syringe resulted in more variable levels of platelet activation, hence the use of Vacutainers® for sample acquisition. The blood was centrifuged at 100 x g for 20 min to separate phases of PRP, buffy coat, and red blood cells (**Fig. 3-5**). To obtain PRP, the supernatant of the centrifuged samples was collected by pipette. An additional centrifugation step of 2000 x g for 40 min was used to obtain platelet poor plasma (PPP).

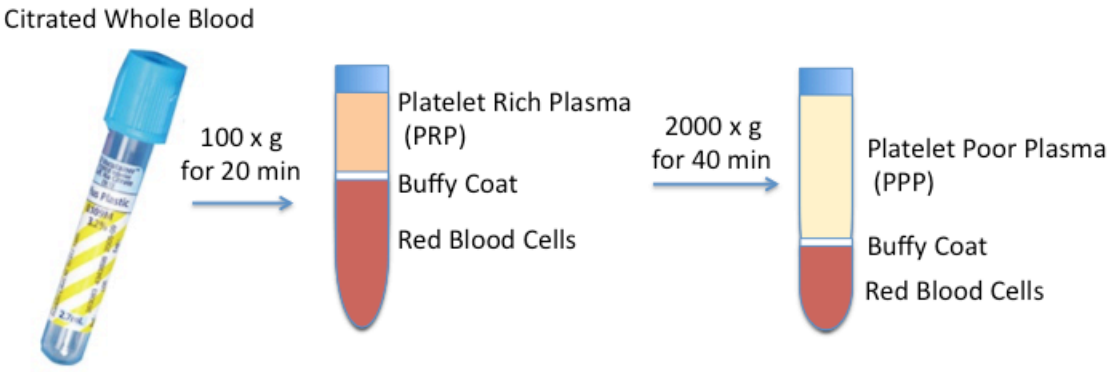

Figure 3-5 | Centrifugation protocol for platelet rich and platelet poor plasma. Citrated whole blood is collected into Vacutainer® tubes. Platelet rich plasma was separated from whole blood by centrifugation at 100 x g for 20 min. A second centrifugation step of 2000 x g for 40 min separated platelet poor plasma from whole blood.

Sonorheometry

The experimental setup (**Fig. 3-6**) consisted of an Isotemp^{TM} 125D block heater (Fisher Scientific, Pittsburgh, PA, USA) which, except where noted, held the samples at body temperature (37 °C). A custom-made saline bath dry-coupled the 10 MHz single-element focused transducer (model IBMF103, NDT Systems, Huntington Beach, CA, USA) to the sample through a flexible plastic film and was held in place with clasp enclosures. The sample was held in a 10 mm x 10 mm x 45 mm cuvette (Sarstedt, Nümbrecht, Germany). The 10 MHz transducer had a diameter of 9.5 mm and a focal length of 19 mm. Time delay estimation was used to determine displacement of scatterers in the sample. Principal component filtering was used to reduce noise and spline-estimation was used to estimate pulse-to-pulse time delays that were assembled into time-displacement curves from which maximum displacements were extrapolated (Viola et al. 2010). The

maximum displacement data was collected and stored as a MATLAB matrix for each pulse sequence acquisition. Relative stiffness, where reported, was the inverse of the maximum displacement determined by the custom program.

a 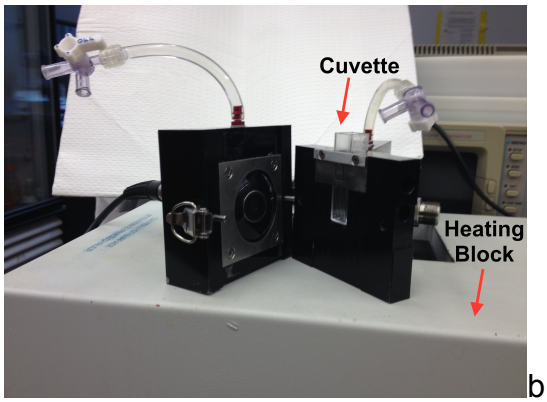

b 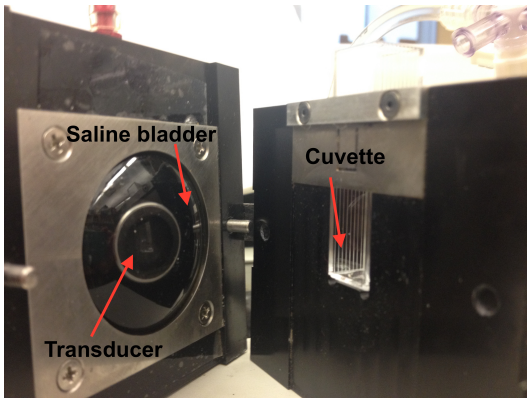

Figure 3-6 | Sonorheometry experimental setup. (a) The sonorheometry device holds the blood sample in a cuvette on a temperature controlled heating block. (b) The blood sample is coupled to the transducer by clamping the cuvette to the transducer with a saline filled flexible membrane.

Sonorheometry blood clot sample preparation

Samples consisted of 1 or 2 mL of fluid volume pipetted into the sample holder. Plasma samples were mixed with 0.5 x 10^6 / mL of 15 µm diameter latex polystyrene beads (Polybead, Polysciences, Warrington, PA, USA) as acoustic scatterers while no beads were added to whole blood samples assessed by sonorheometry because red blood cells act as scatterers. To initiate clotting, samples were recalcified with $CaCl_2$ (Sigma, St. Louis, MO, USA) to bring the PRP to a concentration of 9.525 mM $CaCl_2$. Kaolin (JT Baker, VWR, Radnor, PA, USA) is a coagulation contact pathway activator that, when used, was added to a final concentration between 5 µg/mL and 500 µg/mL. Thrombin, when added,

brought the sample to between 0.25U/mL and 4U/mL thrombin. Clotting and the ARF pulsing sequence were initiated within 15 s of calcium, kaolin, and/or thrombin addition. Displacement information within the sample was collected throughout the initial 30 min of clotting for each sample.

Instrumentation and acoustic pulse sequence

For sonorheometry the 10 MHz transducer used to generate ARF was triggered in all experiments by a custom amplifier circuit connected to a Macbook 2,1 laptop computer (Apple, Cupertino, CA) running a Matlab®/C++ program that controlled the ultrasound transducer firing pattern. A 0.8 μs pulse length (8 wave cycles) was applied. We define the rate of pulse generation used to create an impulse sequence by a pulse repetition frequency (PRF). Pulses were generated at a PRF of 7.5 kHz over a pulse train interval of 0.5 s. Pulse train intervals were separated by 6 or 10 s of rest.

RESULTS

Sonorheometry - influence of kaolin on whole blood clot stiffness

Kaolin blood clot stiffness was assessed for reproducibility by the sonorheometry technique. As shown in **Fig. 3-7**, two whole blood samples initiated by 10 μg/mL kaolin at room temperature both reached their gel point at 12 minutes. The agreement of the clotting kinetics of the two samples supports the reproducibility of sonorheometry blood clot stiffness measurement.

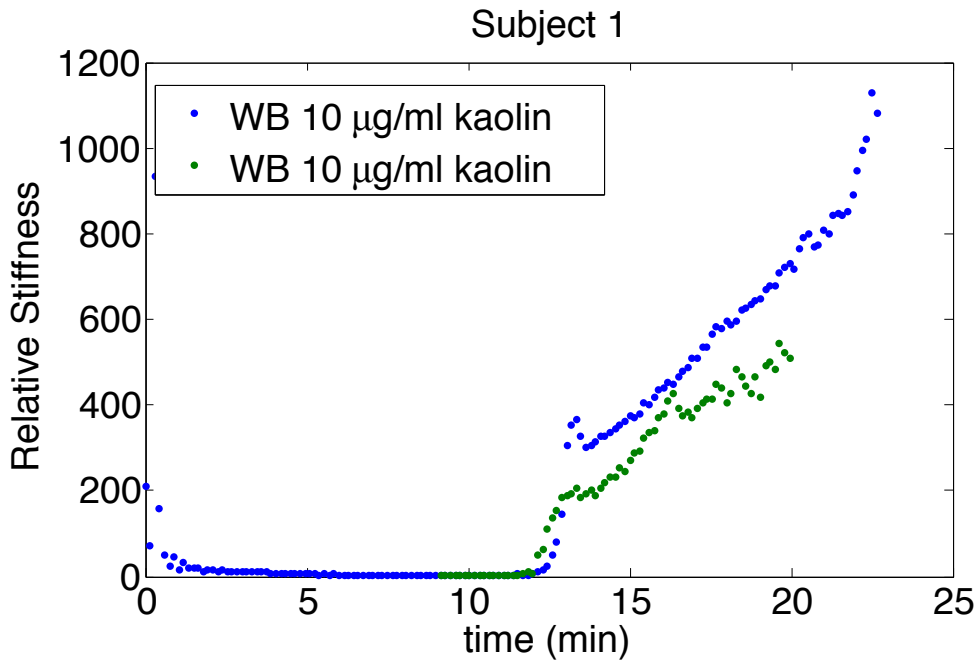

Figure 3-7 | Sonorheometry assessment of kaolin initiated whole blood at room temperature. As assessed by sonorheometry, clotting of two whole blood (WB) samples initiated by10 µg/mL kaolin at room temperature resulted in a change in clot stiffness 12 minutes after initiation.

A titration of kaolin concentrations (**Fig. 3-8**) from 0 µg/mL to 500 µg/mL at 37°C showed both a reduction in time to the gel point and an increase in clot stiffness with increasing kaolin levels. The gel points were also reduced by increasing the sample clotting temperature from room temperature to 37°C; the gel point of 0 µg/mL kaolin at 37°C was at 7 minutes while the gel point of 10 µg/mL kaolin at room temperature was at 12 minutes. Fibronectin was used to coat the cuvette for the high stimulus clot sample 500 µg/mL kaolin due to a likely clot retraction related effect (**Fig. 3-9**) of reduced clot stiffness after a relative stiffness of 2000 or more is reached in the sample. The reduced clot stiffness may be an artifact of

the clot structure pulling away and separating from the cuvette wall creating a pocket of serum and releasing tension on the clot.

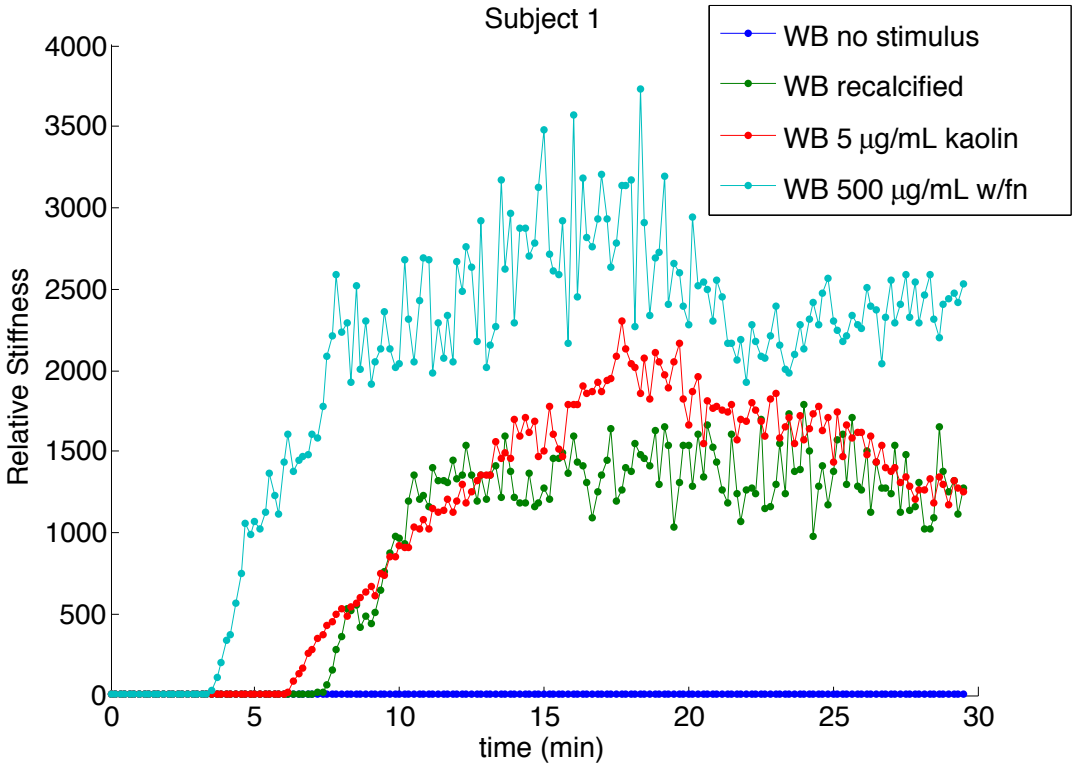

Figure 3-8 | Sonorheometry assessment of kaolin initiated whole blood clot stiffness at 37°C. Increasing kaolin concentration from 0 µg/mL to 5 µg/mL, to 500 µg/mL resulted in reduced gel point time and increased maximum relative stiffness of the clot. The 500 µg/mL kaolin sample cuvette was adsorbed with fibronectin (1 µg/mL) to prevent clot retraction.

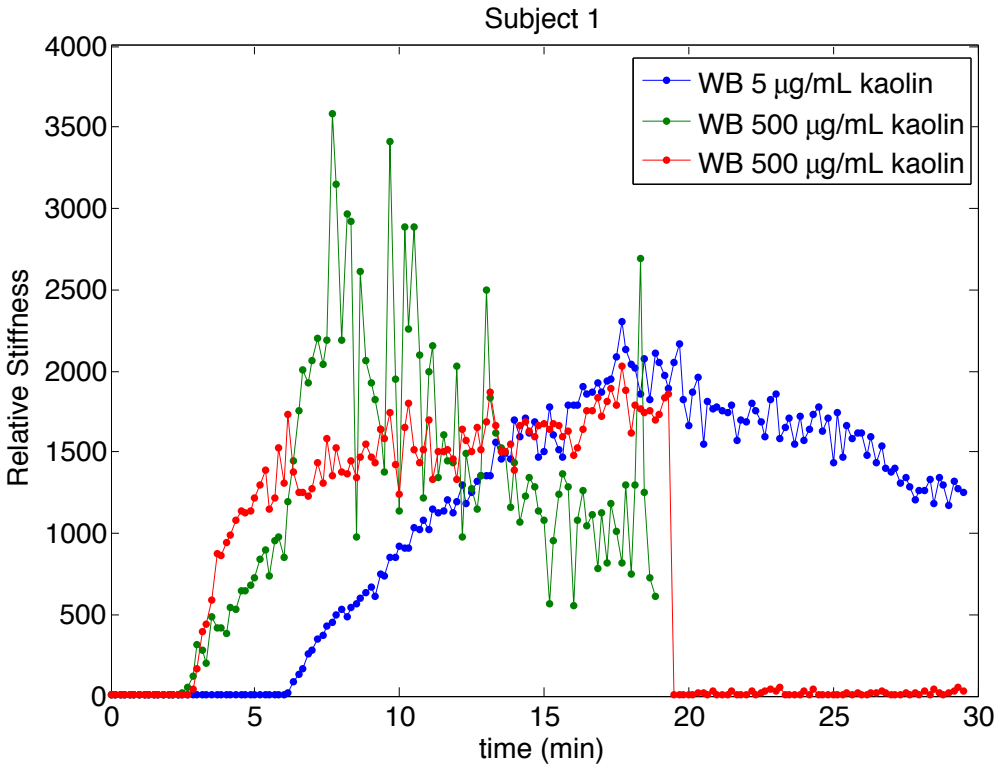

Figure 3-9 | Clot retraction in sonorheometry assessment of high kaolin concentration initiated whole blood clot stiffness. A reduction in relative stiffness measurement in samples that first reached stiffness levels at or above 2000 was observed with kaolin stimulus. The reduced clot stiffness may be due to clot retraction from the cuvette.

Sonorheometry - influence of thrombin on whole blood clot stiffness

A titration of thrombin concentration in whole blood samples (**Fig. 3-10**) was performed to assess clot stiffness in sonorheometry. The gel point time of clotting with increasing thrombin concentration was reduced from 0 U/mL to 0.8 U/mL. Increasing thrombin concentration from 0.8 U/mL to 2.5 U/mL increased the time to gel point.

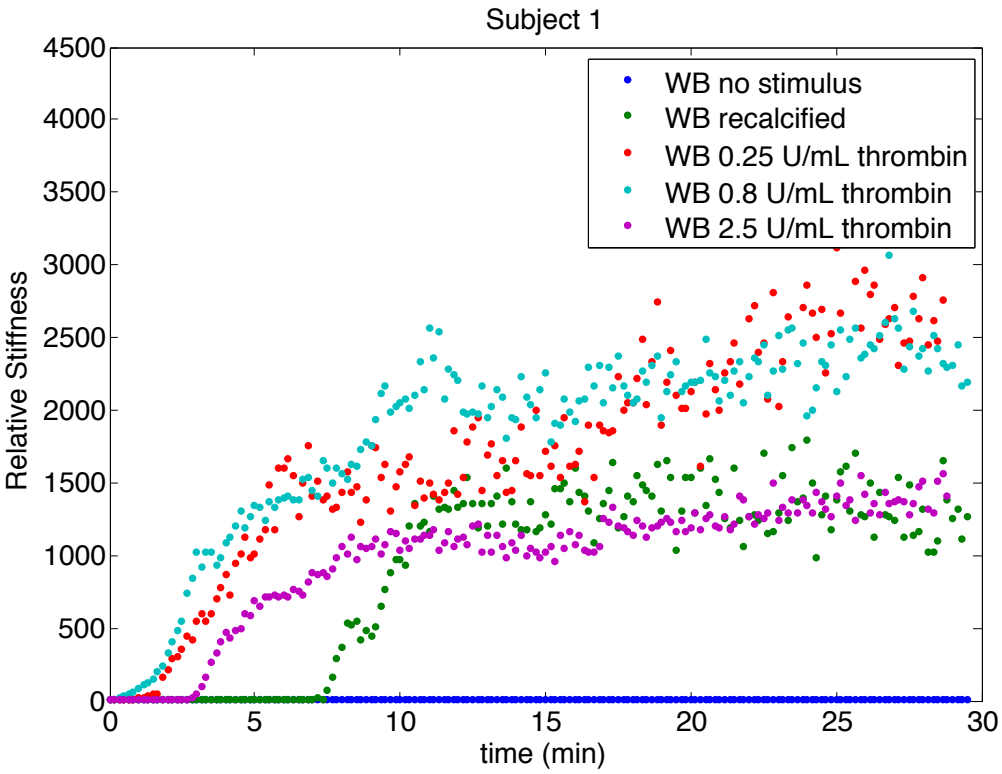

Figure 3-10 | Sonorheometry assessment of titration of thrombin in whole blood. Increased thrombin concentration progressively reduced time to gel point from 0 U/mL to 0.8 U/mL. Time to gel point increased with thrombin concentration increase from 0.8 U/mL to 2.5 U/mL.

The maximum relative stiffness measured for each whole blood clot thrombin concentration (**Fig. 3-11**) was determined by averaging the relative stiffness values after a plateau in clot stiffness was reached. The existence of an optimum thrombin concentration above which maximum clot stiffness is reduced (Ryan et al. 1999) is consistent with the maximum clot stiffness determined for titration of thrombin in whole blood, since concentrations greater than 0.25 U/mL thrombin resulted in reduced maximum clot stiffness as compared to the maximum clot stiffness at 0.25 U/mL.

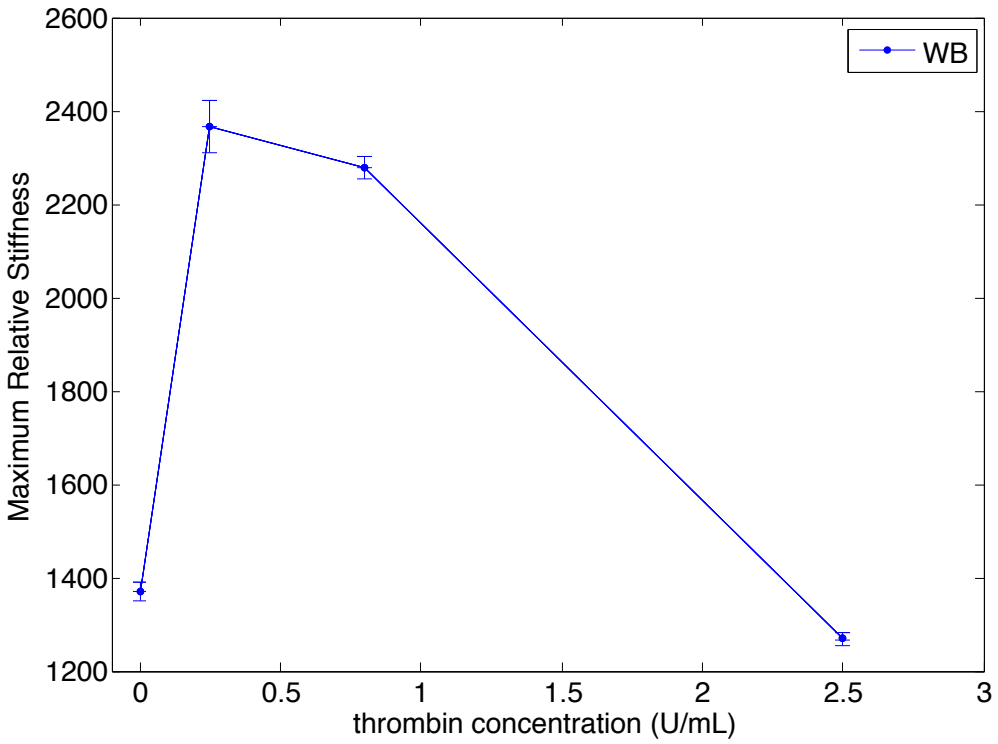

Figure 3-11 | Maximum relative stiffness of whole blood with thrombin titration. Thrombin titration in whole blood increased maximum clot stiffness from 0 U/mL to 0.25 U/mL thrombin while thrombin concentrations greater than 0.25 U/mL reduced maximum clot stiffness relative to the stiffness at 0.25 U/mL. Standard error shown with n=80 points between 15 and 30 minutes after thrombin addition.

Sonorheometry - influence of thrombin on platelet poor plasma clot stiffness

A titration of thrombin concentration in platelet poor plasma (PPP) samples (**Fig. 3-12 and Fig. 3-13**) was performed on two subjects to assess clot stiffness in sonorheometry. In both cases the addition of thrombin at 0.25 U/mL reduced the time to the gel point, as compared to recalcified control, by greater than 7 minutes. The time to gel point was more sensitive to the addition of thrombin in PPP than in whole blood. In PPP the gel point was reduced by 3 minutes with

0.25 U/mL thrombin as compared to 0 U/mL thrombin control. The observation of delay of gel points and greater gel point sensitivity to thrombin in PPP samples as compared to whole blood samples indicates the platelet, likely due to thrombin generation, increases the rate of reaction of clotting. Platelet thrombin generation would cause thrombin levels in whole blood samples to be higher than those in PPP samples.

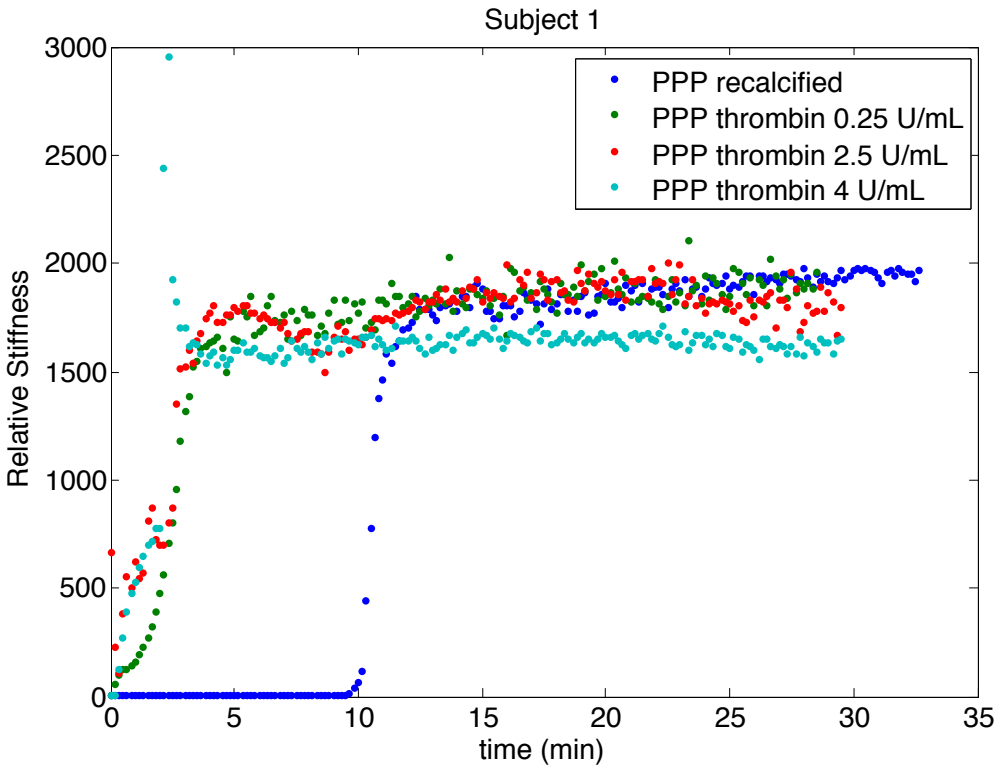

Figure 3-12 | Sonorheometry assessment of titration of thrombin in platelet poor plasma from subject 1. In platelet poor plasma from subject 1, increased thrombin concentration reduced time to gel point from 0 U/mL (recalcified) to 0.25 U/mL by 8 minutes, a larger time difference than was observed in whole blood.

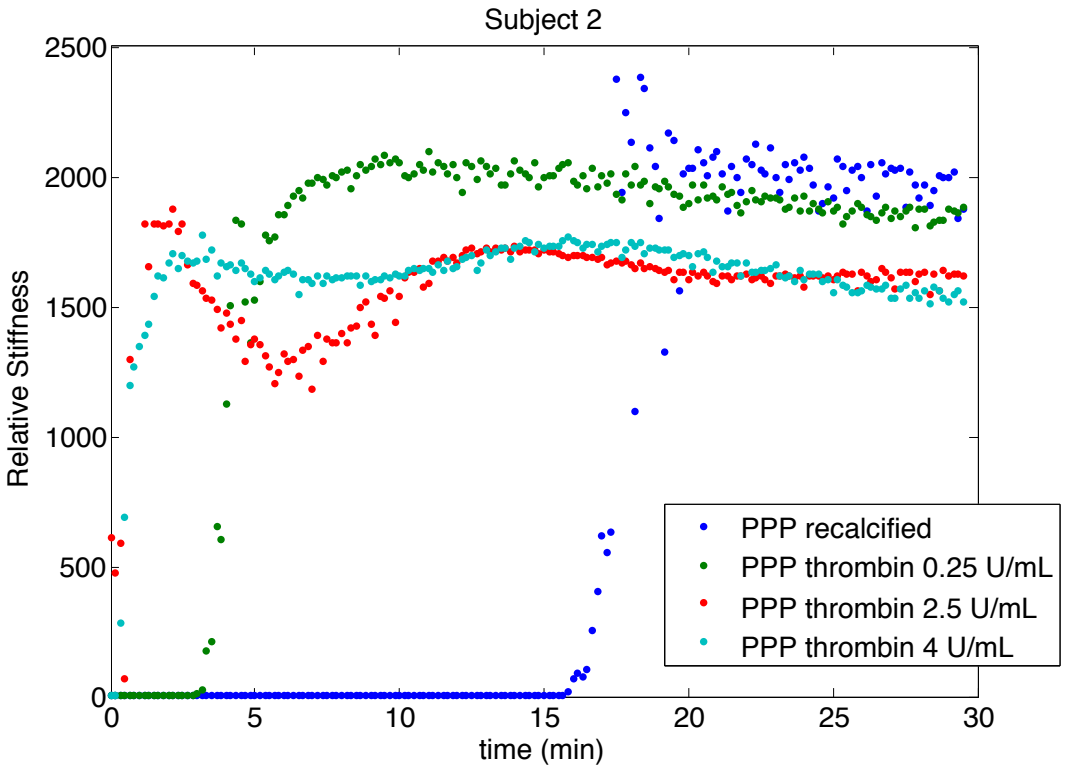

Figure 3-13 | Sonorheometry assessment of titration of thrombin in platelet poor plasma from subject 2. In platelet poor plasma from subject 2, increased thrombin concentration reduced time to gel point from 0 U/mL (recalcified) to 0.25 U/mL by 12 minutes, a larger time difference than was observed in whole blood (4 minutes).

The maximum relative stiffness measured for each thrombin concentration in platelet poor plasma (**Fig. 3-14 and Fig. 3-15**) was reduced with increasing thrombin concentration in both samples. The reduction of maximum relative stiffness with increasing thrombin concentration appeared particularly large in the case of subject 2 (**Fig. 3-15**); even the initial addition of thrombin at 0.25 U/mL reduced maximum relative clot stiffness.

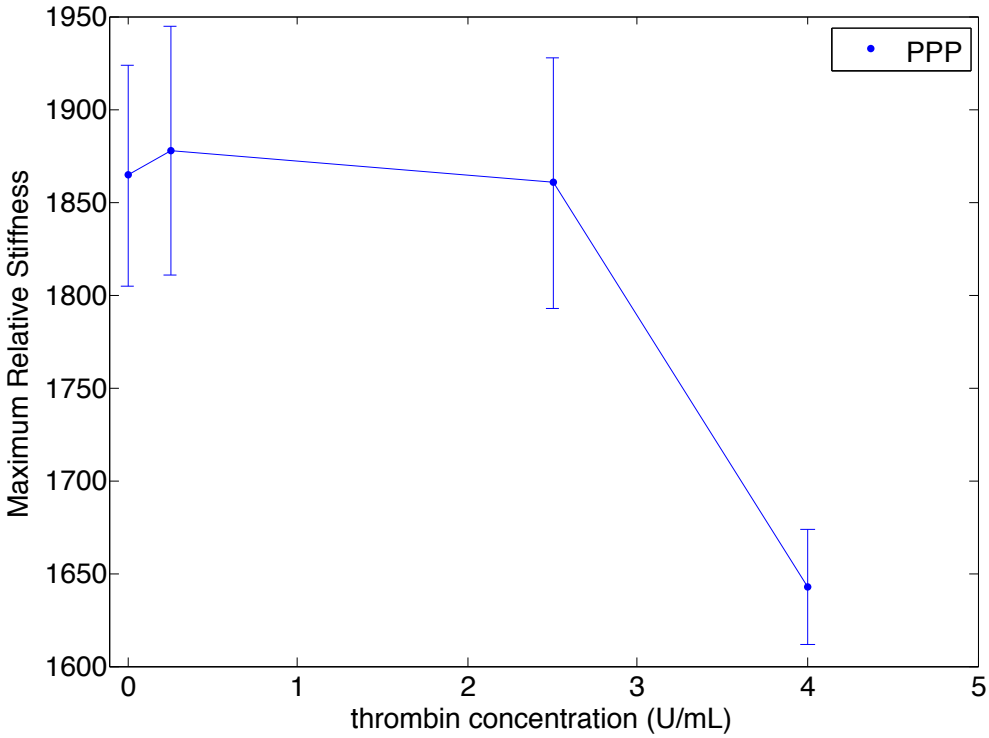

Figure 3-14 | Maximum relative stiffness of platelet poor plasma from subject 1 with thrombin titration. Thrombin titration in platelet poor plasma increased maximum clot stiffness from 0 U/mL to 0.25 U/mL thrombin while thrombin concentrations greater than 0.25 U/mL reduced maximum clot stiffness relative to the stiffness at 0.25 U/mL. Standard error shown with n=80 points between 15 and 30 minutes after thrombin addition.

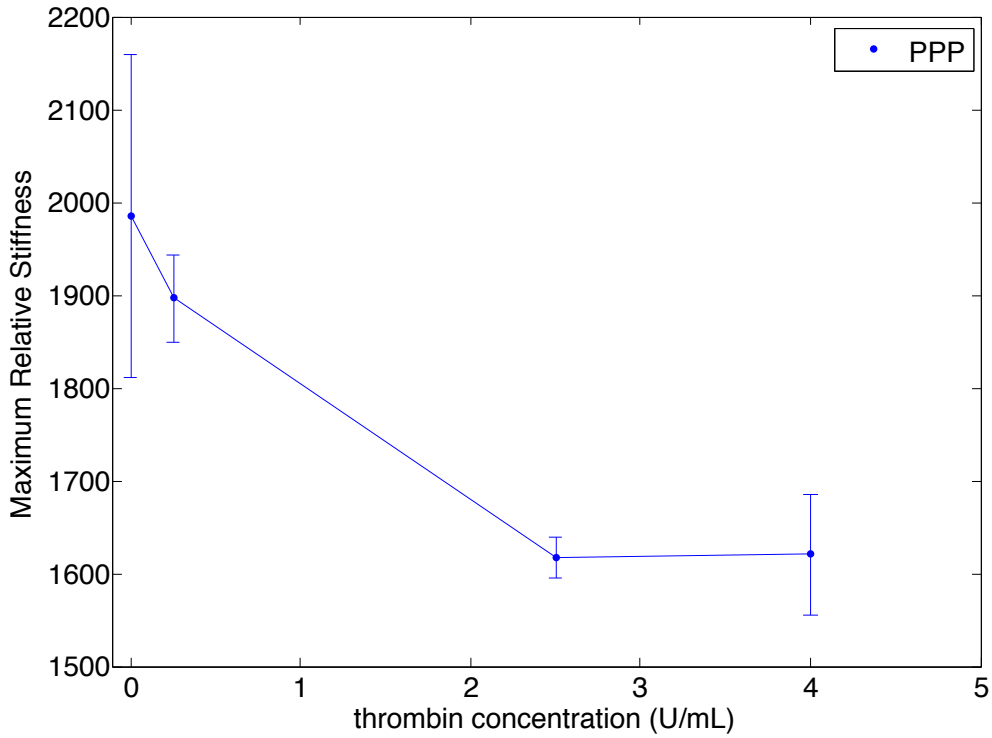

Figure 3-15 | Maximum relative stiffness of platelet poor plasma from subject 2 with thrombin titration. Thrombin titration in platelet poor plasma reduced maximum clot stiffness with increasing thrombin concentration from 0 U/mL to 2.5 U/mL. Thrombin concentration increase from 2.5 U/mL to 4 U/mL had little effect on maximum clot stiffness. Standard error shown with n=65 points between 18 and 30 minutes after thrombin addition.

Sonorheometry - influence of thrombin on Factor Xa inhibited whole blood clot stiffness

Apixaban inhibition (10 μM) of Factor Xa was used to block thrombin generation by the platelet in clot stiffness assessment of thrombin titration experiments. In order to demonstrate the inhibition of thrombin generation by apixaban, recalcification of apixaban whole blood was measured by sonorheometry (**Fig. 3-16**). Where no additional thrombin is used, in apixaban inhibited whole blood no change in clot stiffness is observed over the 30 minute experimental window,

which is consistent with inhibition of platelet thrombin generation, or any thrombin generation independent of addition of exogenous thrombin to the whole blood. Addition of thrombin at 0.25 U/mL to apixaban inhibited whole blood (**Fig. 3-16**) resulted in a gel point at 5 minutes and a slow clot stiffness formation, such that after 30 minutes of clotting the sample had not yet reached a maximum clot stiffness.

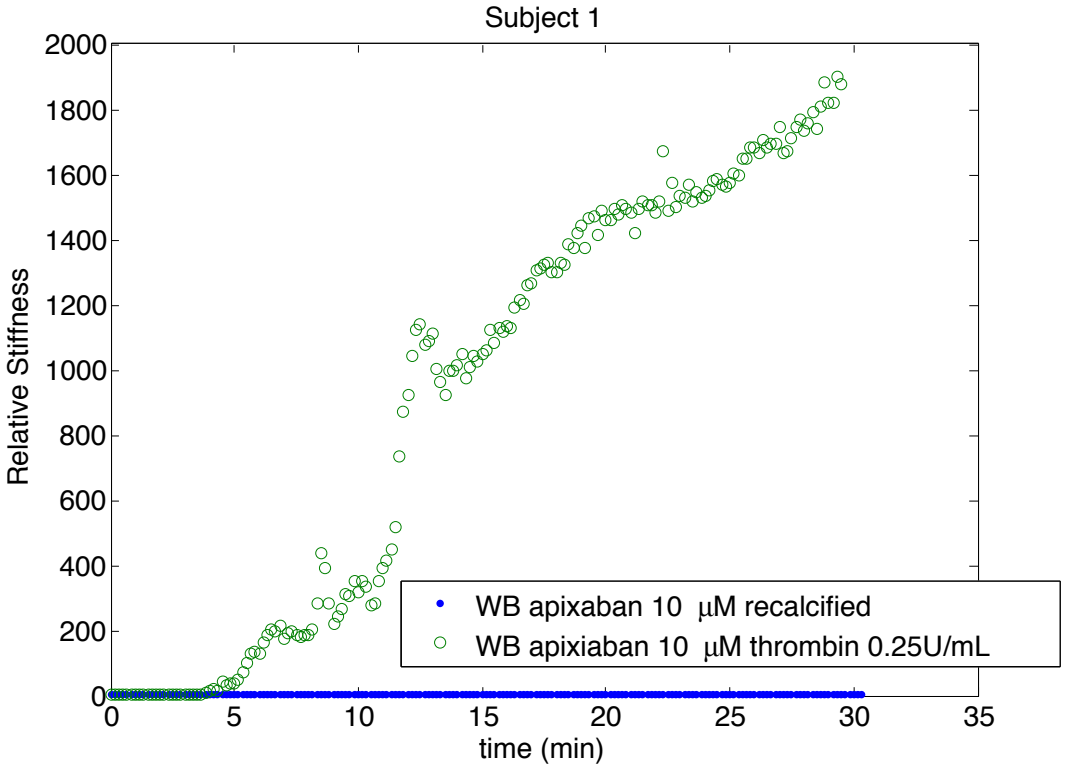

Figure 3-16 | Sonorheometry assessment of influence of thrombin on apixaban inhibited whole blood from subject 1. In recalcified whole blood from subject 1, apixaban inhibition of Factor Xa prevented clot stiffness formation. With addition of 0.25 U/mL thrombin, apixaban inhibited whole blood slowly increased in stiffness over the course of the 30 minute experiment, but never reached a maximum clot stiffness.

The maximum relative stiffness measured for apixaban inhibited whole blood with and without addition of thrombin (0.25 U/mL) is shown in **Fig. 3-17**. Maximum relative stiffness of the whole blood clot was increased with the addition of thrombin at 0.25 U/mL. Higher concentrations of thrombin addition would be required to determine if an optimal maximum clot stiffness above which thrombin addition reduces clot stiffness exists in apixaban inhibited whole blood clots. Additionally a longer time course of whole blood clotting may be required to better assess maximum relative stiffness, since 30 minutes of clotting did not result in a maximum for apixaban inhibited whole blood following activation with 0.25 U/mL thrombin.

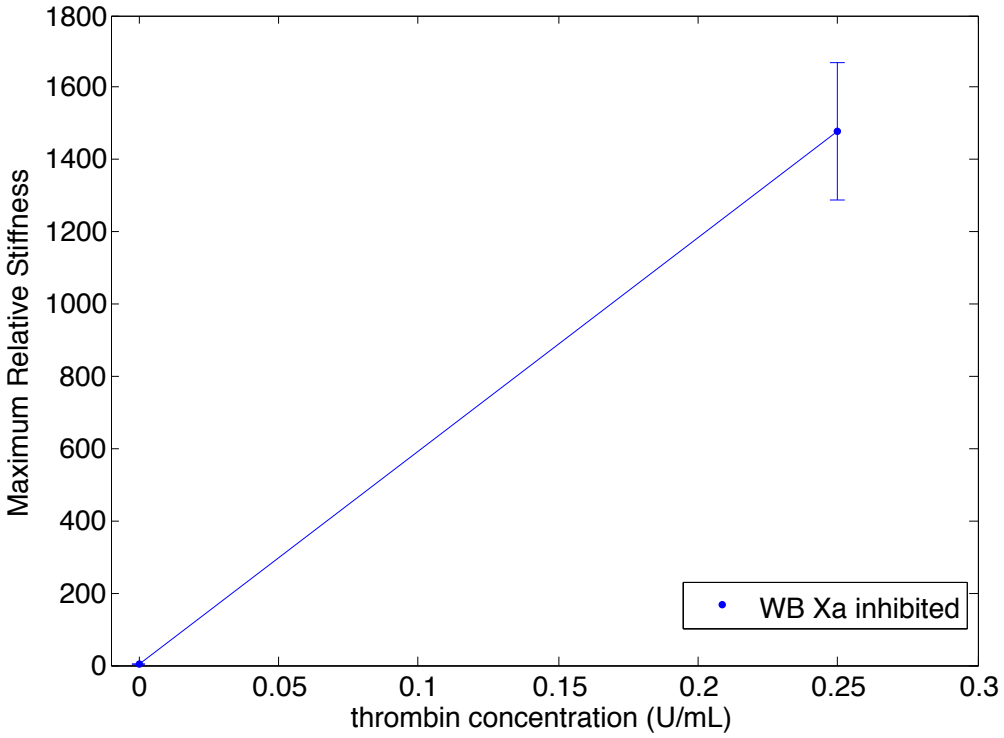

Figure 3-17 | Maximum relative stiffness of apixaban inhibitied whole blood from subject 1 with and without thrombin. Addition of thrombin (0.25 U/mL) to whole blood increased maximum clot stiffness as compared to 0 U/mL thrombin recalcified control in which clot stiffness increase was not observed. A true maximum relative stiffness was not observed during the 30 minute time course of the experiment for the 0.25 U/mL thrombin sample because a plateau of clot stiffness was not reached. Standard error shown with n=80 points between 15 and 30 minutes after thrombin addition.

Sonorheometry assessment of clot stiffness of a titration of thrombin concentration on apixaban inhibited citrated whole blood was performed (**Fig. 3-18**). With apixaban inhibition, the thrombin concentration of 0.25 U/mL does not significantly increase clot stiffness in citrated whole blood. Concentrations of 2.5 U/mL and 4 U/mL thrombin resulted in gel points at 1 minute and 30 seconds respectively.

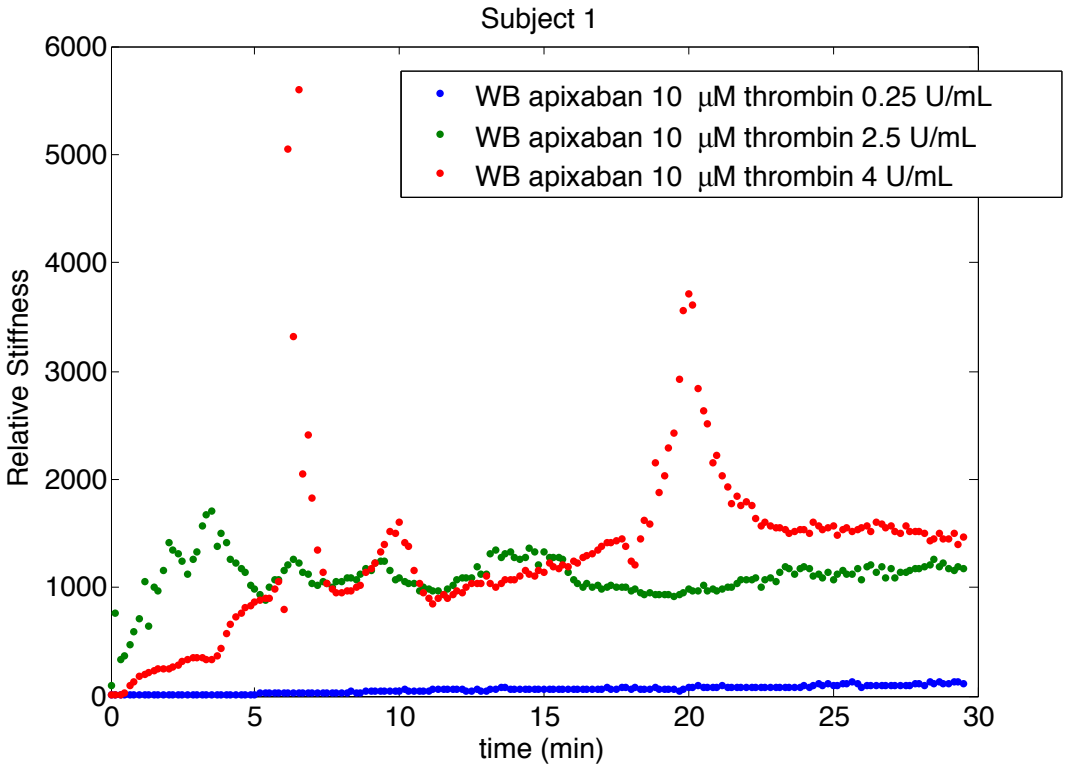

Figure 3-18 | Sonorheometry assessment of influence of thrombin on apixaban inhibited citrated whole blood from subject 1. In citrated whole blood from subject 1, apixaban inhibition of Factor Xa resulted in greatly reduced clot stiffness formation as compared to uninhibited recalcified whole blood samples at comparable thrombin concentrations. With addition of 0.25 U/mL thrombin, apixaban inhibited citrated whole blood did not increase significantly in clot stiffness. The kinetics of 2.5 U/mL and 4 U/mL thrombin apixaban inhibited citrated whole blood samples were comparable to uninhibited recalcified whole blood samples. The spikes in measurement values of 4 U/mL thrombin sample are likely signal noise.

The maximum relative stiffness measured for apixaban inhibited citrated whole blood thrombin titration is shown in **Fig. 3-19**. Maximum relative stiffness of the citrated whole blood clot increased linearly with increasing thrombin concentration up to the highest concentration measured, 4 U/mL. Higher concentrations of thrombin addition would be required to determine if an optimal

maximum clot stiffness above which thrombin addition reduces clot stiffness exists in apixaban inhibited citrated whole blood clots.

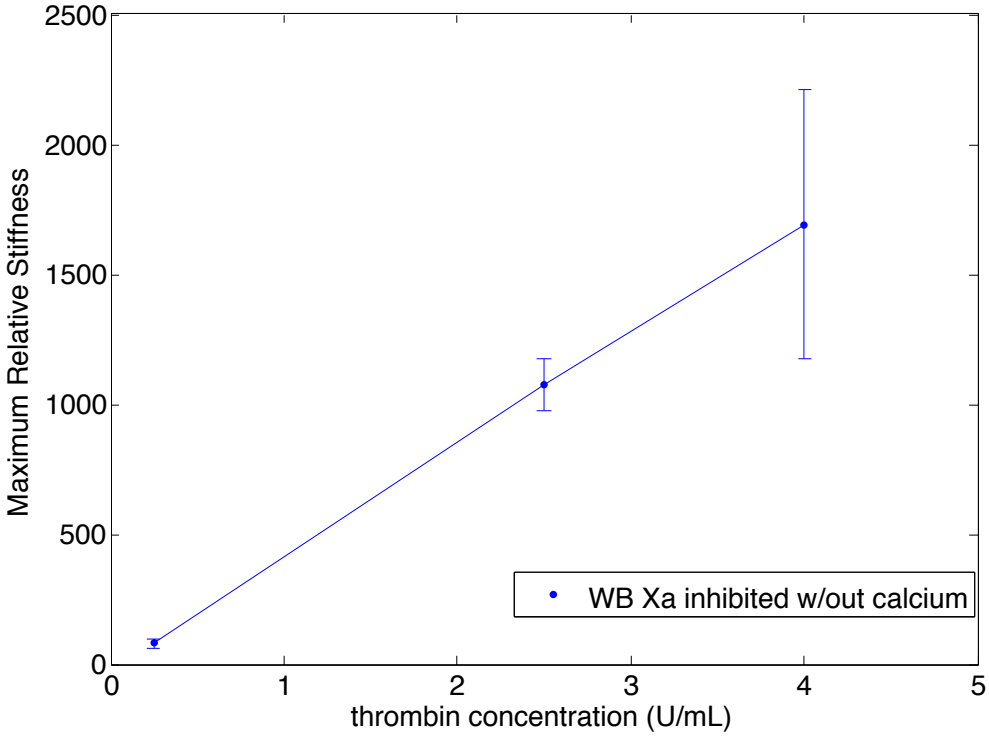

Figure 3-19 | Maximum relative stiffness of a citrated thrombin titration of apixaban inhibitied whole blood from subject 1. Thrombin titration in citrated whole blood increased maximum clot stiffness measured by sonorheometry with increasing thrombin concentration from 0 U/mL to 4 U/mL. Standard error shown with n=80 points between 15 and 30 minutes after thrombin addition.

DISCUSSION

The experiments described in Chapter 3 demonstrate the thrombin concentration dependence of clot stiffness where thrombin can both promote and inhibit clot stiffness in a concentration dependent manner. The role of platelets in thrombin concentration has also been examined and it has been demonstrated that

platelets generate significant amounts of thrombin during clot formation. With inhibition of Factor Xa by apixaban clots containing platelets had significantly reduced stiffness and the inhibitory clot stiffness effects of addition of thrombin concentrations were not observed. Inhibition of Factor Xa allowed for comparison of the clot stiffness of whole blood and platelet poor plasma without the confounding complication of additional thrombin produced by the platelet through the prothrombinase complex. Due to inhibition of Factor Xa and the prothrombinase complex on the platelet, the thrombin levels in each sample can be assumed to be equal to the thrombin concentration added. Further experiments at higher thrombin concentrations could be performed to determine the point at which thrombin concentrations become inhibitory to clot stiffness in Factor Xa inhibited clots containing platelets. It was shown that in platelet poor plasma samples thrombin levels of 2.5 U/mL or larger reduced maximum clot stiffness, whereas in Xa inhibited whole blood clots at 2.5 U/mL and 4 U/mL maximum clot stiffness continued to increase. The increased maximum clot stiffness in Xa inhibited whole blood may be due to platelet functions independent of thrombin generation, such as platelet adhesion through integrin IIb-IIIa. A study of platelet adhesion as a modulator of clot stiffness and clot structure is described in Chapter 4.

Sonorheometry was used for the assessment of the influence of platelet thrombin generation on clot stiffness. Sonorheometry, as opposed to optical acoustic radiation force based clot stiffness assessment, allowed for a faster screening of

characteristics of blood clot stiffness with perturbations, with the tradeoff for relative rather than quantitative assessment of clot stiffness.

Additional experiments could be done in order to establish a pattern of influence of platelet thrombin generation on fibrin network characteristics in addition to clot stiffness, such as fibrin fiber diameter, network porosity, branchpoints, and tortuosity. The observation of changes in clot stiffness due to platelet thrombin generation and independent of platelet thrombin generation suggests that changes in clot structure would also be found to occur due to thrombin generation and other platelet functions. Clot structural changes likely are responsible for changes in clot stiffness, but detecting the structural changes and understanding which features of the clot lead to clot stiffness may be challenging. It would likely be important going forward with studying structural changes in clot properties due to platelet functions to assess a host of possible clot structural properties in order to determine a key set of parameters that correlate most strongly with modulation of clot stiffness.

The purpose of the study of influence of platelet thrombin generation on clot stiffness was to begin to parse out the multiple effects of the platelet. With better understanding of the role of specific platelet functions such as thrombin generation, adhesion through integrin IIb-IIIa, and granule secretion we may be able to engineer desirable clot properties in order to mitigate coagulopathies and improve clinical outcomes.

REFERENCES

Bale, M D, and J D Ferry. 1988. “Strain Enhancement of Elastic Modulus in Fine Fibrin Clots.” *Thrombosis Research* 52: 565–72. doi:10.1016/0049-3848(88)90129-6.

Mockros, L F, W W Roberts, and L Lorand. 1974. “Viscoelastic Properties of Ligation-Inhibited Fibrin Clots.” *Biophysical Chemistry* 2 (2): 164–69. doi:10.1016/0301-4622(74)80037-2.

Rivera, J, M L Lozano, L Navarro-Nunez, and V Vicente. 2009. “Platelet Receptors and Signaling in the Dynamics of Thrombus Formation.” *Haematologica* 94 (5): 700–711. doi:10.3324/haematol.2008.003178.

Ryan, Esther A, Lyle F Mockros, John W Weisel, and Laszlo Lorand. 1999. “Structural Origins of Fibrin Clot Rheology.” *Biophysical Journal* 77 (5): 2813–26. doi:10.1016/S0006-3495(99)77113-4.

Viola, Francesco, F William Mauldin, Xiefan Lin-Schmidt, Doris M Haverstick, Michael B Lawrence, and William F Walker. 2010. “A Novel Ultrasound-Based Method to Evaluate Hemostatic Function of Whole Blood.” *Clinica Chimica Acta* 411: 106–13. doi:10.1016/j.cca.2009.10.017.

Weisel, JW. 2004. “The Mechanical Properties of Fibrin for Basic Scientists and Clinicians.” *Biophysical Chemistry* 112: 267–76.

Weisel, JW. 2010. “Biomechanics in Hemostasis and Thrombosis.” *Journal of Thrombosis and Haemostasis* 8: 1027–29. doi:10.1111/j.1538-7836.2010.03808.x.

Wolberg, Alisa S. 2007. “Thrombin Generation and Fibrin Clot Structure.” *Blood Reviews* 21 (3): 131–42. doi:10.1016/j.blre.2006.11.001.

Chapter 4: Influence of platelet adhesion on clot stiffness and fibrin network structure

INTRODUCTION

What are integrins?

Integrins are membrane proteins that principally mediate cell adhesion, but also signal bi-directionally across the plasma membrane of the cell (Hynes 2002). Binding of integrins with their ligands serves to connect cells to other cells or extracellular matrix. Integrins are heterodimers made up of alpha and beta subunits (Ginsberg, Partridge, and Shattil 2005). There are 18 different alpha subunits and 8 different beta subunits (**Table 4-1**).

Alpha subunits	Beta subunits
α_1, CD49a, VLA1	β_1, CD29, FNRB, MSK12, MDF2
α_2, CD49b, VLA2	β_2, CD18, LFA-1, MAC-1, MF17
α_3, CD49c, VLA3	β_3, CD61, GP3A, GPIIIA
α_4, CD49d, VLA4	β_4, CD104
α_5, CD49e, VLA5	β_5, ITGB5, FLJ26658
α_6, CD49f, VLA6	β_6, ITGB6
α_7, ITGA7, FLJ25220	β_7, ITGB7
α_8, ITGA8	β_8, ITGB8
α_9, ITGA9, RLC	
α_{10}, ITGA10	
α_{11}, ITGA11, HsT18964	
α_D CD11D, FLJ39841	
α_E CD103, HUMINAE	
α_L CD11a, LFA1A	
α_M CD11b, MAC-1	
α_V CD51, VNRA, MSK8	
α_{IIb} CD41, GPIIb	
α_X CD11c	

Table 4-1 | Integrin alpha and beta subunits. There are 18 alpha subunits and 8 beta subunits. This table was modified from Hynes 2002 with alternative names from NCBI gene search.

This heterodimer assembly allows integrins to interact with a variety of ligands (**Table 4-2**) that have common peptide sequences such as RGD (Campbell and Humphries 2011). Integrins are involved in multiple diverse processes of cells from blood clotting to immune response and leukocyte recruitment. In addition, integrins are implicated in auto-immune and genetic diseases as well as cancer (Hynes 2002). Integrin IIb-IIIa ($\alpha_{IIb}\beta_3$) is involved in blood clotting. Integrin IIb-IIIa is expressed on platelets and interacts with an RGD peptide sequence on fibrin or fibrinogen, the blood protein that forms the polymer matrix of the blood clot.

Integrins by Receptor Class				
Collagen	Laminin	RGD	Leukocyte specific	Other
$\alpha_1\beta_1$	$\alpha_3\beta_1$	$\alpha_5\beta_1$	$\alpha_L\beta_2$	$\alpha_4\beta_1$
$\alpha_2\beta_1$	$\alpha_6\beta_1$	$\alpha_8\beta_1$	$\alpha_M\beta_2$	$\alpha_9\beta_1$
$\alpha_{10}\beta_1$	$\alpha_7\beta_1$	$\alpha_V\beta_1$	$\alpha_X\beta_2$	
$\alpha_{11}\beta_1$	$\alpha_6\beta_4$	$\alpha_V\beta_5$	$\alpha_D\beta_2$	
		$\alpha_V\beta_6$	$\alpha_4\beta_7$	
		$\alpha_V\beta_8$	$\alpha_E\beta_7$	
		$\alpha_V\beta_3$		
		$\alpha_{IIb}\beta_3$		

Table 4-2 | Integrins and their receptors. Integrins bind to a variety of receptors including collagen, laminin, RGD bearing peptides such as fibrinogen, leukocyte specific receptors, and others. This table was modified from a figure from Hynes 2002.

What is integrin activation?

Integrin activation leads to an increase in its ligand binding affinity (Ma, Qin, and Plow 2007). The activation of integrins is regulated by cellular signaling and is induced by inside-out signaling, or stimuli from inside the cell (Shattil, Kim, and Ginsberg 2010). In blood clotting integrin activation helps to promote platelet aggregation and adhesion to the fibrin network. Integrin activation may involve conformational change of the integrin from a closed bent conformation to a high affinity open extended conformation (**Fig. 4-1**). In addition ligand binding may further extend the conformation transmitting a signal into the cell (outside-in signaling). Cytoskeletal changes in the cell occur both with inside-out and outside-in signaling (Goggs and Poole 2012).

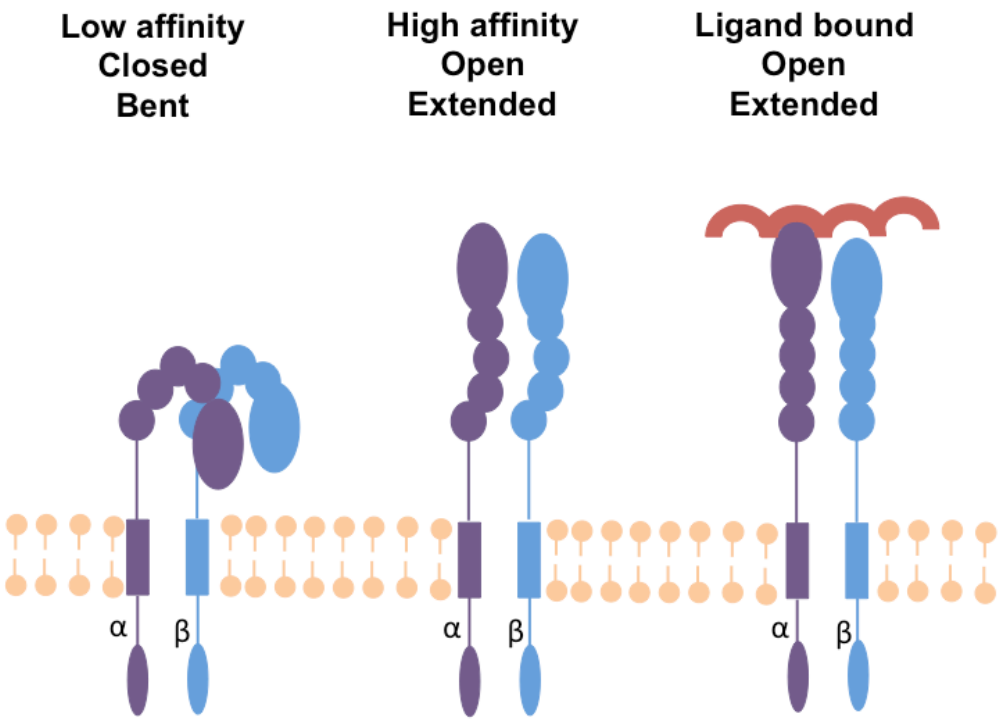

Figure 4-1 | Integrin activation and conformation. Integrins modulate between closed bent and open extended conformations. The open extended conformation has greater affinity for the integrin ligand.

What do integrins do?

Integrins, with their ability to “activate”, or change binding affinity in a controlled manner, can signal between the inside and the outside of the cell and are involved in processes such as hemostasis, immune response, cell motility, cancer, development, genetic processes, and auto-immune diseases (Hynes 2002). Integrins, because they are involved in so many processes, can be targets for drug treatment or used as targeting agents for drug delivery to diseases of a tissue with a specific integrin expression. In the process of hemostasis or blood clotting the platelet-expressed integrin IIb-IIIa, also known as $\alpha_{IIb}\beta_3$, binds to the fibrin extracellular clot matrix. Drugs targeted to integrin IIb-IIIa for the maintenance of hemostasis such as abciximab (Reopro®), eptifibatide (Integrilin®), and tirofiban (Aggrastat®) have been shown to reduce incidents of thrombotic events during myocardial infarction and percutaneous coronary intervention (E Hagemeyer and Peter 2010). Although integrin IIb-IIIa inhibiting drugs are effective at reducing thrombosis, bleeding complications can arise. Kinases in the platelet integrin IIb-IIIa signaling pathways (**Fig. 4-2**) may be potential targets for therapeutic treatment to maintain hemostasis with a reduced bleeding risk as compared to IIb-IIIa inhibiting drugs.

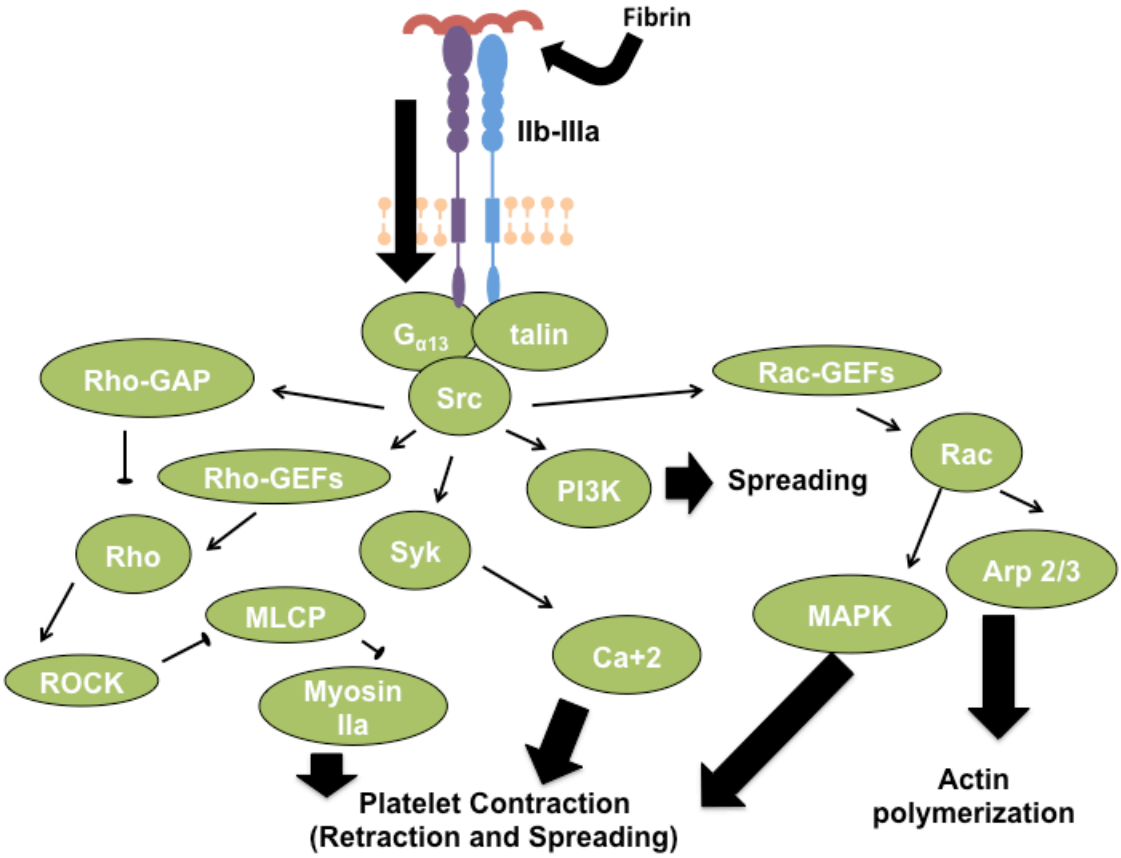

Figure 4-2 | Platelet integrin IIb-IIIa signaling. Platelet integrin IIb-IIIa outside-in signaling initiated in blood clotting by fibrin binding to the integrin involves a network of protein kinase signaling that is that regulates platelet spreading and contractility. Effects of these integrin signaling processes on clot stiffness and structural properties are largely unknown. This figure was modified from Shen 2012.

What are platelet integrin IIb-IIIa signaling pathways?

Platelet signaling in coagulation is a process that involves the interaction of multiple stimuli and feedback loops that result in a coordinated platelet response in clotting. The processes of platelet integrin IIb-IIIa signaling can be generally categorized as outside-in (**Fig. 4-3**) and inside-out, where outside-in signaling is initiated from stimuli from outside the cell to the integrin and inside-out signaling is initiated from inside the cell.

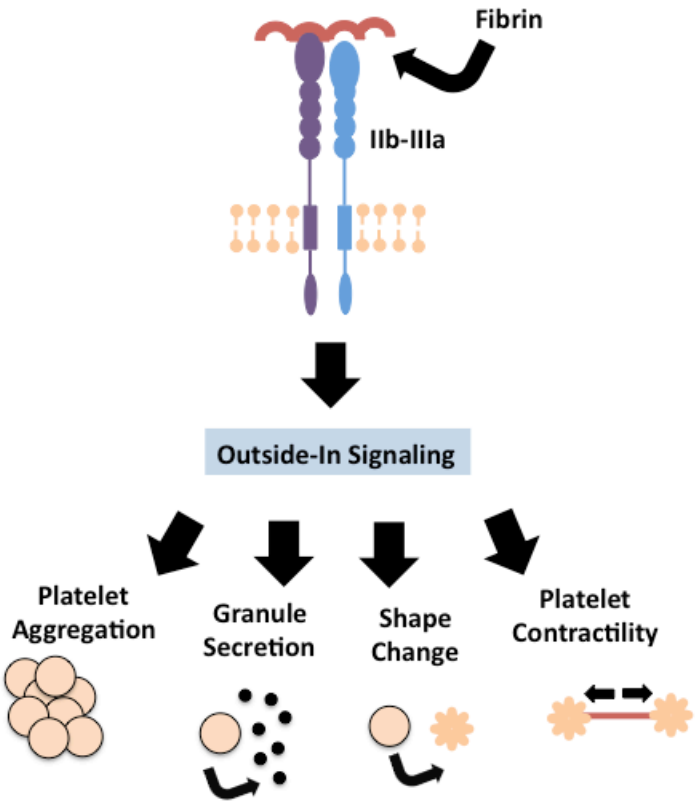

Figure 4-3 | Integrin IIb-IIIa outside in signaling. Outside-in signaling of integrin IIb-IIIa is initiated by binding of fibrin to the integrin and leads to platelet aggregation, granule secretion, shape change, and contractility.

Outside-in signaling to integrin IIb-IIIa can be initiated by the binding of fibrin or fibrinogen to the integrin. The integrin then undergoes conformational changes that lead to platelet aggregation, granule secretion, shape change, and platelet contractility (Shattil, Kashiwagi, and Pampori 1998). Granule secretion releases a variety of coagulation related effectors that feedback and amplify both pro-coagulation and anti-coagulation systems (Blair and Flaumenhaft 2009).

Integrin IIb-IIIa inside-out signaling involves stimuli to other receptors on the platelet surface that initiate processes resulting in transient integrin activation (Cosemans et al. 2008). Receptors on the platelet that could lead to inside-out signaling include collagen receptor glycoprotein VI (GPVI), thrombin receptors protease activated receptor-1 (PAR1) and protease activated receptor 4 (PAR4), adenosine diphosphate (ADP) receptors P_2Y_1 and P_2Y_{12}, and thromboxane A2 (TXa_2) receptor (TP) (Tran et al. 2013; J. Weisel 2010). For example, when GPVI binds collagen, which is exposed to the blood following blood vessel severance or puncture, a series of signaling events is induced. These signaling events result in PI3K activation, calcium release, and Src and Syk kinase activation, and ultimately lead to focal adhesion formation on integrin IIb-IIIa and subsequent integrin activation (Goggs and Poole 2012).

What are protein kinases?

Protein kinases mediate most signaling events in human cells. These kinases operate by reversibly phosphorylating and dephosphorylating other proteins (**Fig. 4-4**) (Manning 2002). Because protein kinases can regulate other protein kinases they can form chains and networks of protein kinase reactions that regulate a host of cellular processes including platelet signaling in hemostasis. All protein kinases have a general homology of structure. Protein kinases have also been further classified by gene sequence analysis into 10 evolutionary subcategories which include tyrosine kinases, tyrosine kinase-like proteins, and AGCs which are named for the protein kinase A, G, and C families (Manning 2002). The

protein kinases of platelet signaling in hemostasis likely include a mix of several subcategories. For instance, while Src kinase and protein kinase C are both involved in the platelet signaling process in hemostasis, Src kinase is a tyrosine kinase (Boggon and Eck 2004) and protein kinase C is a member of the AGC group.

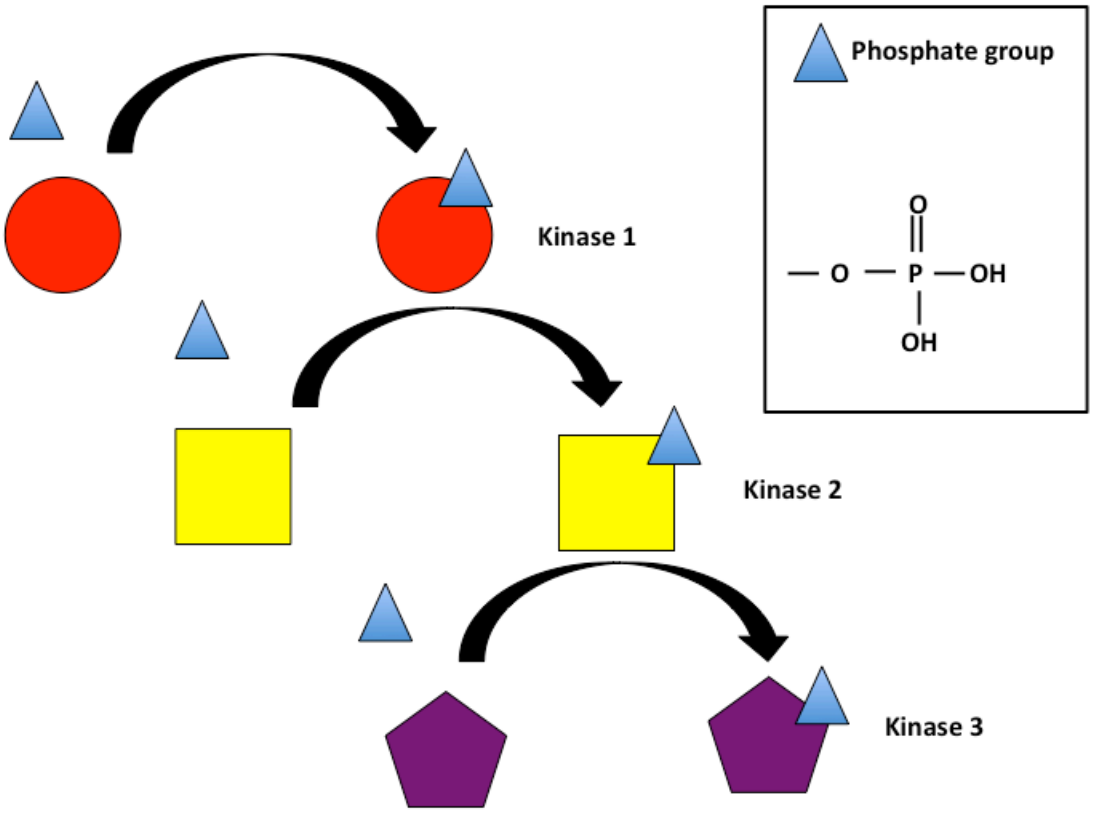

Figure 4-4 | A chain of protein kinase phosphorylation. Protein kinases can transmit signals from one protein to another by acting on each other in a chain of phosphorylation (activation) or dephosphorylation (inactivation) steps.

What is the role of calcium signaling in platelet activation and hemostasis?

Calcium is released in platelets due to multiple stimuli. Increases in the cytosolic levels of calcium in the platelet occur both through entrance of calcium through

the plasma membrane and from release of intracellular calcium stores (Varga-Szabo, Braun, and Nieswandt 2009). The release of calcium into the platelet stimulates platelet activation in blood clotting and leads to major cytoskeletal reorganization involving actin polymerization as well as integrin IIb-IIIa activation, phosphatidylserine exposure, and platelet granule secretion (Lee and Diamond 2015).

How is cytoskeletal reorganization involved in platelet response to hemostasis?

The platelet cytoskeleton reorganizes during platelet activation. Based on studies of platelets on fibrin coated surfaces, the reorganization transforms the platelet shape from rounded to a more flattened form with sheet-like lamellipodia protrusions or long thin filopodia protrusions from the platelet body (**Fig. 4-5**) (K. Park, Mao, and Park 1990; Goodman 1999). The platelet cytoskeleton is composed of the protein actin which forms filaments and polymerizes in a dynamic process that regulates cell shape and rigidity (Janmey 1998). The motor protein myosin is also involved in the cytoskeletal processes and acts as a intracellular transporter or stress generator (Janmey 1998).

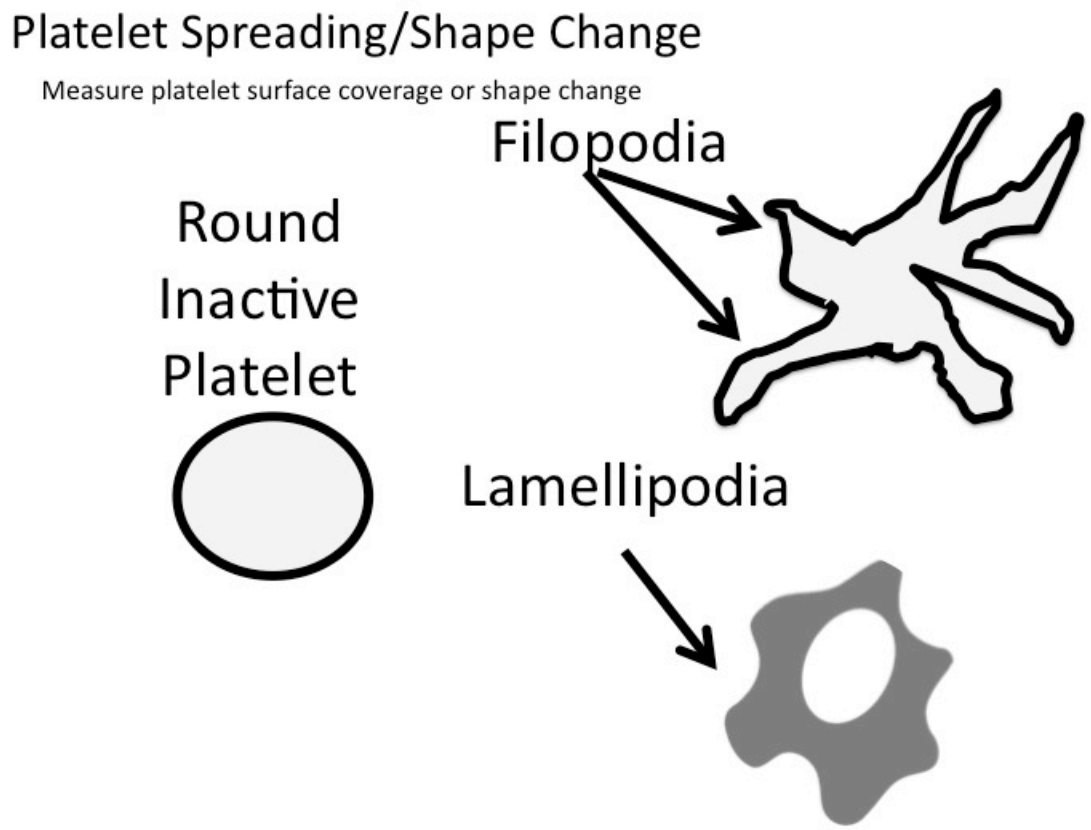

Figure 4-5 | Platelet shape change assessment. In platelet shape change assays platelets contact a surface and their morphological characteristics in response to various clotting stimuli from the surface are visually assessed. Platelet shape changes include a round inactive shape, platelet spreading, formation of sheet-like protrusions called lamellipodia, or formation of long thin protrusions called filopodia.

Together actin and myosin work to regulate cellular mechanics. Actin and myosin are involved in cell motility where actin tends to form dense branched structures at the leading and protruding edge of the cell and become most polymerically active in the leading edge region as well (Mitchison and Cramer 1996). Actin and myosin have been shown to coordinate to build tension in the classic example of striated muscle cells (Huxley 1957). It is likely then that the actin and myosin of

the platelet may be mobilized in response to platelet activation in order to generate force and tension the blood clot.

What is clot retraction?

The platelet cytoskeletal reorganization that occurs after clotting stimulus may be involved in a bulk clot phenomenon called clot retraction. Clot retraction is characterized by a reduction in thrombus volume, measured by pipetting serum volume from the clot, over the course of hours (Weiner 1963; Nicholson et al. 1998; Tucker, Sage, and Gibbins 2012). The mechanism of the volume reduction in clot retraction has not been determined. The process has been shown to be a platelet function dependent however (Goschnick 2006). The long term effects of platelet contractility are measured by the clot retraction assay. However platelet contractility is not measured directly. Additionally the retraction assay has not been systematically studied to assess mechanical tension or material stiffness, although platelet contraction has been studied in mechanical testing devices (Carr 2003; Jen and McIntire 1982).

Integrin signaling and platelet contractility

Impaired outside-in signaling of the integrin IIb-IIIa reduces clot retraction, platelet aggregation, platelet spreading on fibrinogen, and thrombus stability (Goschnick 2006). It is thought that IIb-IIIa mediates clot retraction through the platelet contractile apparatus and the activity of myosin IIa. Inhibition of myosin IIa with blebbistatin results in reduced clot contraction (Suzuki-Inoue et al. 2007;

Kovacs 2004). The role of platelet contractile mechanism and IIb-IIIa on clot contraction and later stages of clot formation is well understood however any influence of the platelet contractile apparatus on primary hemostasis or early stages of clotting is limited (Ono et al. 2008).

IIb-IIIa outside in signaling and mediation of platelet spreading and clot retraction involves interaction with tyrosine-protein kinase Src (Src), Ras homolog gene family member A (RhoA), and myosin IIa (**Fig. 4-6**) (Shen, Delaney, and Du 2012). Inhibition of RhoA by Src reduces myosin IIa activity and platelet contractility, leading to platelet spreading (A. P. Somlyo and Somlyo 2003; Calaminus et al. 2007; Bresnick 1999).

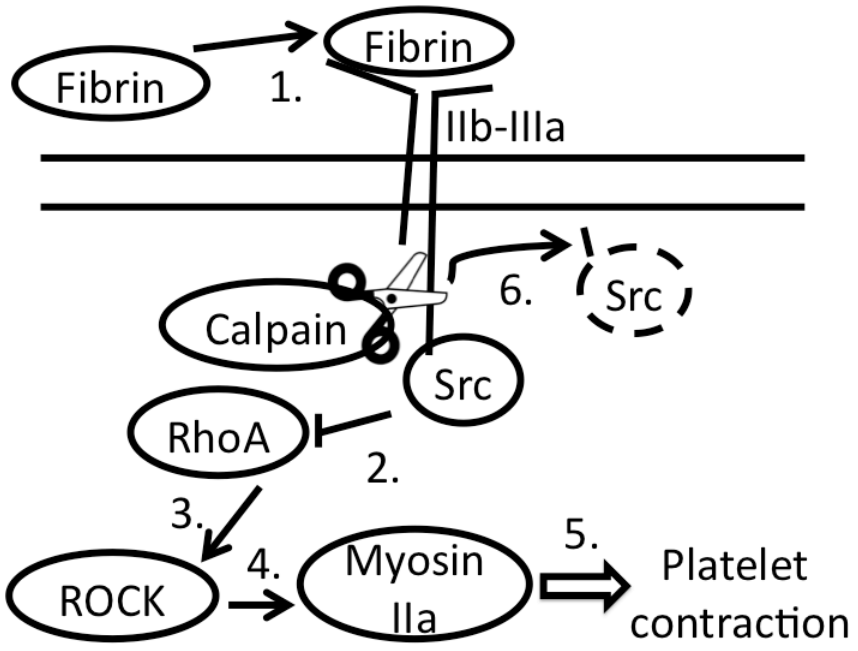

Figure 4-6 | Outside-in signaling through IIb-IIIa integrin. Outside-in signaling by integrin IIb-IIIa promotes platelet contraction by the following pathway: (1) Fibrin binds to IIb-IIIa, initiating Src activation. (2) Src inhibits RhoA. (3) RhoA activates ROCK (Rho kinase). (4) ROCK activates Myosin IIa. (5) Myosin IIa activity promotes platelet contraction. (6) Calpain cleavage of the β_3 tail and Src inactivation.

Platelets in their resting state undergo shape regulation or “rounding” through Rho kinases that activate myosin IIa to maintain the spherical resting shape of the platelet. Src kinase is constitutively bound to the cytoplasmic tail of IIb-IIIa and is activated after fibrinogen binding to the integrin (Hanke et al. 1996; Obergfell 2002; Petrich et al. 2007). In addition, Src kinase inhibition suppresses platelet spreading on fibrinogen (Hanke et al. 1996; Obergfell 2002; Petrich et al. 2007), which suggests that a Src kinase dependent pathway, following fibrin binding to IIb-IIIa, leads to cytoskeletal connection of integrin IIb-IIIa. It has been shown that ligand bound IIb-IIIa forms clusters while unbound IIb-IIIa remains diffusely on the platelet membrane (Loftus 1984; Fox and Shattil 1996; Kucik 2002). Cytochalasin D suppresses clustering of bound IIb-IIIa. These findings suggest cytoskeletal attachment controls IIb-IIIa binding affinity and that fibrin binding to IIb-IIIa integrin in outside in signaling causes changes in Src kinase association that triggers selective integrin clustering. PP2 was found to not inhibit IIb-IIIa binding to fibrin (Munnix et al. 2007). It has also been shown that blocking IIb-IIIa binding to fibrin with abciximab or Src inhibition by PP2 results in decreased calcium release, which is important for sustaining calcium dependent contractile force generation (Goncalves 2003; van der Meijden et al. 2012).

After fibrin binding to IIb-IIIa, Src is activated by G alpha 13 and inhibits the activity of RhoA, an initiator of clot retraction, through RhoGEF (Li et al. 2010). This inhibition of RhoA activity leads to reduced myosin IIa activity and a period

of platelet spreading. Calpain cleavage of the β_3 cytoplasmic tail on which Src is constitutively bound eventually allows for reactivation of RhoA and clot retraction.

The effect of this period of platelet spreading on clot stiffness is ill defined. The platelet spreading may increase interaction between the platelet and fibrin fibers, allowing for a more firm attachment to the network. Platelet outside in signaling of IIb-IIIa mediates temporal changes in platelet contractility, and this modulation of platelet contractility may impact clot stiffness and clot structure. Because most platelet biology research has been done out of the context of the fibrin network and most fibrin mechanics and structure research has been done in the absence of platelets, the impact of all platelet functions, both catalytic and adhesive, on clot stiffness and clot structure is ill defined. A striking inconsistency in the recent literature regarding Src kinase and platelet function in clotting is that Src kinase inhibition by PP2 has been shown to both accelerate and inhibit clot retraction (Suzuki-Inoue et al. 2007; Flevaris et al. 2007) . This disagreement in the platelet signaling field regarding the role of Src kinase in clot retraction is demonstrative of the need to further investigate platelet contributions to clot stiffness. The differing reports on Src kinase effects on clot stiffness may suggest that it has a temporally sensitive effect on platelet contraction and spreading.

Experimental Objective

This study was designed to determine the impact of the platelet adhesion interaction with the fibrin network on modulation of clot stiffness and fibrin fiber

structure. Integrin IIb-IIIa binding to fibrin was inhibited in plasma clots and fibrin fiber structure was analyzed. In addition clot stiffness was measured in IIb-IIIa inhibited plasma clots. Differences observed in fibrin fiber structure and clot stiffness as compared to control clots were assessed to determine the effect of platelet adhesion to the fibrin network on clot structural and mechanical properties

METHODS

The Ethics statement and Blood clotting experiments sections are included in Chapters 2-4. Optical ARF Clot Stiffness Assessment: Experimental Setup and Bead tracking and processing of displacement data sections are included in Chapters 2 and 4. The Sonorheometry section is included in Chapters 3 and 4. This repetition allows for each chapter to stand alone.

Ethics statement

All participants provided written signed informed consent after explanation of study procedures. Experiments and study protocol as described in IRB-HSR # 12600 were approved by the Institutional Review Board for Health Sciences Research of the University of Virginia.

Blood clotting experiments

Blood was collected from three healthy volunteers using the protocol described in IRB-HSR # 12600 in 1.8 mL or 2.7 mL citrated 3.2% Vacutainer® tubes (BD,

Franklin Lakes, NJ, USA). Venipuncture drawn by syringe resulted in more variable levels of platelet activation, hence the use of Vacutainers® for sample acquisition. The blood was centrifuged at 100 x g for 20 min to separate phases of platelet rich plasma (PRP), buffy coat, and red blood cells (**Fig. 4-7**). To obtain PRP, the supernatant of the centrifuged samples was collected by pipette. An additional centrifugation step of 2000 x g for 40 min was used to obtain platelet poor plasma (PPP).

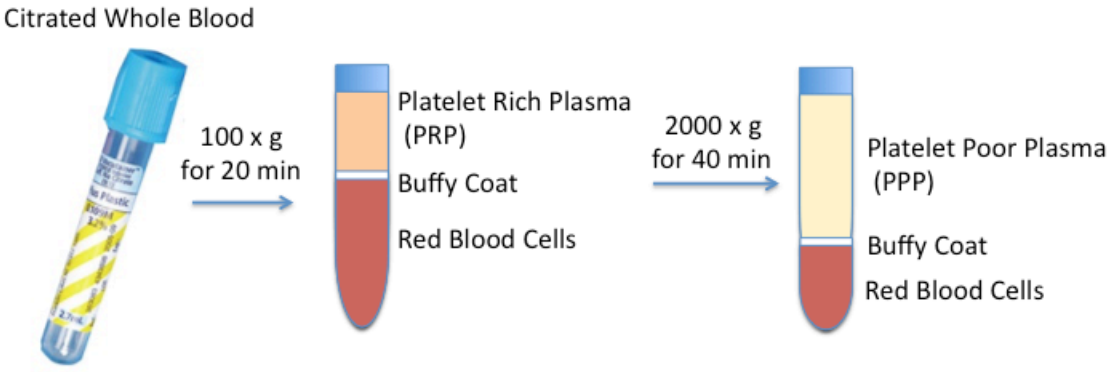

Figure 4-7 | Centrifugation protocol for platelet rich and platelet poor plasma. Citrated whole blood is collected into Vacutainer® tubes. Platelet rich plasma was separated from whole blood by centrifugation at 100 x g for 20 min. A second centrifugation step of 2000 x g for 40 min separated platelet poor plasma from whole blood.

Reagents

Abciximab (Reopro®) was used to block IIb-IIIa binding to fibrinogen (Eli Libby, Indianapolis, IN, USA). Apixaban (Eliquis®) was used to inhibit Factor Xa activity (Selleckchem, Munich, Germany). Src kinase inhibitor PP2 (R&D Systems, Minneapolis, MN, USA) was used to inhibit the intracellular signaling between the binding event of IIb-IIIa with fibrin and the myosin IIa activity modulations

(ROCK/Rac dependent). The inactive PP3 was used as a negative control (R&D Systems, Minneapolis, MN, USA). Calcium ionophore (Sigma, St. Louis, MO, USA) was used to open platelet calcium channels on the plasma membrane.

Optical ARF clot stiffness assessment

Experimental setup

The experimental setup (**Fig. 4-8a**) consisted of a platform, which positioned the ultrasound transducer relative to the microscope objective at the transducer focal distance. The sample was held in place over the objective and acoustically coupled to the transducer with ultrasound gel (Aquasonic, Parker Laboratories, Fairfield, NJ, USA). A 2.54 cm square polystyrene box (8.2 mL) (Ted Pella, Redding CA, USA) was used to hold the fluid or plasma sample. An acoustically absorbent V-shaped polydimethylsiloxane form (**Fig. 4-9**) was inserted into the box to minimize acoustic reflections and reduce the required sample volume to 2 mL. A 10 MHz single-element focused transducer (model IBMF103, NDT Systems, Huntington Beach, CA, USA) was coupled to the sample holder with ultrasound gel. The 10 MHz transducer had a diameter of 9.5 mm and a focal length of 19 mm. The transducer and sample holder were held in place by a custom stage mounted on an air table. The sample holder was mounted above a microscope (Diaphot 300, Nikon, Melville, NY, USA) with a 10 X microscope air objective, which permitted focusing into the sample at varying depths. For optimal foci alignment of the ultrasound beam with the objective plane of focus, the optical focal plane was fixed at 1300 μm above the sample holder surface for

all stiffness measurements. The motion of beads dispersed within the sample was acquired at 30 fps by a video camera (Canon Vixia HF S21, Canon, Melville, NY, USA) mounted to the microscope camera port.

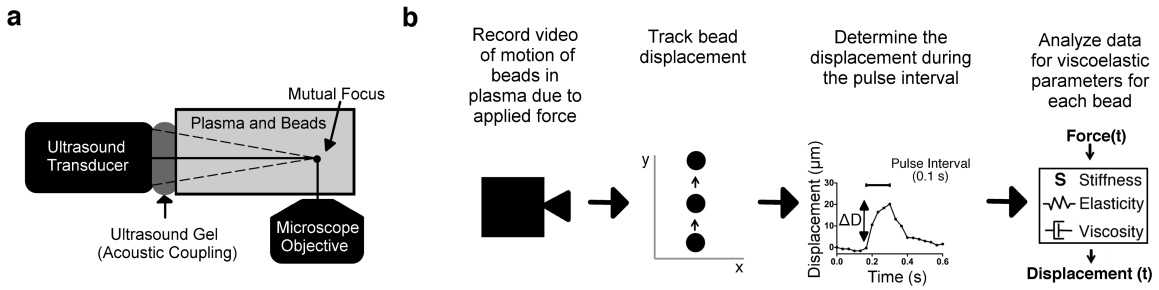

Figure 4-8 | Acoustic Radiation Force (ARF) based clot stiffness measurement. (**a**) The ARF based measurement setup used a 10 MHz ultrasound transducer to apply ARF to blood plasma in which beads were suspended. A microscope with 10 X objective and video camera had a mutual focus with the ultrasound transducer so application of ARF to the sample was imaged. (**b**) To assess blood plasma stiffness: 1) Video microscopy of the blood plasma sample was collected during application of ARF, 2) The bead motion due to applied ARF was tracked by an ImageJ program, 3) Displacements during the ARF pulse interval were determined, and 4) The displacement data was analyzed for the sample's viscoelastic parameters.

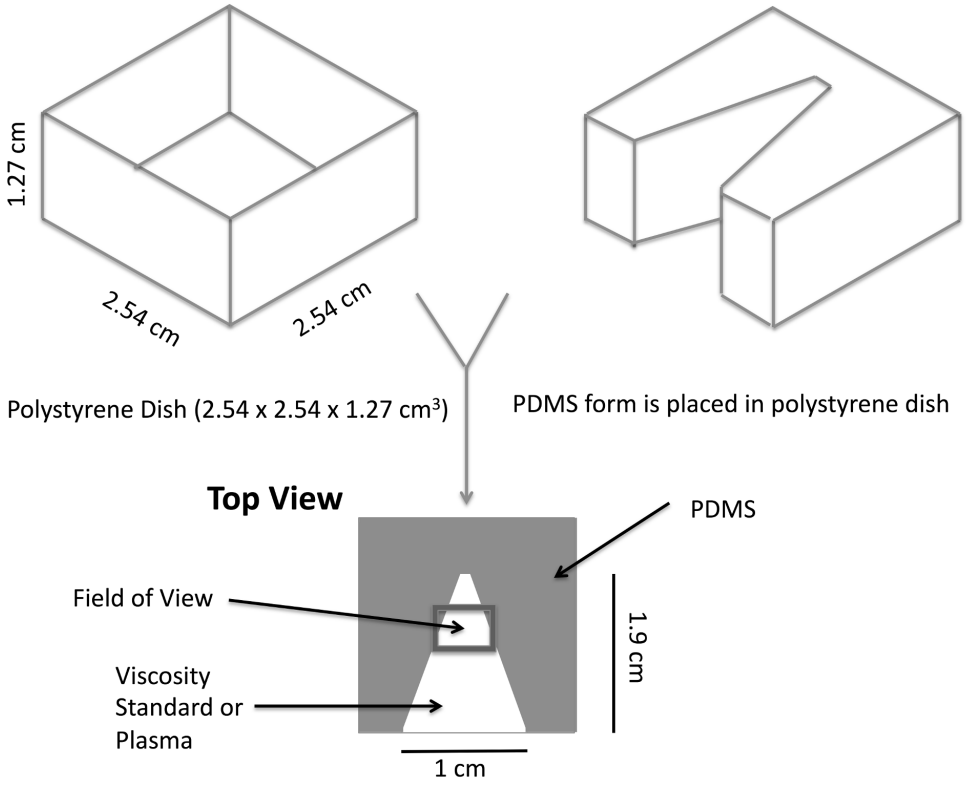

Figure 4-9 | The sample holder. The field of view for the 10 X objective is 2000 μm x 1200 μm. The shape of the PDMS mold works to reduce volume requirements for the blood sample, while the PDMS material properties allow it to act as an ultrasonic absorber reducing container reflections.

Bead tracking and processing of displacement data

Two methods of single particle tracking implemented in the image processing software ImageJ (NIH, Bethesda, MD, USA) were used to quantify bead displacement due to incident ARF: a manual particle tracking protocol and an automated tracking algorithm (Schneider, Rasband, and Eliceiri 2012). Manual tracking was used when bead velocities were greater than 400 μm/s and the automated algorithm was used in all other cases. At high velocities manual

tracking was more effective due to edge detection limitations in the automated tracking algorithm. The automated tracking algorithm utilized a cross-correlation technique to measure sub-pixel and sub-micron displacements (Cheezum, Walker, and Guilford 2001).

Manual tracking was performed using the point tool in ImageJ with the "auto-measure" and "auto-next slice" features turned on. Determination of the elastic and viscous parameters of the Kelvin-Voigt viscoelastic model from position data was performed using curve fitting with the built-in function lsqcurvefit in the computational software Matlab® (Natick, MA, USA) where the lower and upper bounds for viscosity (μ) and elasticity (k) were set to 0.1 and 10 $pN \cdot s \cdot \mu m^{-1}$ and 0.1 and 10,000 $pN \cdot \mu m^{-1}$, respectively.

Sonorheometry

The experimental setup (**Fig. 4-10**) consisted of an Isotemp™ 125D block heater (Fisher Scientific, Pittsburgh, PA, USA) which held the samples at body temperature (37 °C). A custom-made saline bath dry-coupled the 10 MHz single-element focused transducer (model IBMF103, NDT Systems, Huntington Beach, CA, USA) to the sample through a flexible plastic film and was held in place with clasp enclosures. The sample was held in a 10 mm x 10 mm x 45 mm cuvette (Sarstedt, Nümbrecht, Germany). The 10 MHz transducer had a diameter of 9.5 mm and a focal length of 19 mm. Time delay estimation was used to determine displacement of scatterers, either red blood cells or microbeads, in the sample.

Principal component filtering was used to reduce noise and spline-estimation was used to estimate pulse-to-pulse time delays that were assembled into time-displacement curves from which maximum displacements were extrapolated (Viola et al. 2010). The maximum displacement data was collected and stored as a MATLAB matrix for each pulse sequence acquisition. Relative stiffness, where reported, was the inverse of the maximum displacement determined by the custom program.

a 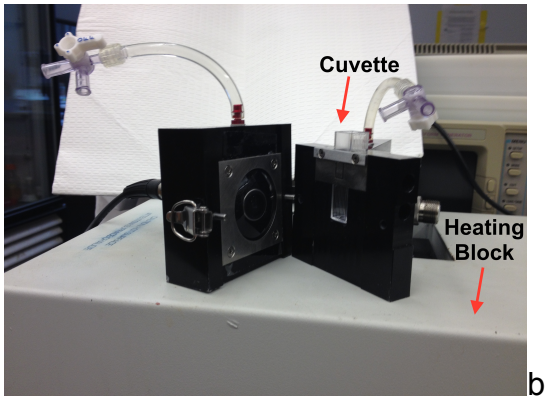

b 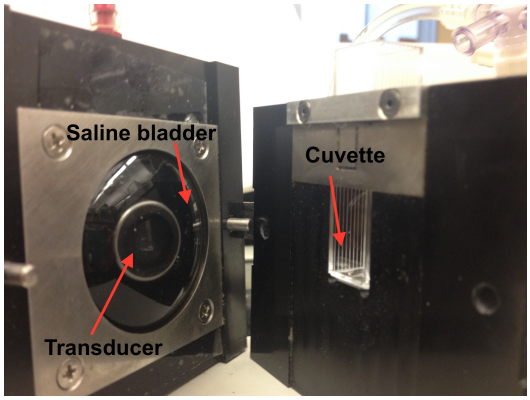

Figure 4-10 | Sonorheometry experimental setup. (a) The sonorheometry device holds the blood sample in a cuvette on a temperature controlled heating block. (b) The blood sample is coupled to the transducer by clamping the cuvette to the transducer with a saline filled flexible membrane.

Optical ARF clot stiffness assessment and sonorheometry blood clot sample preparation

Samples consisted of 1 or 2 mL of fluid volume pipetted into the sample holder. Plasma samples were mixed with 0.5 x 10^6 / mL of 15 µm diameter latex polystyrene beads (Polybead, Polysciences, Warrington, PA, USA) as acoustic scatterers while no beads were added to whole blood samples assessed by sonorheometry because red blood cells act as scatterers. To initiate clotting,

samples were recalcified with $CaCl_2$ (Sigma, St. Louis, MO, USA) to bring the PRP to a concentration of 9.525 mM $CaCl_2$. Kaolin (JT Baker, VWR, Radnor, PA, USA) is a coagulation contact pathway activator that, when used, was added to a final concentration of 5 µg/mL. Thrombin, when added, brought the sample to between 0.25U/mL and 4U/mL thrombin. Clotting and the ARF pulsing sequence were initiated within 15 s of calcium, kaolin, and/or thrombin addition. Displacement information within the sample was collected throughout the initial 30 min of clotting for each sample.

Instrumentation and acoustic pulse sequence

For optical ARF clot stiffness assessment and sonorheometry the 10 MHz transducer used to generate ARF was triggered in all experiments (except where noted) by a custom amplifier circuit connected to a Macbook 2,1 laptop computer (Apple, Cupertino, CA) running a Matlab®/C++ program that controlled the ultrasound transducer firing pattern. A 0.8 µs pulse length (8 wave cycles) was applied. We define the rate of pulse generation used to create an impulse sequence by a pulse repetition frequency (PRF). Pulses were generated at a PRF of 7.5 kHz over a pulse train interval of 0.5 s. Pulse train intervals were separated by 6 or 10 s of rest.

Scanning electron microscopy (SEM) sample preparation

For preparation of SEM imaging samples (**Fig. 4-11**) where Factor Xa inhibition is indicated apixaban was added to 1 mL of plasma (PRP or PPP) at a

concentration of 10 μM. 60μL of the plasma was then pipetted onto a 12 mm circular coverslip (Fisher Scientific, Pittsburgh, PA, USA). To initiate clotting the plasma was recalcified at 11.811 mM $CaCl_2$ and brought to between 0.25U/mL and 4U/mL thrombin, where used. The samples were then humidified at room temperature for 1 hour before fixation with 4% paraformaldehyde for 20 minutes. A series of increasingly concentrated ethanol washes each lasting 5 minutes were performed: 25, 50, 75, and 100% ethanol were washed 3 times each over the plasma samples. The samples were then either allowed to air dry in the laminar flow hood followed by placement in the vacuum chamber overnight or critical point dried with CO_2 in a Samdri 780 (Tousimis, Rockville, MD, USA).

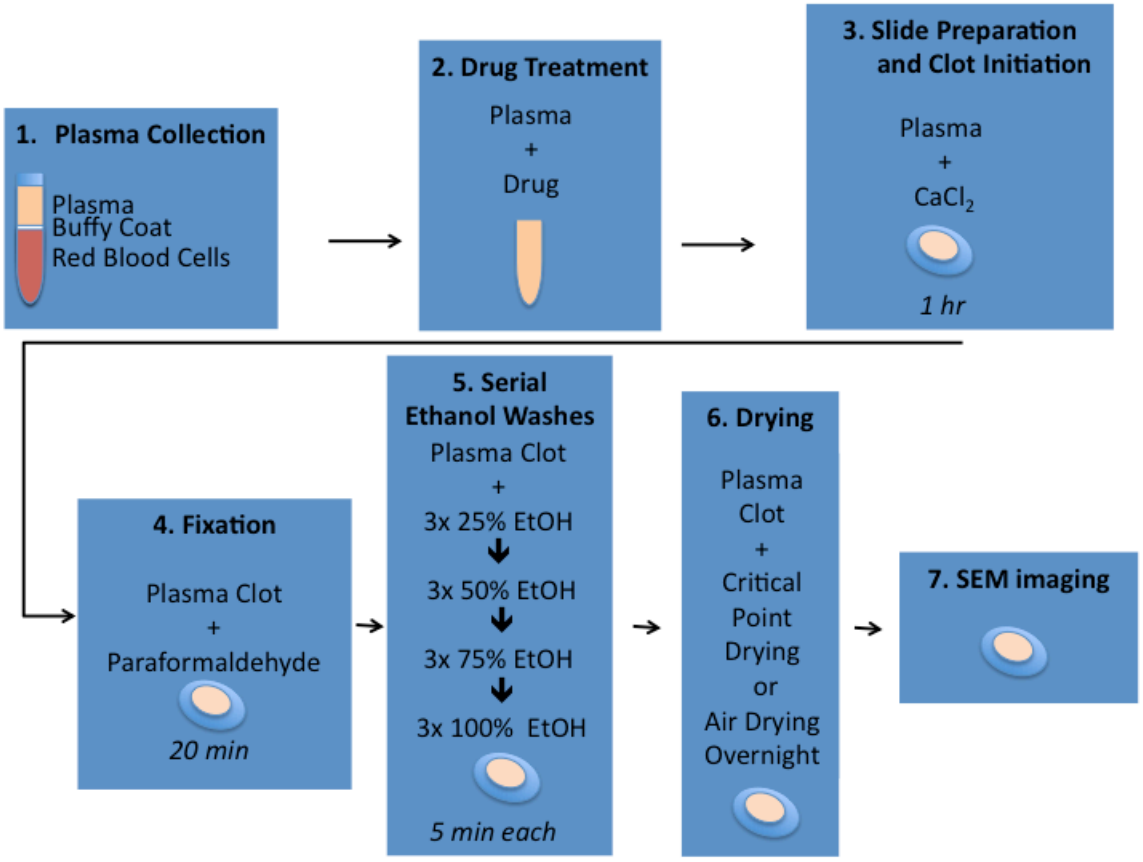

Figure 4-11 | SEM sample preparation protocol. In preparation for SEM imaging citrated plasma clot samples were drug treated and then recalcified, placed on a glass coverslip and allowed to clot for 1 hour. The plasma clot was then fixed with paraformaldehyde for 20 minutes and then washed with a series of increasing ethanol washes. The samples were then dried either by critical point drying or air drying in a vacuum chamber overnight.

SEM imaging

PELCO© colloidal graphite (Ted Pella, Redding, CA, USA) was used to attach the coverslip to a 1/2 inch diameter aluminum specimen mount (pedestal) with a 1/8 inch pin (Ted Pella, Redding, CA, USA). A carbon bridge (**Fig. 4-12**) was made by applying the colloidal graphite on one section of the coverslip continuously from the top of the coverslip to the side of the pedestal. The sample pedestal was left at room temperature for 5 minutes to dry. SEM images were collected using a

Phenom™ Pure (PhenomWorld, Eindhoven, Netherlands). The sample was placed into a sample holder cartridge for loading and inserted into the machine for imaging. Images were collected using the Phenom™ imaging software and saved in TIFF format.

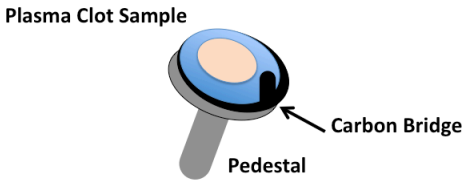

Figure 4-12 | SEM pedestal schematic. Colloidal graphite was used to bond the glass coverslip to the pedestal and a line of graphite (carbon bridge) was made to contact the top surface of the coverslip with the base of colloidal paint to reduce charge buildup on the sample.

Fibrinogen fluorescent label conjugation

The fluorescent dye Oregon Green® 488 carboxylic acid succinimidyl ester, 5 isomer (Life Technologies, Grand Island, NY, USA) was conjugated to human fibrinogen (Sigma Aldrich, St. Louis, MO, USA) for fluorescence microscopy imaging by a succinimidyl ester amine reaction to the fibrinogen protein. A 100 µL volume of 10mg/mL Oregon Green® 488 succinimidyl ester in DMSO was added to 1mL of a 10mg/mL solution of fibrinogen in 0.1M sodium bicarbonate buffer. Due to light sensitivity of the dye, the microcentrifuge tube containing the reaction solution was wrapped in foil for 1 hr on a Roto-torque (Cole Parmer, Vernon Hills, IL, USA) for mixing.

Differential Interference Contrast (DIC) and fluorescence microscopy

For DIC and Fluorescence microscopy imaging (**Fig. 4-13**) 0.5 mL of plasma were collected into a microcentrifuge tube and where required fibrin was fluorescently labeled at ~2% of the normal plasma fibrin concentration of 2500 µg/mL (J. W. Weisel 2005) (40 µg/mL) by addition of human fibrinogen Oregon Green® 488 conjugate (Life Technologies, Grand Island, NY, USA) or human fibrinogen Oregon Green® 488 conjugate produced by succinimidyl ester amine reaction as described in the fibrinogen fluorescent label conjugation section. Drug treatments such as PP2 (10 µM), PP3 (10 µM), abciximab (20 µg/mL), or calcium ionophore (10 µM) when used were added at this time to the specified concentration. When calcium imaging was performed Fluo 4 AM (Life Technologies, Grand Island, NY, USA) was added to a final concentration of 8 µM and the sample was kept at room temperature for 30 minutes. The samples were initiated to clot by recalcification of the sample to 7.681mM with $CaCl_2$. A 20 µL volume of the plasma was transferred onto a 24 mm x 50 mm glass coverslip (Fisher Scientific, Pittsburgh, PA, USA) and covered with a 18 mm square glass coverslip for clotting (Fisher Scientific, Pittsburgh, PA, USA). Samples were left in a humidified chamber at room temperature for 20 min before imaging. Imaging was performed on either an Eclipse TE300 (Nikon Instruments, Melville, NY, USA) with a 60x oil immersion objective using a VIXIA HF S21 camcorder (Canon, Melville, NY, USA) or an Olympus IX51 microscope with a 40x air objective (Olympus America, Center Valley, PA, USA) using a Retiga-4000RV

digital CCD camera (QImaging, Burnaby, BC, Canada) controlled via Q-Capture Pro 7 software (QImaging, Burnaby, BC, Canada).

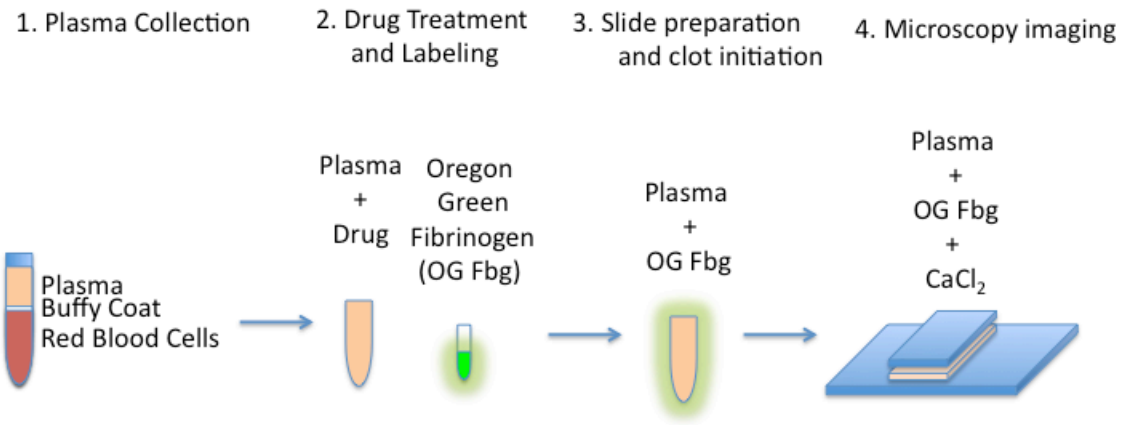

Figure 4-13 | DIC and fluorescence microscopy sample preparation protocol. Citrated plasma samples were drug treated, Oregon Green fibrinogen was added to fluorescently label fibrin, and finally the samples were recalcified to initate clotting and placed on a glass coverslip for imaging.

Fiber diameter analysis

Fluorescence and SEM images were analyzed for fibrin fiber diameters (**Fig. 4-14**) using the line tool and plot profile function in ImageJ. Lines were drawn perpendicularly across the fiber and the position of the line was saved as a region of interest and the line histogram intensities (**Fig. 4-15**) produced by the plot profile function were saved as a matrix. A MATLAB function created by Patrick Egan and available at (http://www.mathworks.com/matlabcentral/fileexchange/10590-fwhm) for full width half max determination was used to determine the fibrin fiber diameters from the line histogram matrices. The fiber diameter determination for the line

histograms was accepted if the histogram was determined to have a positive polarity and the diameter determined was not a NaN.

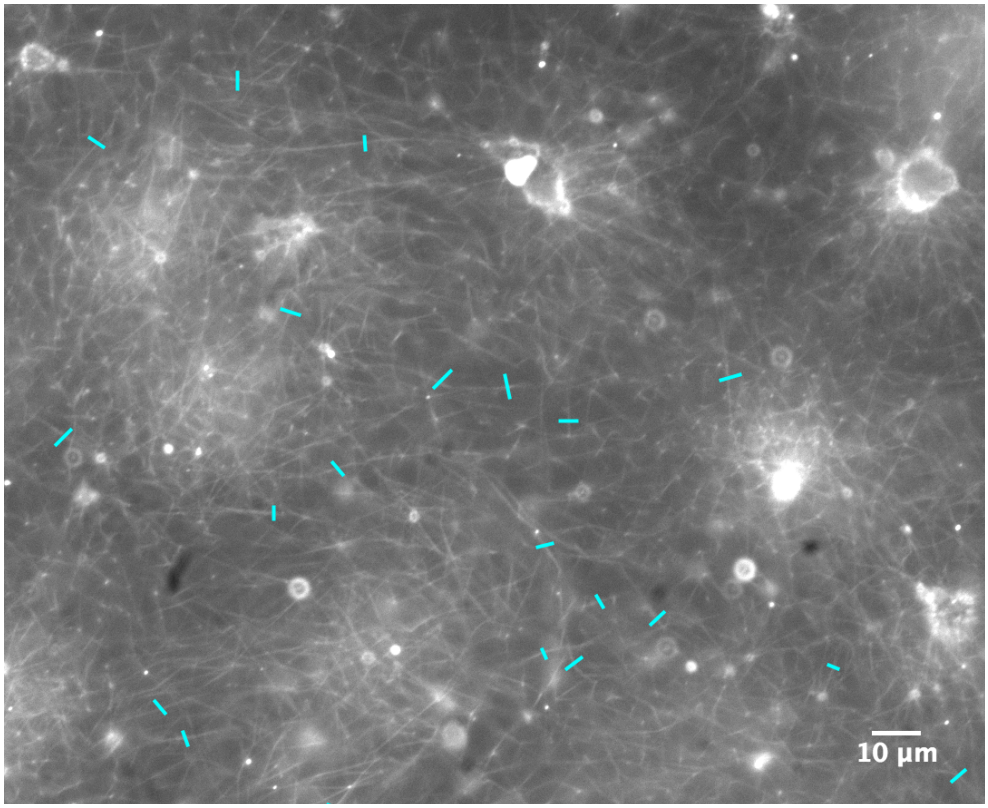

Figure 4-14 | Fiber diameter analysis. Fiber diameters were measured in fluorescence images of fibrin labeled platelet rich plasma clots by drawing lines perpendicular to the fiber with the line tool in ImageJ.

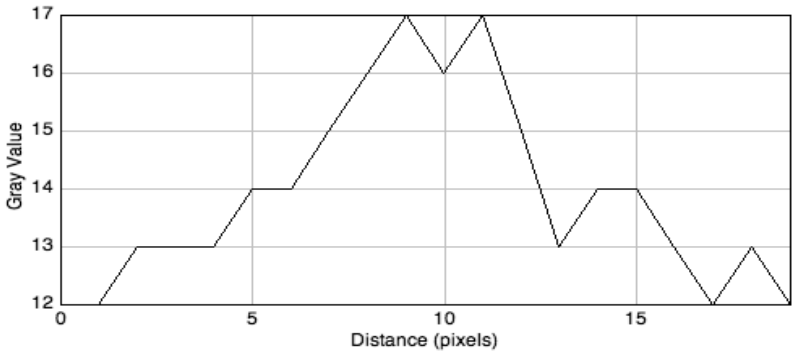

Figure 4-15 | Fiber diameter line histogram. Line histograms of pixel number along the line versus pixel intensity were generated using the plot profile function in ImageJ. The full width half max of the histogram was determined to measure the fibrin fiber diameter.

Fiber porosity analysis

Fluorescence and SEM images were analyzed for fibrin network porosity (**Fig. 4-16**) using thresholding with the Otsu function in ImageJ. The regions selected by the Otsu method thresholding were saved as regions of interest and converted to a binary image for determination of porosity of the fibrin network by the area fraction function of the image.

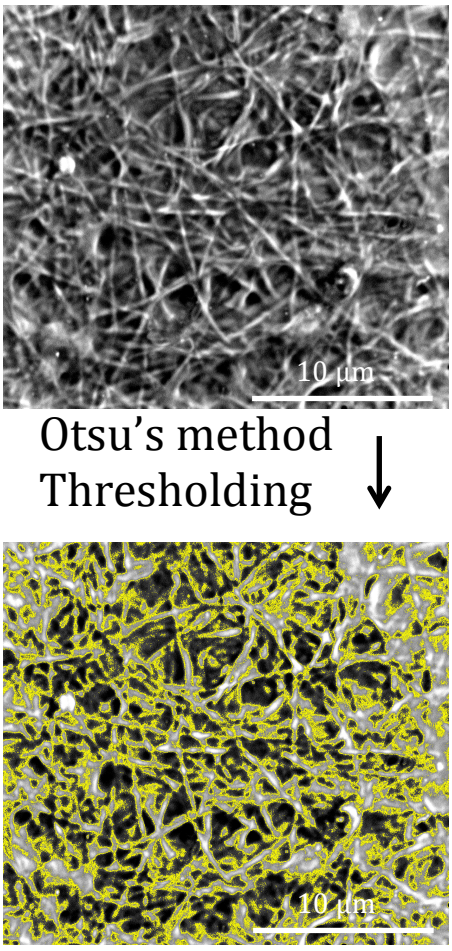

Figure 4-16 | Fibrin network porosity analysis. The porosity of the fibrin network was determined in images of plasma clots by thresholding using Otsu's method creating a region of interest that separates the fibers in the foreground from the background space.

Cell cluster size analysis

DIC microscopy images were analyzed for cell cluster size using the polygon selection tool (**Fig. 4-17**) and saving each cell cluster polygon as a region of interest. The selected regions of interest were analyzed for surface area using the area measurement tool.

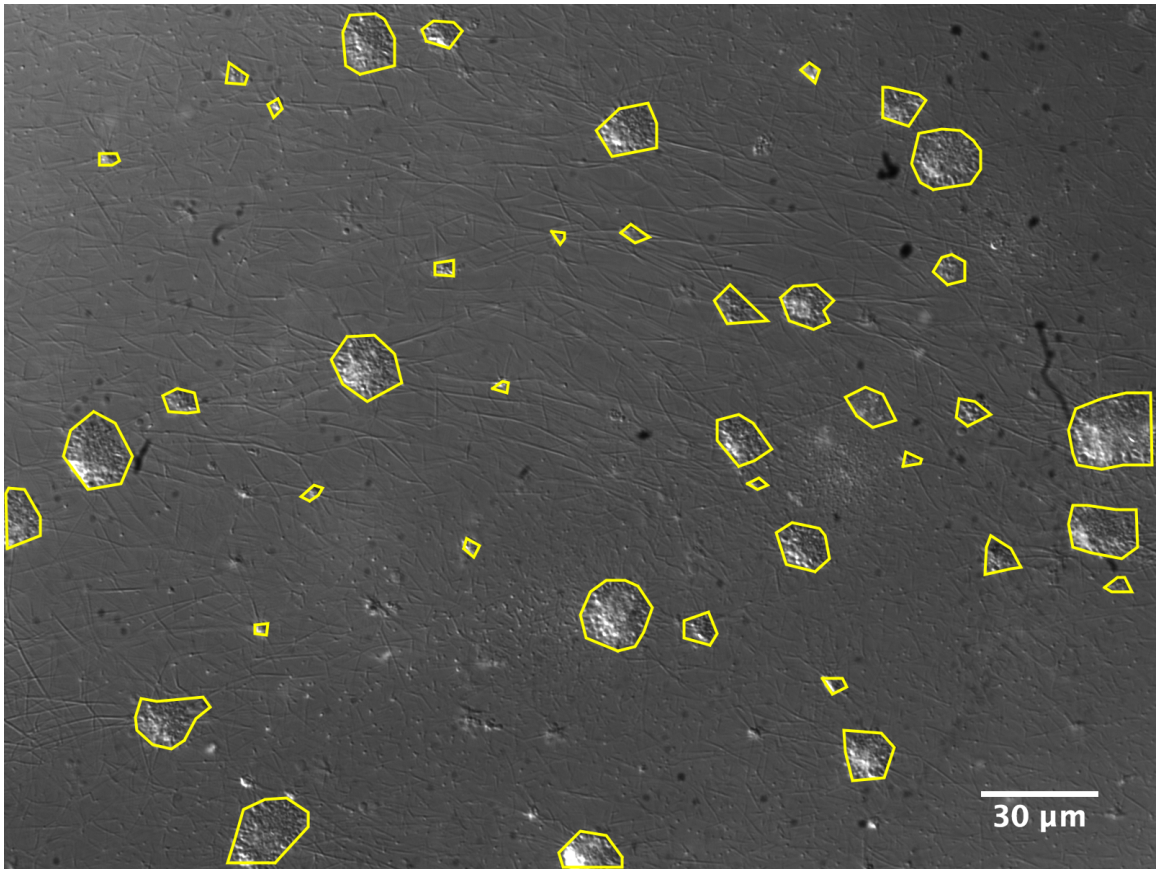

Figure 4-17 | Cell cluster size analysis. Polygon regions of interest were drawn around cell clusters in DIC images of platelet rich plasma clots using ImageJ. Cell clusters that were not greater than the platelet diameter (4 µm) were excluded.

Calcium imaging analysis

Fluorescence microscopy images were analyzed for platelet calcium levels using thresholding by the Otsu method in ImageJ. The regions selected by the Otsu method thresholding were saved as regions of interest. The regions of interest were then analyzed using the mean grey value measurement function. The platelet calcium levels were normalized and reported as Fluo 4 platelet relative fluorescence based on citrated platelet rich plasma as a negative control and calcium ionophore treated platelet rich plasma as a positive control by the following equation

$$Fluo\ 4\ Platelet\ Relative\ Fluorescence = \frac{(FIU - Citrated_m)}{(Ca\ Ionophore_m - Citrated_m)}, \quad (1)$$

where *FIU* is the mean fluorescence intensity of the image as determined by the mean grey value function, $Citrated_m$ is the mean fluorescence intensity of images of citrated platelet rich plasma samples, and $Ca\ Ionophore_m$ is the mean fluorescence intensity of images of calcium ionophore treated platelet rich plasma samples.

RESULTS

Platelet rich and platelet poor plasma - optical ARF clot stiffness measurement

The optical ARF clot stiffness assessment technique was used to assess the contribution of platelets to clot stiffness (**Fig. 4-18**). When kaolin was added to

platelet rich plasma and platelet poor plasma clot stiffness increased within minutes, as measured using optical ARF clot stiffness assessment. The maximum stiffness of platelet rich plasma was 6.9 fold stiffer than platelet poor plasma. Analysis using the Kelvin-Voigt model showed that the elasticity of platelet rich plasma clots develops more quickly and to a greater maximum elasticity than the platelet poor plasma clot, while viscosity developed in a comparable manner in both plasma clots.

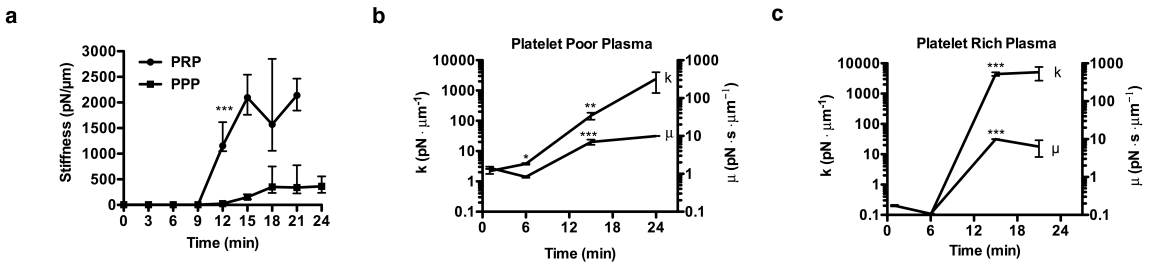

Figure 4-18 | Stiffness of clotting platelet rich (PRP) and platelet poor plasma (PPP) as optically assessed by ARF application. (**a**) Clot stiffness of 5 μg/mL kaolin induced clotting PRP and PPP was determined. Bead displacements (n = 5) were averaged to compute stiffness, which is displayed with 60% quartiles (***, p<0.0005 between PPP and PRP from t > 12 min). (**b-c)** Kelvin-Voigt viscous (μ) and elastic (k) parameters of PPP and PRP were determined. Standard error is shown with n=5 beads per time point (* ,p<0.05)(**, p<0.006)(***,p<0.0005). (**b**) During clotting in the PPP sample the Kelvin-Voigt viscous (μ) and elastic (k) parameters increased 1107 fold and 6.9 fold respectively. (**c**) During clotting in the PRP sample the average fold difference of viscous (μ) and elastic (k) parameters of the clot as compared to PPP between 15 and 21 min were 1.3 fold and 11 fold larger, respectively.

While removing platelets by centrifugation demonstrated that platelets contribute to clot stiffness the mechanism of action of platelet stiffening of the clot was not elucidated. Catalysis of thrombin generation leading to higher thrombin concentrations in clots with platelets may lead to increased clot stiffness. Platelets may also create tension and increased stiffness in the clot by

contracting on fibrin through integrin IIb-IIIa binding and myosin activity on the actin cytoskeleton. Platelet inhibiting drugs could be used to determine the relative contributions of thrombin generation and integrin IIb-IIIa related platelet contractility on clot stiffness.

Platelet rich and platelet poor plasma –SEM imaging

SEM imaging was performed on platelet rich and platelet poor plasma clots (**Fig. 4-19**) in order to assess clot structural properties of fibrin fiber tortuosity, fiber diameter, and fibrin network porosity. Tortuosity is a property of how bent or loopy fibers are in a network. Platelet rich plasma clots fibrin networks were qualitatively less tortuous than those of platelet poor plasma clots. The reduced tortuosity may indicate platelet tensioning of the fibrin fibers.

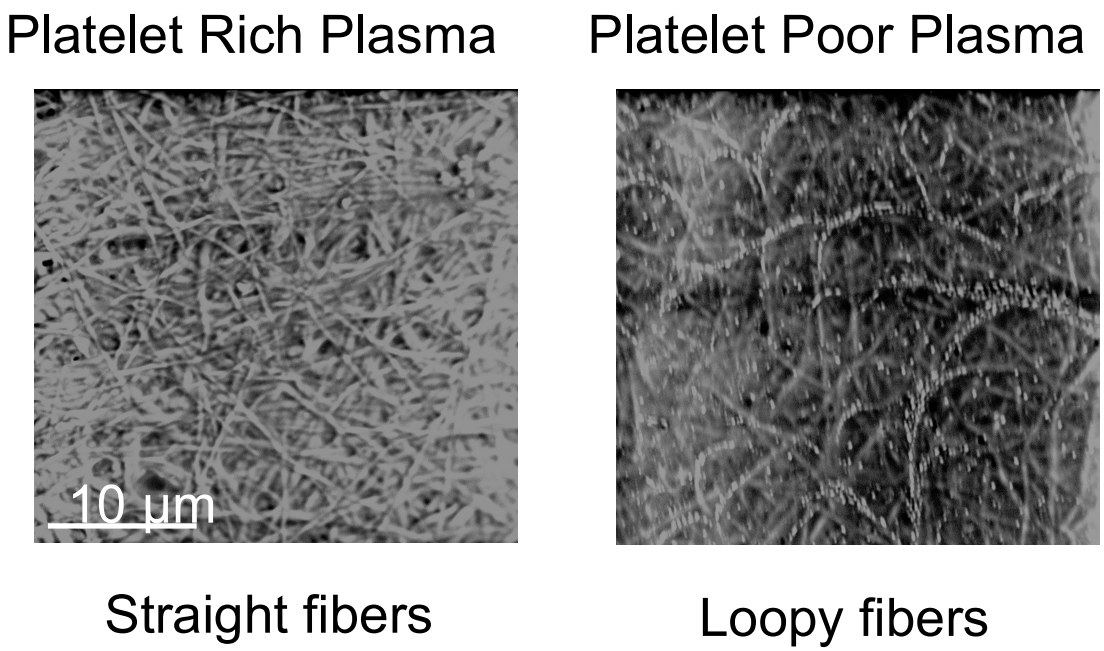

Figure 4-19 | SEM images of platelet rich and platelet poor plasma clots. Platelet rich and platelet poor plasma samples were recalcified with $CaCl_2$ (11.811 mM) to initiate clotting and fixed with paraformaldehyde after 1 hr. Platelet rich plasma clots had qualitatively reduced fibrin fiber tortuosity.

With fibrin fiber diameter analysis (**Figure 4-20**) platelet poor plasma clots had fibrin fiber diameters that were 18% reduced as compared to fibers in platelet rich plasma clots. The reduced fibrin fiber diameter with removal of platelets from plasma clots suggested that platelets may modulate clot structure correlated with the changes in clot stiffness described above, but the mechanism of platelet action was not interrogated.

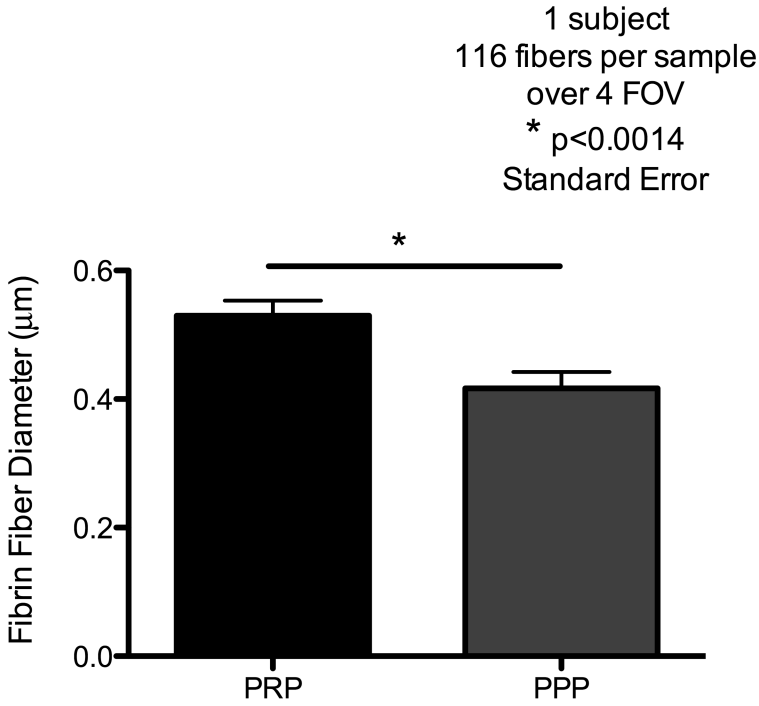

Figure 4-20 | Fibrin fiber diameter analysis of SEM images of platelet rich and platelet poor plasma clots. Platelet rich and platelet poor plasma samples were recalcified with $CaCl_2$ (11.811 mM) to initiate clotting and fixed with paraformaldehyde after 1 hr. Fibrin fiber diameter was reduced 18% in platelet poor plasma clots as compared to platelet rich plasma clots.

Porosity analysis (**Fig. 4-21**) of the platelet rich and platelet poor plasma clots showed the platelet poor plasma clots to be 50% more porous than the platelet rich plasma. The presence of platelets creating a less porous fibrin clot again demonstrated that platelets alter the fibrin structure in a profound way. Platelets have been shown to influence clot structure in fiber tortuosity, diameter, and fibrin network porosity.

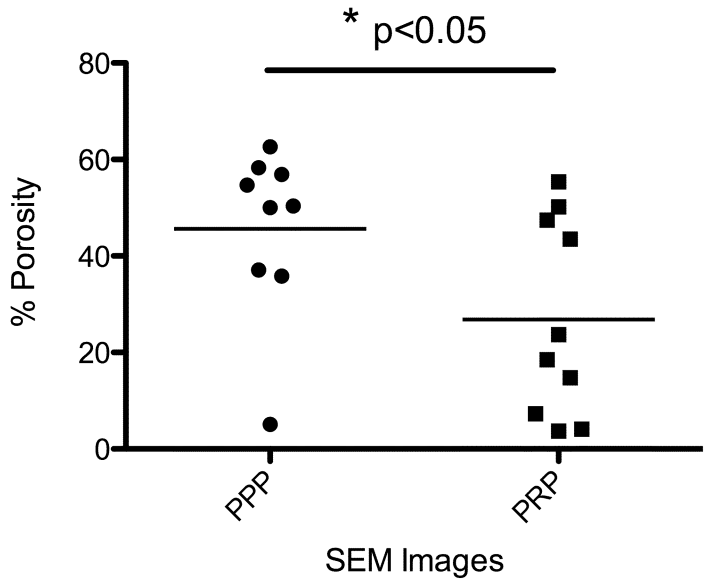

Figure 4-21 | Porosity analysis of SEM images of platelet rich and platelet poor plasma clots. Platelet rich and platelet poor plasma samples were recalcified with $CaCl_2$ (11.811 mM) to initiate clotting and fixed with paraformaldehyde after 1 hr. Platelet rich plasma clots had reduced fibrin network porosity as compared to platelet poor plasma clots. 1 subject, each point represents one field of view.

IIb-IIIa inhibited platelet rich plasma - optical ARF clot stiffness measurement

With abciximab inhibition of integrin IIb-IIIa binding to fibrin optical ARF clot stiffness assessment was performed (**Fig. 4-22**). The abciximab treated plasma clots were 50% less stiff than control platelet rich plasma clots. The reduced stiffness with abciximab treatment showed the influence of integrin IIb-IIIa adhesion on clot stiffness. Because thrombin generation by the platelet is not

controlled in the experiment, however, the effect was not conclusively separated from platelet thrombin generation by the experiment.

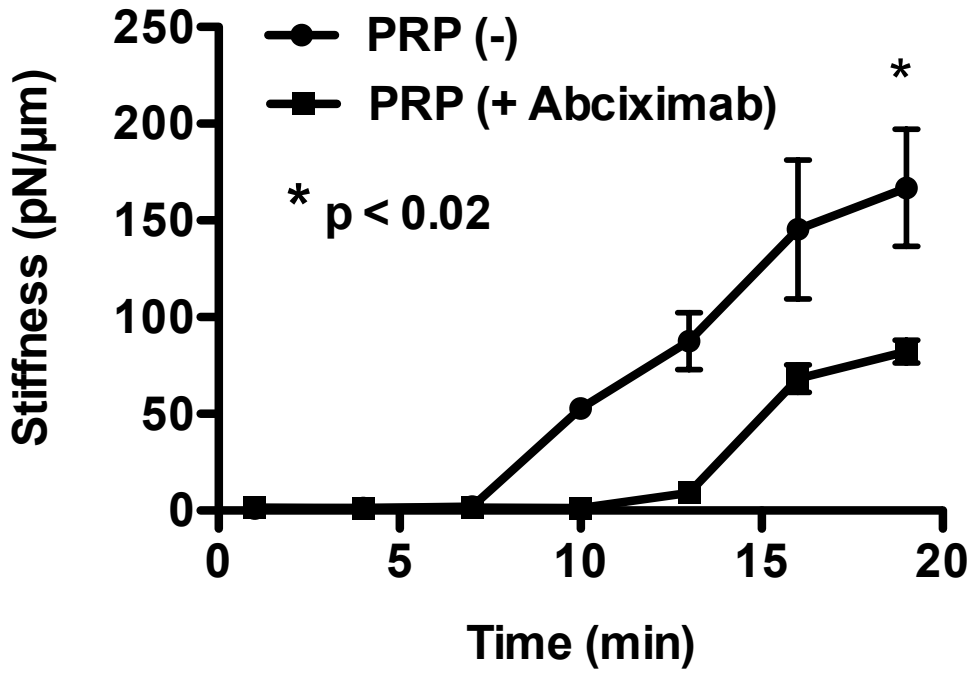

Figure 4-22 | Stiffness of clotting abciximab IIb-IIIa inhibition of platelet rich plasma (PRP) as optically assessed by ARF application. Abciximab treated platelet rich plasma had 50% reduced clot stiffness as compared to control. Abciximab (18 µg/mL) and 15 µm polystyrene beads (0.5 x 10^6 / mL) were added. 1 subject, standard error is shown with n=5 beads per time point.

IIb-IIIa inhibited platelet rich plasma - DIC and fluorescence Imaging

Clot structure was examined in abciximab inhibited plasma clots using DIC and fluorescence microscopy imaging (**Fig. 4-23**). Fibrin fiber diameter analysis and platelet cluster size determination were performed on the plasma clots that were labeled for fibrin fluorescence.

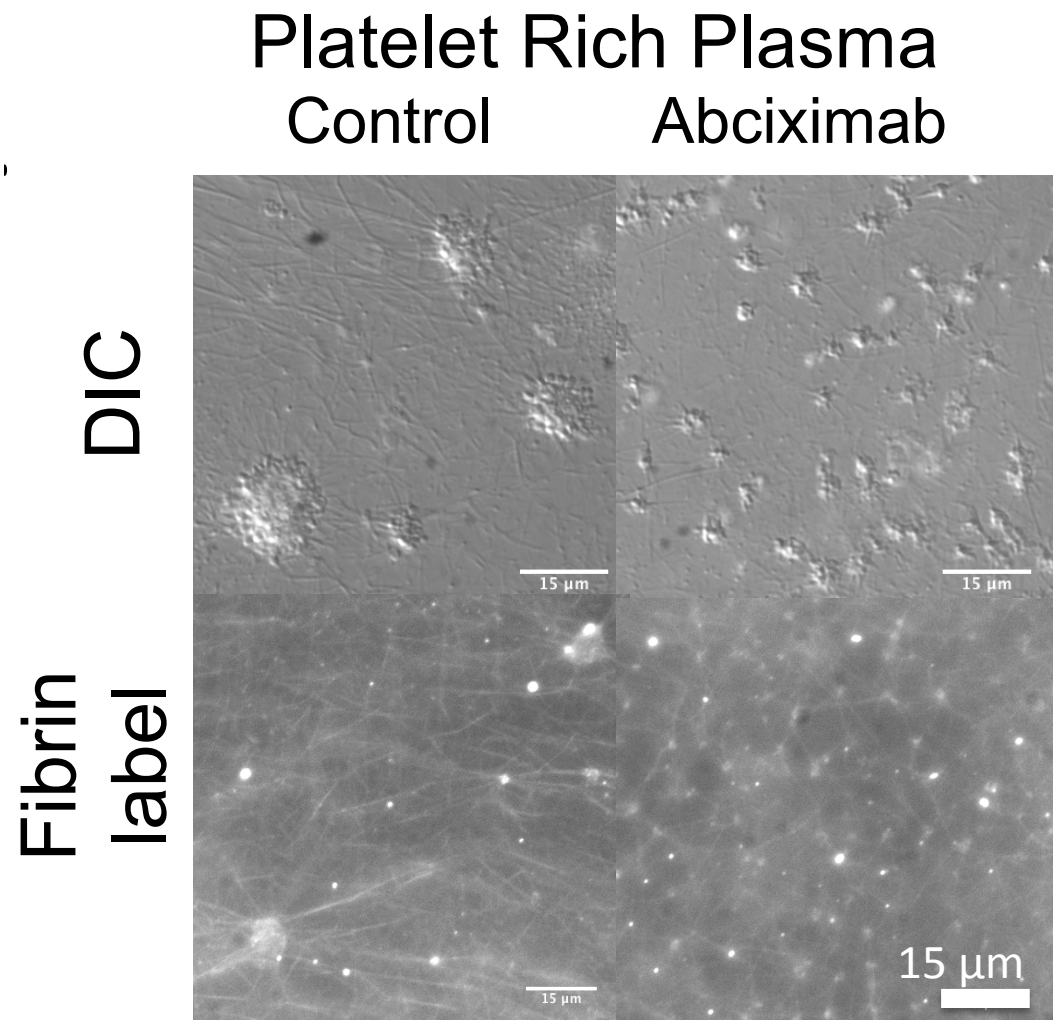

Figure 4-23 | DIC and fluorescence microscopy images of platelet rich plasma with abciximab IIb-IIIa inhibition. Fibrin fiber diameter and platelet cluster size qualitatively appear to be reduced with abciximab inhibition (20 µg/mL) of IIb-IIIa. Images were taken 1 hour after recalcification with $CaCl_2$ (11.811 mM).

With abciximab inhibition fibrin fiber diameter was reduced by 40% (**Fig. 4-24**). The reduced fibrin fiber diameter of abciximab treated plasma clots as compared to control platelet rich plasma clots showed that the integrin IIb-IIIa is involved in modulating clot structure. With a correlation between clot stiffness and fibrin fiber

diameter reduction with abciximab treatment of plasma clots, integrin IIb-IIIa may be altering fibrin fiber size and increasing clot stiffness.

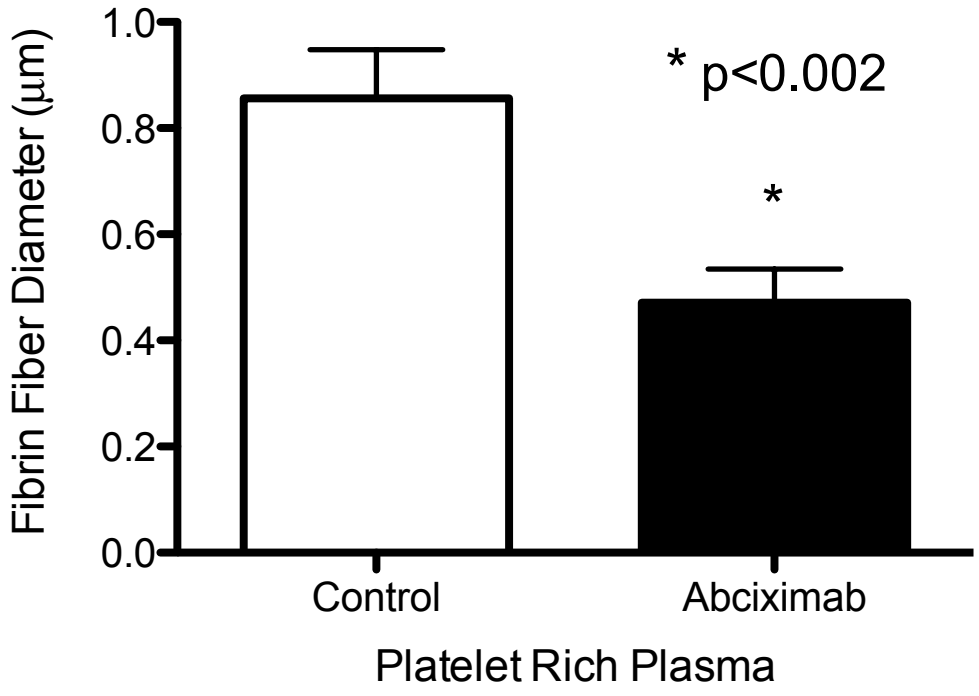

Figure 4-24 | Fibrin fiber diameter analysis of fluorescence microscopy images of abciximab IIb-IIIa inhibited platelet rich plasma. Abciximab inhibition (20 μg/mL) of IIb-IIIa in platelet rich plasma clots reduced fibrin fiber diameter by 40% as compared to uninhibited platelet rich plasma control. Images were taken 1 hour after recalcification with $CaCl_2$ (11.811 mM). 1 subject, standard error is shown with 150 fibers per sample over at least 3 fields of view.

With abciximab treatment platelet cluster size in the clots, reported as surface area per cell cluster (**Fig. 4-25**), is reduced 79%. Platelet clustering due to interaction of integrin IIb-IIIa with fibrin may be important for clot stiffening.

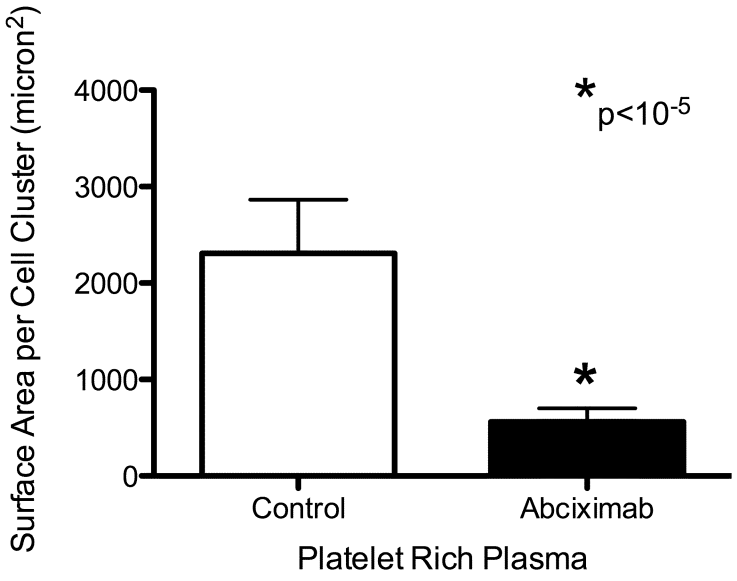

Figure 4-25 | Platelet cluster size analysis. Platelet cluster size was reduced with abciximab inhibition (20 μg/mL) of IIb-IIIa in platelet rich plasma. Images were taken 1 hour after recalcification with $CaCl_2$ (11.811 mM). 1 subject, standard error is shown for cell cluster traces over 9 fields of view.

DISCUSSION

The experiments described in Chapter 4 suggest that increased fibrin network density, fibrin fiber diameter, and platelet cluster size due to platelet adhesion to fibrin through integrin IIb-IIIa are correlated with increased clot stiffness. Integrins are known to cluster with activation, or increased ligand binding affinity (**Fig. 4-1**). Integrin clustering may serve to additionally increase the interaction of the integrin with fibrin, due to avidity. Integrin IIb-IIIa binding to fibrin may initiate changes in the platelet that lead to integrin clustering. Larger fibrin fiber formation may occur if integrins and fibrin are brought into close proximity during integrin clustering. The close proximity of fibrin protofibrils may lead to bundling of the protofibrils into larger fibrin fibers.

Integrin IIb-IIIa interaction with fibrin may also increase stiffness through platelet contractility. The platelet cytoskeleton is linked to the integrin IIb-IIIa through talin (O'Halloran, Beckerle, and Burridge 1985). During platelet activation, the action of myosin IIa on the cytoskeleton and integrin signaling regulated cytoskeletal remodeling may result in changes in platelet contractility. The timing of platelet contractile response may be important for the development of clot stiffness and for the formation of fibers and the size of the fibers formed. Platelet contractility may drive the formation of integrin clusters. If, however, membrane diffusion drives integrins to cluster, reduced platelet contractility might allow clustering, while contractility after clustering could increase tension on the fibrin fiber network and stiffen the blood clot. Because platelet contractility may tension the fibrin network, fibrin fibers formed with integrin IIb-IIIa fibrin interactions may be less tortuous, in addition to being larger.

Some preliminary experiments were performed that explore the possible link between signaling events downstream of integrin IIb-IIIa binding to fibrin and modulation of clot structure and clot stiffness. Prior literature suggests that protein kinase activity initiated by integrin IIb-IIIa binding to fibrin modulates myosin activity and platelet spreading. The signaling of these protein kinases may effect the interaction of the platelet with the fibrin network and have implications for the fibrin network structure and clot stiffness.

The link between a signaling molecule Src kinase and potential downstream effects of platelet signaling on contractility, clot stiffness, and fibrin fiber structure was investigated using Src kinase inhibitor PP2. A speculative schematic of temporal changes in Src kinase activity and myosin IIa activity is shown in **Fig. 4-26**. The impact of such a temporal change in Src kinase on clot stiffness might be to allow for greater interaction of the platelet with the fibrin network through a period of reduced myosin IIa activity (platelet spreading), after which the platelet can generate more tension in the fibrin network when myosin IIa activity is increased (clot retraction).

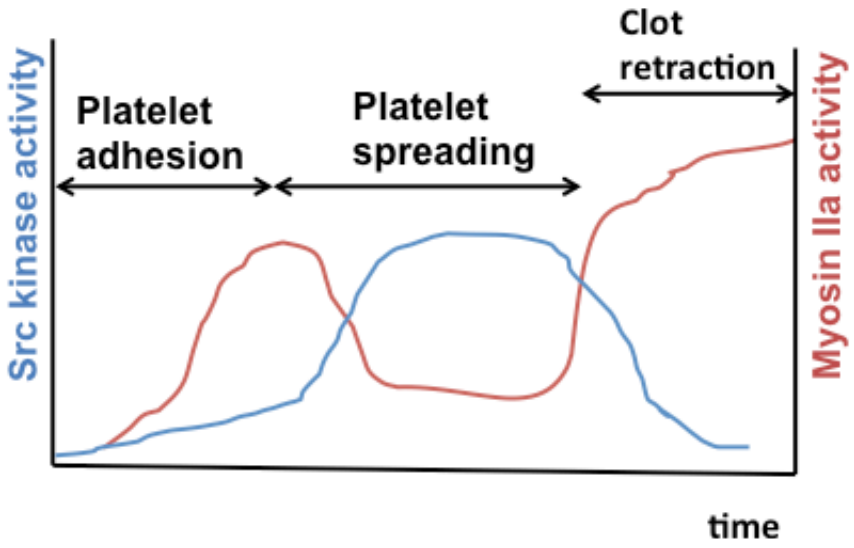

Figure 4-26 | Proposed transient platelet contraction and clot stiffness model. We propose a model of integrin IIb-IIIa outside-in signaling in which fibrin binding leads to a transient Src kinase activation disrupting myosin IIa activity and platelet contraction and causing a period of platelet spreading (Shen, Delaney, and Du 2012). The implications of such a signaling process on clot stiffness and structure are not known.

Platelet rich plasma with Src kinase inhibition – Clot stiffness assessment by sonorheometry

In a preliminary experiment, sonorheometry was used to assess the inhibitory effect of PP2, a Src kinase inhibitor, on plasma clot stiffness (**Fig. 4-27**). PP2 inhibition of Src kinase increased the rate of clot stiffness development in the plasma clot, but the clot stiffness was sharply reduced after 15 minutes. The reduced clot stiffness was an unexpected result of the PP2 treatment. Repeated clot stiffness measurements of PP2 inhibited plasma clotting could be performed to further investigate the PP2 inhibitory effect on plasma clot stiffness.

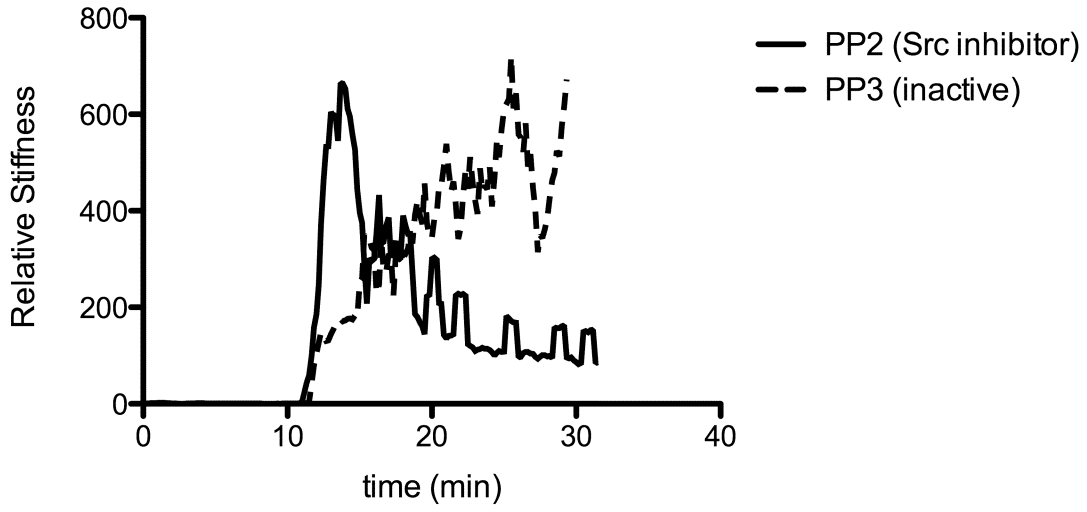

Figure 4-27 | Sonorheometry assessment of PP2 Src kinase inhibited plasma clot stiffness. Clotting was initiated by addition of kaolin (5 µg/mL) and recalcification with $CaCl_2$ to (9.525 mM). With sonorheometry assessment of platelet rich plasma clot stiffness Src kinase inhibition (10 µM) resulted in an initial sharp increase in clot stiffness and then a precipitous drop off of clot stiffness relative to control, inactive PP3 (10 µM) treated plasma clot. Subject 1, n=1 .

Platelet rich plasma with Src kinase inhibition – Calcium imaging using fluorescence microscopy

Platelet intracellular calcium levels were measured in plasma clots using DIC and fluorescence microscopy imaging and calcium sensitive fluorescent dye Fluo 4 (**Fig. 4-28**).

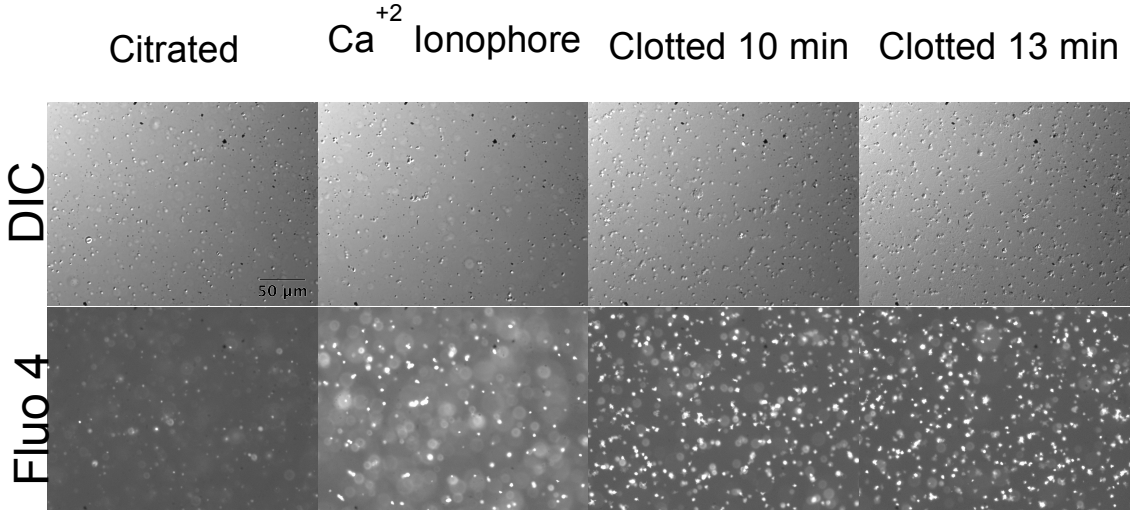

Figure 4-28 | Calcium imaging of platelet rich plasma clots. In platelet rich plasma clots calcium imaging using Fluo 4 (8 µM) shows an increase in platelet calcium levels with initiation of clotting and between clots at 10 minutes and 13 minutes. Calcium ionophore (10 µM) opens platelet plasma membrane calcium channels and is a positive control for resting platelet calcium concentration.

Platelet calcium levels in plasma with PP2 inhibition were significantly reduced, nearly to the level of citrated plasma (**Fig. 4-29**). Although PP3 controls were also significantly reduced in their platelet intracellular calcium, the effect appears to be more pronounced with the PP2 inhibition. PP3 inhibitory effect may be due to the DMSO vehicle of both PP2 and PP3. Repetitions of the calcium signaling experiment could be performed to improve characterization of platelet intracellular calcium inhibition with PP2. Because myosin IIa activity is calcium

sensitive, and platelet calcium release is one of the processes of platelet signaling in activation from clotting stimulus, reduced platelet calcium levels suggest reduced platelet contractile ability with Src kinase inhibition.

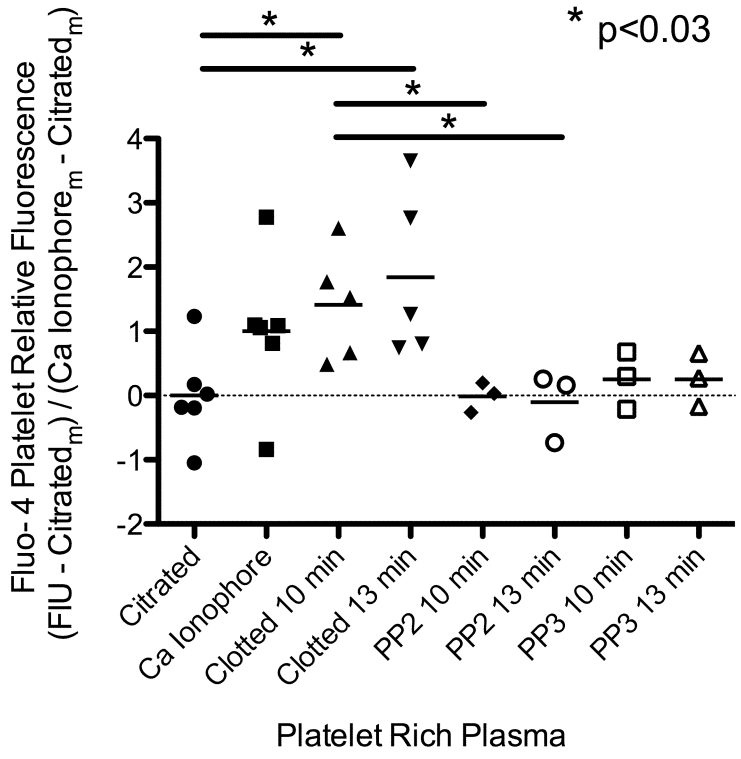

Figure 4-29 | Analysis of calcium levels in platelet rich plasma clots with PP2 inhibition of Src kinase. In platelet rich plasma clots calcium imaging using Fluo 4 (8 μM) shows calcium levels were reduced with PP2 inhibition. Calcium levels were also significantly reduced in PP3 inactive control, perhaps due to inhibitory effects of the DMSO vehicle. Calcium ionophore (10 μM) opens platelet plasma membrane calcium channels and is a positive control for resting platelet calcium concentration.

The preliminary work presented examining the impact of Src kinase activity on clot stiffness and platelet calcium levels suggests that Src kinase activity may promote increased clot stiffness in platelet rich plasma clots and involve changes in myosin IIa activity. Clot stiffness was reduced with Src kinase inhibition by PP2

in a sonorheometry clot stiffness assessment and calcium imaging of Src kinase inhibited platelet rich plasma clots revealed reduce calcium levels as compared to uninhibited controls. Although these experiments support the hypothesis of integrin IIb-IIIa related signaling processes promoting clot stiffness and structural modulation through regulation of myosin IIa activity the phenomenon could be better characterized and additional specific inihibitions in clot stiffness and structural studies could be performed including blebbistatin inhibition and manganese enhancement of integrin IIb-IIIa binding affinity.

In future work, image analysis techniques analyzing clot structure could be designed to reduce potential for human bias. The analysis technique used for determination of fibrin fiber diameter used manual choice of fiber and alignment of the line perpendicular to the fiber of interest. The human bias of choice could be limited for example by use of a random point generator to direct the user to draw a line perpendicular to the nearest fiber to the point. Human bias in the fibrin fiber diameter analysis could be additionally reduced by use of a computational algorithm that skeletonizes the fibrin network through image thresholding. With a skeletonized image the fibrin fiber diameter analysis could be performed in the context of a fibrin fiber skeleton.

For image analysis to quantify fibrin network properties, additional analysis techniques could identify new fibrin network structural characteristics that are modulated by the interaction of platelet integrin IIb-IIIa with the fibrin network.

Although parameters of fibrin network structure explored in this dissertation (fibrin fiber diameter, fibrin network porosity, and platelet cluster size) were shown to be correlated with integrin IIb-IIIa interaction with fibrin and clot stiffness, other parameters describing clot structure may more sensitively track with clot stiffness. A sensitivity analysis of fibrin network parameters and modulation of clot stiffness could be performed and might guide a choice of clot structural attributes to engineer to produce desirable clot mechanical properties.

REFERENCES

Blair, Price, and Robert Flaumenhaft. 2009. “Platelet A-Granules: Basic Biology and Clinical Correlates.” *Blood Reviews* 23 (4): 177–89. doi:10.1016/j.blre.2009.04.001.

Boggon, Titus J, and Michael J Eck. 2004. “Structure and Regulation of Src Family Kinases.” *Oncogene* 23 (48): 7918–27. doi:10.1038/sj.onc.1208081.

Bresnick, A R. 1999. “Molecular Mechanisms of Nonmuscle Myosin-II Regulation.” *Current Opinion in Cell Biology* 11: 26–33. doi:10.1016/S0955-0674(99)80004-0.

Calaminus, S D J, J M Auger, O J T McCarty, M J O Wakelam, L M Machesky, and S P Watson. 2007. “MyosinIIa Contractility Is Required for Maintenance of Platelet Structure During Spreading on Collagen and Contributes to Thrombus Stability.” *Journal of Thrombosis and Haemostasis* 5 (10): 2136–45. doi:10.1111/j.1538-7836.2007.02696.x.

Campbell, I D, and M J Humphries. 2011. “Integrin Structure, Activation, and Interactions.” *Cold Spring Harbor Perspectives in Biology* 3 (3): a004994. doi:10.1101/cshperspect.a004994.

Carr, Marcus E, Jr. 2003. “Development of Platelet Contractile Force as a Research and Clinical Measure of Platelet Function.” *Cell Biochemistry and Biophysics* 38 (1): 55–78. doi:10.1385/CBB:38:1:55.

Cheezum, M K, WF Walker, and W H Guilford. 2001. “Quantitative Comparison of Algorithms for Tracking Single Fluorescent Particles.” *Biophysical Journal* 81: 2378–88. doi:10.1016/S0006-3495(01)75884-5.

Cosemans, J M E M, B F Iserbyt, H Deckmyn, and J W M Heemskerk. 2008. “Multiple Ways to Switch Platelet Integrins on and Off.” *Journal of Thrombosis and Haemostasis* 6 (8): 1253–61. doi:10.1111/j.1538-7836.2008.03041.x.

E Hagemeyer, Christoph, and Karlheinz Peter. 2010. “Targeting the Platelet Integrin GPIIb/IIIa.” *Current Pharmaceutical Design* 16 (37): 4119–33. doi:10.2174/138161210794519255.

Flevaris, P, A Stojanovic, H Gong, A Chishti, E Welch, and X Du. 2007. “A Molecular Switch That Controls Cell Spreading and Retraction.” *The Journal of Cell Biology* 179 (3): 553–65. doi:10.1083/jcb.200703185.

Fox, Joan E B, and Sanford J Shattil. 1996. “The Platelet Cytoskeleton Stabilizes the Interaction Between Alpha(IIb)Beta(3) and Its Ligand and Induces Selective Movements of Ligand-Occupied Integrin.” *Journal of Biological Chemistry* 271 (12): 7004–11. doi:10.1074/jbc.271.12.7004.

Ginsberg, M H, A Partridge, and S J Shattil. 2005. “Integrin Regulation.” *Current Opinion in Cell Biology* 17: 509–16.

Goggs, Robert, and Alastair W Poole. 2012. “Platelet Signaling-a Primer.” *Journal of Veterinary Emergency and Critical Care* 22 (1): 5–29. doi:10.1111/j.1476-4431.2011.00704.x.

Goncalves, I. 2003. “Integrin αIIb B3-Dependent Calcium Signals Regulate Platelet-Fibrinogen Interactions Under Flow: Involvement of Phospholipase Cγ2.” *Journal of Biological Chemistry* 278 (37): 34812–22.

doi:10.1074/jbc.M306504200.
Goodman, S L. 1999. “Sheep, Pig, and Human Platelet-Material Interactions with Model Cardiovascular Biomaterials.” *Journal of Biomedical Materials Research* 45 (3): 240–50. doi:10.1002/(SICI)1097-4636(19990605)45:3<240::AID-JBM12>3.0.CO;2-C.
Goschnick, M W. 2006. “Impaired ‘Outside-in’ Integrin IIbbeta3 Signaling and Thrombus Stability in TSSC6-Deficient Mice.” *Blood* 108 (6): 1911–18. doi:10.1182/blood-2006-02-004267.
Hanke, Jeffrey H, Joseph P Gardner, Robert L Dow, Paul S Changelian, William H Brissette, Elora J Weringer, Brian A Pollok, and Patricia A Connelly. 1996. “Discovery of a Novel, Potent, and Src Family-Selective Tyrosine Kinase Inhibitor.” *Journal of Biological Chemistry* 271 (2): 695–701. doi:10.1074/jbc.271.2.695.
Huxley, A F. 1957. “Muscle Structure and Theories of Contraction.” *Progress in Biophysics and Biophysical Chemistry*, January, 255–318.
Hynes, Richard O. 2002. “IntegrinsBidirectional, Allosteric Signaling Machines.” *Cell* 110 (6): 673–87. doi:10.1016/S0092-8674(02)00971-6.
Janmey, Paul A. 1998. “The Cytoskeleton and Cell Signaling: Component Localization and Mechanical Coupling.” *Physiological Reviews* 78 (3): 763–81.
Jen, Chauying J, and Larry V McIntire. 1982. “The Structural Properties and Contractile Force of a Clot.” *Cell Motility* 2 (5): 445–55. doi:10.1002/cm.970020504.
Kovacs, M. 2004. “Mechanism of Blebbistatin Inhibition of Myosin II.” *Journal of Biological Chemistry* 279 (34): 35557–63. doi:10.1074/jbc.M405319200.
Kucik, Dennis F. 2002. “Rearrangement of Integrins in Avidity Regulation by Leukocytes.” *Immunologic Research* 26 (1-3): 199–206. doi:10.1385/IR:26:1-3:199.
Lee, Mei Yan, and Scott L Diamond. 2015. “PLOS Computational Biology: a Human Platelet Calcium Calculator Trained by Pairwise Agonist Scanning.” *PLoS Computational Biology* 11 (2): e1004118. doi:10.1371/journal.pcbi.1004118.
Li, Zhenyu, M Keegan Delaney, Kelly A O'Brien, and Xiaoping Du. 2010. “Signaling During Platelet Adhesion and Activation.” *Arteriosclerosis, Thrombosis, and Vascular Biology* 30: 2341–49. doi:10.1161/ATVBAHA.110.207522.
Loftus, J C. 1984. “Redistribution of the Fibrinogen Receptor of Human Platelets After Surface Activation.” *The Journal of Cell Biology* 99 (3): 822–29. doi:10.1083/jcb.99.3.822.
Ma, Y Q, Hao Qin, and E F Plow. 2007. “Platelet Integrin αIIb B3: Activation Mechanisms.” *Journal of Thrombosis and Haemostasis* 5 (7): 1345–52. doi:10.1111/j.1538-7836.2007.02537.x.
Manning, G. 2002. “The Protein Kinase Complement of the Human Genome.” *Science* 298 (12): 1912–34. doi:10.1126/science.1075762.
Mitchison, T J, and L P Cramer. 1996. “Actin-Based Cell Motility and Cell Locomotion.” *Cell* 84 (2): 371–79. doi:10.1016/S0092-8674(00)81281-7.

Munnix, Imke C A, Marijke J E Kuijpers, Jocelyn Auger, Christella M L G D Thomassen, Peter Panizzi, Marc A M van Zandvoort, Jan Rosing, Paul E Bock, Steve P Watson, and Johan W M Heemskerk. 2007. “Segregation of Platelet Aggregatory and Procoagulant Microdomains in Thrombus Formation.” *Arteriosclerosis* 27: 2484–90. doi:10.1161/ATVBAHA.107.151100.

Nicholson, Nancy S, Susan G Panzer-Knodle, Neal F Haas, Beatrice B Taite, James A Szalony, Jimmy D Page, Larry P Feigen, David M Lansky, and Anita K Salyers. 1998. “Assessment of Platelet Function Assays.” *American Heart Journal* 135 (5): S170–78. doi:10.1016/S0002-8703(98)70245-5.

O'Halloran, Theresa, Mary C Beckerle, and Keith Burridge. 1985. “Identification of Talin as a Major Cytoplasmic Protein Implicated in Platelet Activation.” *Nature* 317 (10): 449–51. doi:10.1038/317449a0.

Obergfell, A. 2002. “Coordinate Interactions of Csk, Src, and Syk Kinases with alphaIIbbeta3 Initiate Integrin Signaling to the Cytoskeleton.” *The Journal of Cell Biology* 157 (2): 265–75. doi:10.1083/jcb.200112113.

Ono, A, E Westein, S Hsiao, W S Nesbitt, J R Hamilton, S M Schoenwaelder, and S P Jackson. 2008. “Identification of a Fibrin-Independent Platelet Contractile Mechanism Regulating Primary Hemostasis and Thrombus Growth.” *Blood* 112 (1): 90–99. doi:10.1182/blood-2007-12-127001.

Park, K, F W Mao, and H Park. 1990. “Morphological Characterization of Surface-Induced Platelet Activation.” *Biomaterials* 11 (1): 24–31. doi:10.1016/0142-9612(90)90047-T.

Petrich, Brian G, Per Fogelstrand, Anthony W Partridge, Nima Yousefi, Ararat J Ablooglu, Sanford J Shattil, and Mark H Ginsberg. 2007. “The Antithrombotic Potential of Selective Blockade of Talin-Dependent Integrin αIIbβ3 (Platelet GPIIb–IIIa) Activation.” *J Clin Invest* 117 (8): 2250–59. doi:10.1172/JCI31024.

Schneider, C A, W S Rasband, and K W Eliceiri. 2012. “NIH Image to ImageJ: 25 Years of Image Analysis.” *Nature Methods* 9 (7): 671–75. doi:10.1038/nmeth.2089.

Shattil, Sanford J, Chungho Kim, and Mark H Ginsberg. 2010. “The Final Steps of Integrin Activation: the End Game.” *Nature Reviews Molecular Cell Biology* 11 (4). Nature Publishing Group: 288–300. doi:10.1038/nrm2871.

Shattil, Sanford J, Hirokazu Kashiwagi, and Nisar Pampori. 1998. “Integrin Signaling: the Platelet Paradigm.” *Blood* 91: 2645–57.

Shen, Bo, M Keegan Delaney, and Xiaoping Du. 2012. “Inside-Out, Outside-in, and Inside–Outside-in: G Protein Signaling in Integrin-Mediated Cell Adhesion, Spreading, and Retraction.” *Current Opinion in Cell Biology* 24 (5): 600–606. doi:10.1016/j.ceb.2012.08.011.

Somlyo, Andrew P, and Avril V Somlyo. 2003. “Ca2+ Sensitivity of Smooth Muscle and Nonmuscle Myosin II: Modulated by G Proteins, Kinases, and Myosin Phosphatase..” *Physiological Reviews* 83 (4): 1325–58. doi:10.1152/physrev.00023.2003.

Suzuki-Inoue, K, C E Hughes, O Inoue, and M Kaneko. 2007. “Involvement of Src Kinases and PLCγ2 in Clot Retraction.” *Thrombosis Research* 120: 251–58. doi:10.1016/j.thromres.2006.09.003.

Tran, Reginald, David R Myers, Jordan Ciciliano, Elaissa L Trybus Hardy, Yumiko Sakurai, Byungwook Ahn, Yongzhi Qiu, Robert G Mannino, Meredith E Fay, and Wilbur A Lam. 2013. “Biomechanics of Haemostasis and Thrombosis in Health and Disease: From the Macro- to Molecular Scale.” *Journal of Cellular and Molecular Medicine* 20 (10): 1–18. doi:10.1111/jcmm.12041.

Tucker, Katherine L, Tanya Sage, and Jonathan M Gibbins. 2012. “Clot Retraction.” *Methods in Molecular Biology* 788: 101–7. doi:10.1007/978-1-61779-307-3_8.

van der Meijden, Paola E J, Marion A H Feijge, Frauke Swieringa, Karen Gilio, Reyhan Nergiz-Unal, Karly Hamulyák, and Johan W M Heemskerk. 2012. “Key Role of Integrin A(IIb)B (3) Signaling to Syk Kinase in Tissue Factor-Induced Thrombin Generation..” *Cellular and Molecular Life Sciences* 69 (20): 3481–92. doi:10.1007/s00018-012-1033-2.

Varga-Szabo, D, A Braun, and B Nieswandt. 2009. “Calcium Signaling in Platelets.” *Journal of Thrombosis and Haemostasis* 7 (7): 1057–66. doi:10.1111/j.1538-7836.2009.03455.x.

Viola, Francesco, F William Mauldin, Xiefan Lin-Schmidt, Doris M Haverstick, Michael B Lawrence, and William F Walker. 2010. “A Novel Ultrasound-Based Method to Evaluate Hemostatic Function of Whole Blood.” *Clinica Chimica Acta* 411: 106–13. doi:10.1016/j.cca.2009.10.017.

Weiner, Murray. 1963. “Clot Retraction and Fibrinolysis.” *Clinical Chemistry* 9 (2): 182–87.

Weisel, John W. 2005. *Fibrinogen and Fibrin*. Vol. 70. Advances in Protein Chemistry. doi:10.1016/S0065-3233(05)70008-5.

Weisel, JW. 2010. “Biomechanics in Hemostasis and Thrombosis.” *Journal of Thrombosis and Haemostasis* 8: 1027–29. doi:10.1111/j.1538-7836.2010.03808.x.

Chapter 5: Future work

INTRODUCTION

There are a number of research questions and device development steps that are relevant to the work discussed in this dissertation that have not been resolved. I have broken up the list of potential future directions for my research project into sections relevant to Chapters 2, 3, and 4 of the dissertation, dealing with clot stiffness measurement device development, study of platelet thrombin generation related effects, and study of platelet IIb-IIIa adhesion related effects, respectively.

DISCUSSION

Optical ARF based clot stiffness assessment device development and applications, next steps

I have validated the clot stiffness assessment device by assessing the material properties of an agarose gel and comparing to prior literature for measurement of agarose gel material properties by standard mechanical properties measurement devices. Measurement of agarose clot stiffness by a standard mechanical properties measurement device in parallel with measurement by the optical acoustic radiation force (ARF) based clot stiffness assessment device could provide more evidence of validation of the mechanical testing capabilities of the new approach.

Additionally, whereas I have demonstrated a comparison of agarose stiffness as compared to plasma clot stiffness by mechanical testing at matched ultrasound

wave application, the acoustic properties (attenuation) of the materials differ and the forces applied in each sample were not equal in an attenuation dependent manner. Experiments could be performed to determine ultrasound settings at which forces applied in agarose and plasma would be equal, such that the displacements could be directly compared to determine the stiffness ratio of the two materials. A comparison of force matched conditions would further validate the approach, since material properties can be force application dependent.

Fluorescence imaging of embedded fluorescent microbeads was implemented effectively in the work described in this dissertation to allow for late stage detection of clot stiffness in turbid plasma clots 1 hour or longer after clot initiation. The potential applications of fluorescence imaging and longer time point measurement in plasma clots could be further explored. Imaging at later time points in plasma clot development could allow for detection of fibrinolysis or clot retraction related effects. It would be of great interest to determine whether there is loss or increase in clot stiffness at late time stages. Loss of clot stiffness at time points greater than 1 hour may be associated with the breakdown of clot matrix due to fibrinolytic processes, whereas increases in clot stiffness could reflect the long term effects of platelet contractility in clot retraction. Additionally, fluorescence imaging could be performed with multi-color imaging to detect labeled fibrin fibers and platelets in the clot as well as fluorescent beads. Experiments in which bead motion and fibrin fibers are both detectable would allow for examination of active microrheological effects on clot structure.

Whereas the experiments performed and presented in this dissertation provide a correlation of clot structural changes and clot stiffness, experiments with platelet and fibrin fiber labeling and fluorescent beads could allow for direct observation of structural responses to force application and local differences in structure that lead to bead motion differences.

Clot plasticity is a feature of blood clotting that may be relevant to how clots deform and change under application of flow in a blood vessel. Optical ARF based clot stiffness assessment is able to detect clot plasticity. Experiments could be performed to determine influences of flow on a blood sample to plastically deform the blood clot. Features of clot deformation may be protective in thrombotic conditions or exacerbate coagulopathies. Optical ARF based clot stiffness assessment could be used to begin to understand the role of plasticity in coagulation.

Platelet thrombin generation influences on clot stiffness and clot structure, next steps

While thrombin generation can be controlled for by inhibition of Factor Xa, as was demonstrated in this dissertation, I did not measure thrombin levels in clot samples instead assuming equal thrombin concentrations in samples where Factor Xa was inhibited. To measure thrombin levels in clot samples a thrombin substrate could be used such as Z-Gly-Gly-Arg-MCA (Colace, Muthard, and Diamond 2012) such that fluorescence intensity in the clot would indicate the

extent of thrombin production. This would allow for blood samples to be matched for comparison of clot structure and clot stiffness based on measured thrombin levels. Z-Gly-Gly-Arg-MCA could be added to blood samples at 800 μM and a fluorometer could be used to assess fluorescence intensity in the sample periodically over the course of 30 minutes with excitation at 390nM and emission at 460nM. Measurement of clot stiffness and structural differences in thrombin concentration matched plasma samples with and without platelets would provide another level of confirmation to the effects of platelet function and thrombin concentration studied in this dissertation.

An experiment described in this dissertation demonstrated the influence of thrombin in Factor Xa inhibited, or thrombin generation inhibited, platelet rich whole blood to resist a reduction in clot stiffness at high thrombin concentration that did occur in platelet poor plasma samples. This experiment is consistent with a hypothesis that platelet functions independent of thrombin generation resist a reduction in clot stiffness at high thrombin concentration. A thrombin titration experiment that employs inhibition of Factor Xa by apixaban and IIb-IIIa-fibrin adhesion by abciximab in combination could be used to test consistency of the hypothesis that platelet adhesion through integrin IIb-IIIa is one platelet function that may contribute to the resistance to loss of clot stiffness at high thrombin concentration. The combination Factor Xa and IIb-IIIa-fibrin inhibition would assess platelet adhesion and its influence on clot stiffness. If with inhibition of IIb-IIIa adhesions, in a situation where through Factor Xa inhibition the thrombin

levels are controlled for, any changes in clot stiffness observed as compared to thrombin titrations in thrombin level controlled plasma without IIb-IIIa inhibition could be attributed to inhibited platelet adhesive function.

Changes in clot structure due to thrombin concentration were not considered in this dissertation although they are of interest. The same perturbations in clots with and without platelets and in inhibition of Factor Xa and integrin IIb-IIIa binding to fibrin could be performed in a clot structural assay. Differential interference contrast (DIC) and fluorescence microscopy imaging could be used to assess clot structural differences such as platelet cluster size, fibrin fiber diameter, clot porosity, fiber tortuosity, and others in order to determine structural changes in blood clots due to platelet thrombin generation and IIb-IIIa adhesion.

Platelet adhesion through integrin IIb-IIIa influences on clot stiffness and structure, next steps

Additional experiments that could be performed involving integrin IIb-IIIa signaling and clot stiffness and structural changes include performing platelet spreading and clot retraction assays. Platelet spreading and clot retraction assays under conditions of Src kinase inhibition by PP2 could provide insight into possible temporal changes in Src kinase and platelet contractility. A time course examination of clot retraction with Src kinase inhibition by PP2 might provide

information to help interpret the conflicting reports in recent literature regarding clot retraction (Flevaris et al. 2007; Suzuki-Inoue et al. 2007).

Immunoprecipitation could be performed to confirm inhibition of Src kinase activity in platelets by PP2. Confirmation of reduced clot stiffness with Src kinase inhibition by PP2 in sonorheometry performed on blood samples from multiple subjects would further validate the hypothesis of Src kinase involvement in regulation of platelet contractility and clot stiffness. Additionally, sonorheometry to assess clot stiffness with blebbistatin inhibition of platelet myosin IIa activity could be performed to confirm the involvement of myosin IIa platelet contractility in clot stiffness.

It has been demonstrated in this dissertation that abciximab inhibition of integrin IIb-IIIa results in reduced clot stiffness and fibrin fiber diameters. The effect of enhanced adhesion of platelet integrin IIb-IIIa to fibrin on clot stiffness and fibrin fiber diameter has not been determined however. Manganese treatment of platelet rich plasma could be used to enhance integrin IIb-IIIa affinity for fibrin (Moser et al. 2008). The effects of blocking IIb-IIIa mediated binding to fibrin could be compared to effects of enhancement of IIb-IIIa binding affinity for fibrin by Mn^{+2} to determine the influence of platelet adhesion to fibrin on clot stiffness and structure. I hypothesize that IIb-IIIa mediated platelet adhesion to fibrin modulates clot stiffness and clot structure by making platelets weldpoints, or fibrin network nodes, that allow for development of larger fibrin fibers and a stiffer

blood clot. Inhibition of IIb-IIIa mediated platelet adhesion to fibrin (abciximab 10μg/mL) (Viola et al. 2010) would reduce platelet function as a weldpoint in the fibrin network, whereas enhancement of IIb-IIIa affinity for fibrin (Mn^{+2} 3mM) (Moser et al. 2008) would increase platelet interaction with the fibrin network. The data from these two experiments should suggest whether platelet connectivity with the fibrin network contributes to platelet modulation of clot stiffness and clot structure.

The effect of platelet contractility (myosin IIa), a driver of clot retraction (Calaminus et al. 2007), on clot stiffness and fibrin fiber diameter could be determined by comparing stiffness and structure of clots formed with myosin IIa inhibited (blebbistatin 80μM) (Suzuki-Inoue et al. 2007; Ono et al. 2008; Calaminus et al. 2007) platelets to control. This experiment would investigate if platelet contractility plays a role in adhesion dependent modulations of clot stiffness and structure. Because the activity of myosin IIa has been shown to result in platelet retraction (Calaminus et al. 2007), platelet contractility may increase clot stiffness through a IIb-IIIa mediated platelet adhesion mechanism that involves tensioning the fibrin network. Creating tension on the fibrin network could result in increased fibrin fiber diameter as multiple platelet fibrin connections are aligned. Blebbistatin inhibition of myosin IIa then, could reduce clot stiffness in plasma clots and reduce fibrin fiber diameter. Confirmation of this effect would be consistent with a model in which platelet contraction contributes to clot stiffness and changes in clot structure.

A research interest regarding the influence of inhibition of integrin IIb-IIIa on outside-in signal transduction could be examined by a Western blotting experiment. “Outside-in” signal transmission after blocking integrin IIb-IIIa adhesion to fibrin (abciximab) and Src kinase phosphorylation as well as subsequent myosin IIa phosphorylation could be assessed. This experiment could assess whether signal transmission from platelet IIb-IIIa adhesion events to contractile apparatus (myosin IIa) might correlate with modulation of clot stiffness and structure. If inhibition of IIb-IIIa integrin ligation to fibrin (abciximab) prevents Src and myosin IIa phosphorylation, that is consistent with a hypothesis that changes in clot stiffness and clot structure observed with abciximab inhibition are due to coordinated action of platelet adhesion and platelet contractility to modulate clot properties. Platelet rich plasma could be incubated for 30 minutes with concentrations of abciximab between 0-10μg/mL (Viola et al. 2010). Clotting could be initiated and the clot lysed with lysis buffer at time points between 0-30 minutes. Phosphorylation of Src and myosin IIa could then be determined with and without abciximab inhibition by immunoprecipitation. Abciximab inhibition of IIb-IIIa ligation may inhibit Src kinase and myosin IIa phosphorylation, which would suggest that the two processes of platelet adhesion and platelet contractility coordinately modulate clot mechanical properties and clot structure.

The effect of granule secretion on stiffness, structure, and thrombin levels in clots formed with granule secretion inhibited (Ro 32-0432) platelets could be

examined. The experiment would investigate if platelet granule secretion modulates clot stiffness and structure. Because platelet granules contain procoagulant factors such as fibrinogen, von Willebrand factor, and Factor V, granule secretion may significantly alter the enzymatic activity of fibrin polymerization of the clot and change clot stiffness and clot structure.(Harrison and Martin Cramer 1993) Inhibition of α granules by Ro 32-0432 has been shown to not reduce platelet aggregation, so it may not alter the platelet adhesion to fibrin mediated by integrin IIb-IIIa.(Moncada de la Rosa et al. 2013) Monitoring of thrombin levels with Ro 32-0432 inhibition could determine if this inhibition also inhibits thrombin concentrations. Because platelets release procoagulant factors and also store p-selectin and IIb-IIIa,(Harrison and Martin Cramer 1993; Blair and Flaumenhaft 2009) granule secretion may significantly modulate clot stiffness and clot structure. Granule secretion may also significantly alter thrombin and IIb-IIIa affinity. Although granule secretion likely plays a significant role in platelet function in blood clotting it may not be possible to truly separate granule secretion from other platelet processes such as thrombin generation and adhesion. Granule secretion may function to amplify the effects of thrombin and platelet adhesion on clot stiffness and clot structure.

REFERENCES

Blair, Price, and Robert Flaumenhaft. 2009. “Platelet A-Granules: Basic Biology and Clinical Correlates.” *Blood Reviews* 23 (4): 177–89. doi:10.1016/j.blre.2009.04.001.

Calaminus, S D J, J M Auger, O J T McCarty, M J O Wakelam, L M Machesky, and S P Watson. 2007. “MyosinIIa Contractility Is Required for Maintenance of Platelet Structure During Spreading on Collagen and Contributes to Thrombus Stability.” *Journal of Thrombosis and Haemostasis* 5 (10): 2136–45. doi:10.1111/j.1538-7836.2007.02696.x.

Colace, Thomas V, Ryan W Muthard, and Scott L Diamond. 2012. “Thrombus Growth and Embolism on Tissue Factor-Bearing Collagen Surfaces Under Flow: Role of Thrombin with and Without Fibrin.” *Arteriosclerosis, Thrombosis, and Vascular Biology* 32 (6): 1466–76. doi:10.1161/ATVBAHA.112.249789.

Flevaris, P, A Stojanovic, H Gong, A Chishti, E Welch, and X Du. 2007. “A Molecular Switch That Controls Cell Spreading and Retraction.” *The Journal of Cell Biology* 179 (3): 553–65. doi:10.1083/jcb.200703185.

Harrison, P., and E Martin Cramer. 1993. “Platelet A-Granules.” *Blood Reviews* 7 (1): 52–62. doi:10.1016/0268-960X(93)90024-X.

Moncada de la Rosa, C, A Radziwon-Balicka, H El-Sikhry, J Seubert, P P Ruvolo, M W Radomski, and P Jurasz. 2013. “Pharmacologic Protein Kinase C Inhibition Uncouples Human Platelet-Stimulated Angiogenesis From Collagen-Induced Aggregation.” *The Journal of Pharmacology and Experimental Therapeutics* 345 (1): 15–24. doi:10.1124/jpet.112.200881.

Moser, Markus, Bernhard Nieswandt, Siegfried Ussar, Miroslava Pozgajova, and Reinhard Fässler. 2008. “Kindlin-3 Is Essential for Integrin Activation and Platelet Aggregation..” *Nature Medicine* 14 (3): 325–30. doi:10.1038/nm1722.

Ono, A, E Westein, S Hsiao, W S Nesbitt, J R Hamilton, S M Schoenwaelder, and S P Jackson. 2008. “Identification of a Fibrin-Independent Platelet Contractile Mechanism Regulating Primary Hemostasis and Thrombus Growth.” *Blood* 112 (1): 90–99. doi:10.1182/blood-2007-12-127001.

Suzuki-Inoue, K, C E Hughes, O Inoue, and M Kaneko. 2007. “Involvement of Src Kinases and PLCγ2 in Clot Retraction.” *Thrombosis Research* 120: 251–58. doi:10.1016/j.thromres.2006.09.003.

Viola, Francesco, F William Mauldin, Xiefan Lin-Schmidt, Doris M Haverstick, Michael B Lawrence, and William F Walker. 2010. “A Novel Ultrasound-Based Method to Evaluate Hemostatic Function of Whole Blood.” *Clinica Chimica Acta* 411: 106–13. doi:10.1016/j.cca.2009.10.017.